

1 **Key:** Solid Blue = Responses, *Italicized blue* = new text, Quotation marks = new and existing text from the
2 manuscript.

3 We would like to thank the reviewers for taking the time to review our paper and for their thoughtful
4 comments. Their comments have helped us clarify and improve the manuscript. We have reproduced
5 the reviewer comments in black text. For ease of review, our responses are given in blue text, while the
6 new text added to the manuscript is given in blue Italics and the original text from the submitted
7 manuscript remains un-italicized. We would also like to point out that the numbering of the figures from
8 the revised manuscript is used here in the responses and that the figures only used for responses are
9 noted with the prefix “R”.

10 **Referee 1 Comments**

11 **R1.1.** This paper is interesting in that new constraints on S/IVOC emissions are used together with
12 recent VBS yield suggestions, and the results compared to a wide range of measurements. The
13 measurement data range from near-surface to aircraft data, all evaluated using the concept of
14 photochemical age and with SOA/CO ratios. The use of OFR data is also beneficial I think, in helping to
15 place limits on the SOA formation and ageing-process at long photochemical ages.

16 Although the paper does present some interesting analysis, I think that there are some significant
17 problems, and I cannot recommend the paper for publication until these are addressed. One problem is
18 that there have been so many papers by now in which somebody identifies a problem with model-
19 measurement discrepancies in SOA, and by tweaking the VBS parameters in some way one can get
20 better agreement. This paper falls into that pattern, and although the authors have good reasons for
21 their particular choice of parameter-tweaking the fact remains that there are an infinite number of ways
22 of improving SOA predictions. The authors need to demonstrate some advantage of their schemes over
23 others, and this requires a reliable model study.

24 We address to this comment by kindly referring the reviewer to the following paragraph written in the
25 submitted manuscript (p. 5, L152) and by adding some sentences (in *Italics*) for clarity:

26 “The goal of this study is to use several recently published results to better evaluate and
27 constrain the box model introduced in our previous work, and thus facilitate the identification of
28 parameterizations that can be eventually incorporated into 3-D air quality models to accurately
29 predict SOA for the right reasons. *It is important to note that parameterizations used in the box model*
30 *are based on several published measurements taken from laboratory experiments and field studies*
31 *that provide more realistic constraints than in previous versions and that were not available to be*
32 *implemented in Hayes et al. (2015).* In particular, our work here improves the box model by
33 incorporating recently published measurements of P-IVOCs and P-SVOCs that allow better
34 constraining of the concentration, reactivity, yields, and volatility of these precursors (Worton et al.,
35 2014; Zhao et al., 2014). In addition, given that experiments in environmental chambers may
36 underestimate SOA yields for the VOCs due to losses of semi-volatile gases to the chamber walls
37 (Zhang et al., 2014), the SOA yields from VOCs have been re-estimated using a very recent

38 parameterization of these wall-losses (Krechmer et al., 2016). The wall-loss corrected yields obtained
39 are then used in the model in a sensitivity study to evaluate the corresponding change in the modeled
40 SOA concentrations. *The model is modified based on these literature constraints. No model tuning is*
41 *performed with the goal of improving the agreement with the observations.*”

42 We also want to clarify that, contrary to the statement from the reviewer, no model tuning is performed
43 in our work at all. That is to say, we test SOA models and parameters based on the literature, and we do
44 not derive new versions based on fitting the observations. The results are obtained by directly
45 incorporating into the model the results mentioned above from each study (P-IVOC concentrations,
46 volatility, etc.) with no *a priori* knowledge that those model cases would have better (or worse)
47 model/measurement agreement. In other words, in the development of the model cases
48 model/measurement agreement with respect to SOA concentration was not used to determine the
49 model parameters and the parameters in each case are not “tuned”.

50 **Why a box-model?**

51 **R1.1.1** In order to demonstrate that the merits of the tweaks used here are real, I would have wanted to
52 see a thorough demonstration of improved model-observation performance across a range of scales.
53 The box model used here cannot in my opinion provide such a demonstration; this study should have
54 been conducted with a well-evaluated 3-D chemical transport model. In fact, with only four mechanisms
55 being evaluated, and over a short period, I cannot think of any reason not to use a CTM.

56 Although box models are often useful for examination of, for example detailed chemical processes, or
57 basic principles, they are not well suited to studies where comparison with ambient measurements is in
58 focus. This has been well established for years, and is a major reason why air pollution modelling moved
59 from the earlier EKMA-type moving box models to 3-D models such as CAMx or CMAQ. The
60 measurements used in this study also range from near-surface data to aircraft, which places additional
61 constraints on the abilities of a box model. Although the authors (and those of the previous Hayes et al
62 2015 study which preceded this work) have put a lot of effort into the box model setup, I do not believe
63 that any amount of effort can overcome the basic limitations of such models. Box models simply cannot
64 account for the 3-D nature of atmospheric dispersion, and they cannot be expected to cope with
65 pollutant situations where nonlinearity of photochemical/SOA production is expected.

66 We very strongly disagree with these statements about 3-D models always being superior to box
67 models, and in fact think that the opposite is the case in some cases, as already documented by many
68 prominent papers in the literature. We address to this comment by kindly referring the referee to the
69 following paragraph written in the submitted manuscript (p. 4, L138) and by adding some sentences (in
70 *Italic*) for clarity:

71 “Recently, we evaluated three parameterizations for the formation of S-SOA and I-SOA using a
72 constrained 0-D box model that represents the South Coast Air Basin during the California Research at
73 the Nexus of Air Quality and Climate Change (CalNex) campaign (Hayes et al., 2015). *Box models are*
74 *often used to compare with ambient measurements, and have been shown to be of similar usefulness*
75 *or even superior to 3D models if the emissions and atmospheric transport affecting a given case study*

76 *are well constrained, and if the use of ratios to tracers can be used to approximately account for*
77 *dispersion (e.g. Volkamer et al., 2006; Dzepina et al., 2009; Yuan et al, 2015; Hayes et al., 2015). A box*
78 *model allows the evaluation of multiple model parameterizations either previously proposed in the*
79 *literature or developed from recent field and laboratory data sets, as well as the performance of*
80 *sensitivity studies, all of which would be difficult to carry-out in more computationally demanding*
81 *gridded 3D models. There are six model cases presented in this paper that are described in further*
82 *detail below. Given the number of model cases (including three additional model cases from Hayes et*
83 *al. 2015), it would be computationally expensive to use a 3-D model to evaluate all the cases.*

84 *Moreover, there are important limitations to traditional comparisons of 3-D models predicted*
85 *concentrations against measurements, as for example discussed for the Pasadena ground site in*
86 *Woody et al. (2016). In that study, the SOA predicted by the Community Multiscale Air Quality (CMAQ)*
87 *model with a VBS treatment of OA is a factor of 5.4 lower than the measurements during the midday*
88 *peak in SOA concentrations. This underestimation was attributed to several different factors. First, the*
89 *model photochemical age for the site was too low by a factor of 1.5. In the box model presented in this*
90 *current work, that problem is eliminated as the photochemical aging of the urban emissions in the*
91 *model is instead determined from the measured ratio of 1,2,4-trimethylbenzene to benzene as*
92 *described previously (Parrish et al., 2007; Hayes et al., 2013). Second, it is difficult to distinguish errors*
93 *due to model dispersion from those due to emission inventories and photochemical age. Woody et al.*
94 *(2016) conclude that excessive dispersion or low emissions account for an error of about a factor of 2.*
95 *Those errors are also eliminated by the use of emission ratios in this work. After those errors are*
96 *accounted for, by analyzing the 3D model output using similar techniques as in our box model, the real*
97 *under-prediction of SOA formation efficiency by a factor of 1.8 emerged, compared to the initial value*
98 *of 5.4 from the concentration comparisons. These errors (of approximately 300%) in the interpretation*
99 *of 3D model comparisons, which are ignored in most 3D model studies, are far larger than the*
100 *uncertainties due to emission ratios or dispersion in our box model (about 10 - 20%), as demonstrated*
101 *in section 2.4.*

102 *In addition, there are uncertainties in the P-S/IVOC emissions inventories used in 3-D models*
103 *and in the methods used to estimate P-S/IVOC emissions from the traditional POA inventories. In our*
104 *box model, as described in further detail below, we incorporated recently published field*
105 *measurements of P-S/IVOCs to better constrain the concentration of these species. Thus, while 3-D*
106 *models are essential for simulating spatially and temporally complex environments under the*
107 *influence of many sources, in cases where transport is relatively simple and there is a well-defined*
108 *urban plume such in Pasadena during the CalNex campaign, the box model is a valuable*
109 *complementary or even superior approach that is less susceptible to the convoluted uncertainties in*
110 *3-D models discussed above. Another reason to use a box model is that it allows a direct comparison*
111 *against OFR measurements taken in the field (Ortega et al., 2016). The OFR provided (every 20*
112 *minutes at the Pasadena ground site) a measure of SOA formation potential for a photochemical age*
113 *of up to two weeks. To the best of our knowledge, 3-D models have not yet been adapted for*
114 *comparison against OFR data. Finally, box models are more widely usable by experimental groups*
115 *(such as ours) due to reduced complexity, while 3-D models are almost exclusively used by modeling-*

116 *only groups, who tend to be more distant from the availability, use, and interpretation of*
117 *experimental constraints. Thus the use of a range of models by a range of different groups is highly*
118 *beneficial to scientific progress.”*

119 **R1.1.2** The authors may argue that by scaling with CO that they remove dispersion errors but this is only
120 partly true. This does not account for the fact that SVOC partitioning is dependent on absolute OA
121 concentrations, and so requires simulation of e.g. urban plumes and vertical gradients.

122 This is a small effect, which we had already addressed previously with a sensitivity study in Dzepina et al.
123 (2009). We address this comment by adding the following section in the text:

124 *Section 2.4 Correction for changes in partitioning due to emissions into a shallower boundary layer*
125 *upwind of Pasadena*

126 *“As described in Hayes et al. (2015), during the transport of the pollutants to Pasadena, the*
127 *planetary boundary layer (PBL) heights increase during the day. Using CO as a conservative tracer of*
128 *emissions does not account for how the shallow boundary layer over Los Angeles in the morning*
129 *influences gas-particle partitioning due to lower vertical mixing and higher absolute POA and SOA*
130 *concentrations at that time. Thus, as shown in the gas-particle partitioning equation above, there will*
131 *be a higher partitioning of the species to the particle phase and less gas-phase oxidation of primary*
132 *and secondary SVOCs. Later in the morning and into the afternoon the PBL height increases (Hayes et*
133 *al. 2013) diluting the POA and urban SOA mass as photochemical ages increases. However this is a*
134 *relatively small effect as the partitioning calculation in the SOA model is relatively insensitive to this*
135 *effect and the absolute OA concentrations (Dzepina et al., 2009; Hayes et al., 2015). Our previous work*
136 *(Hayes et al., 2015) found in a sensitivity study a +4/-12% variation in predicted urban SOA when*
137 *various limiting cases were explored for simulation of the PBL (e.g. immediate dilution to the*
138 *maximum PBL height measured in Pasadena versus a gradual increase during the morning).*

139 *To account for the effect of absolute OA mass on the partitioning calculation, the absolute*
140 *partitioning mass is corrected using the following method. A PBL height of 345 m is used for a*
141 *photochemical age of 0 h and it reaches a height 855 m at a photochemical age of 9.2 h, which is the*
142 *maximum age for the ambient field data. Between the two points, the PBL is assumed to increase*
143 *linearly. The boundary layer heights are determined using ceilometer measurements from Pasadena*
144 *at 6:00 - 9:00 and 12:00 - 15:00 local time, respectively (Hayes et al. 2013). The second period is chosen*
145 *because it corresponds to when the maximum photochemical age is observed at the site. The first*
146 *period is chosen based on transport times calculated for the plume from downtown Los Angeles*
147 *(Washenfelder et al. 2011) that arrives in Pasadena during the afternoon. There are certain limitations*
148 *to this correction for the partitioning calculation. First, the correction is based on a conceptual*
149 *framework in which a plume is emitted and then transported to Pasadena without further addition of*
150 *POA or SOA precursors. A second limitation is that we do not account for further dilution that may*
151 *occur as the plume is advected downwind of Pasadena. However, such dilution is not pertinent to the*
152 *OFR measurements, and so for photochemical ages beyond ambient levels observed at Pasadena, we*
153 *focus our analysis on the comparison with the OFR measurements.”*

154 **R1.1.3** More fundamentally, the assumption in this box-model work is that one can predict Δ VOC
155 concentrations from Δ CO alone. There may be some merit in this for transport derived VOC (and the
156 VOC profiles shown in Hayes et al 2015 show surprisingly good agreement for such VOC), but such a
157 relationship cannot hold for VOC from solvents and various production processes. Thus, we have
158 sources of VOC and hence SOA which are not constrained. I didn't find a discussion of this in the paper.

159 We address to this comment by adding the following paragraph in the experimental section.

160 *“It should be noted that the use of VOC emission ratios to CO to estimate VOC emissions does*
161 *not assume that VOCs are always co-emitted with CO. Rather, it assumes that VOC emission sources*
162 *are individually small and finely dispersed in an urban area, so that they are spatially intermingled*
163 *with the sources of CO. Moreover, previous studies have measured the emission ratios of*
164 *anthropogenic VOCs with respect to CO and the results show that vehicle exhaust is a major source of*
165 *VOC and CO (Borbon et al. 2013, Warneke et al. 2007). Furthermore, the ratios are consistent both*
166 *temporally and spatially. Thus, when thinking of the entire urban area as a source, the use of emission*
167 *ratios to CO is justified. As shown in Hayes et al. (2015) in the supporting information, the modeled*
168 *VOC concentrations are consistent with the measurements indicating that major VOCs sources have*
169 *not been omitted, and the smooth time variations of the VOC concentrations support the use of a*
170 *“global urban source”.”*

171 **R1.1.4** These problems are even more difficult to deal with when comparing SOA formation at longer
172 photochemical ages, e.g. 3 days as is done here. I would expect problems with any pollutant when
173 running a box model over such time-scales.

174 We address to this comment by adding the following paragraph in section 3.1 of the submitted
175 manuscript:

176 *“As displayed in the graphs for Fig. 3, it should be noted the measurements from the OFR*
177 *(Ortega et al. 2016) and from the NOAA P3 research aircraft (Bahreini et al. 2012) give quite similar*
178 *results for SOA/ Δ CO. The OFR measurements are not affected by particle deposition that would occur*
179 *in the atmosphere at long timescales or photochemical ages. Only a few percent of the particles are*
180 *lost to the walls of the reactor, and this process has been corrected for already in the results of Ortega*
181 *et al. The similarity in the two types of observations suggests that ambient particle deposition and*
182 *plume dispersion do not significantly change the SOA/ Δ CO ratio over the photochemical ages*
183 *analyzed here.”*

184

185 **R1.1.5** The authors (also in Hayes et al. 2015) do not even demonstrate that the model is capable of
186 reproducing pollutants such as CO or NO₂ reliably, and without this it is impossible to explain model-
187 measurement discrepancies in SOA in terms of VBS parameters alone.

188 It was disturbing that the text didn't acknowledge these limitations, but instead all model-measurement
189 discrepancies are assigned to VBS/SOA formation parametrizations.

190 As the NO_x levels and CO are constraints already used in the model set-up, it would not be meaningful to
191 perform the diagnostics described by the reviewer, although we certainly agree that those comparisons
192 would be worthwhile for (unconstrained) 3-D models. The ability to constrain important parameters is
193 one key advantage of constrained box models for this type of application. To better explain how the
194 model set-up is evaluated we have added the following text in section 2.2 of the manuscript.

195 *“It should be noted that the model uses CO and NO_x as inputs to constrain the model and the*
196 *SOA yields for high-NO_x conditions are used, based on our previous work (Hayes et al. 2013; 2015).*
197 *Therefore, to verify model performance both predictions of VOC and POA concentrations have been*
198 *compared against field measurements and the model performance appears to be satisfactory (Hayes*
199 *et al. 2015).”*

200 We agree with the reviewer that it is useful if the conclusions drawn from this study more clearly
201 acknowledge the model uncertainties, which appear to be confusing in the submitted version.
202 Therefore, we have updated the text as described in our response to comment R1.5.12 below.

203 **R1.1.6** Given that CTM models have already been set up and used for the CalNex campaign (Baker et al.,
204 2015, Hayes et al., 2015, Woody et al., 2016), I would suggest that the authors re-do their work in
205 collaboration with one of these teams.

206 Based on our points described above, especially R1.1.1, it seems reasonable to conclude that a box
207 model provides important scientific value that complements 3-D models and is superior to those models
208 for some scientific questions. Indeed, we have contributed to both box modeling as well as collaborated
209 closely in several 3-D modeling studies for CalNex. From those experiences, we have concluded that the
210 box model can be superior to a 3-D model for this application, as it eliminates or greatly reduces many
211 potential errors in, e.g., the photochemical age, dispersion, and emissions, by the use of constraints. We
212 are not saying that box models can always provide a comparable alternative to 3-D models to study
213 chemical processes in all cases, but this is clearly the case when source regions and transport are simple
214 and well-characterized as in this study.

215

216 **2 Experiment design**

217 **R1.2.1** I found the approach confusing in several respects.

218 To start with, the paragraph at the end of P9 (start of 2.2.2) is worrying. The initial POA is calculated
219 from $\Delta\text{POA}/\Delta\text{CO}$ emissions, which implies that POA is an inert pollutant. At the same time the authors
220 use Robinson's volatility distribution to estimate all emitted P/S/IVOCs. How can this be reconciled?

221 This topic has been discussed extensively in previous work (e.g. Dzepina et al., 2009, 2011; Hayes et al.,
222 2015). We address this comment by updating the text below in the submitted manuscript (p. 9, L324).

223 ***“The initial POA concentration is determined from the product of the background-subtracted
224 CO concentration and the $\Delta\text{POA}/\Delta\text{CO}$ emission ratio (Hayes et al., 2015). While this ratio may change
225 due to evaporation/condensation or photochemical oxidation of POA, our previous work (Hayes et al.
226 2013) has shown that $\Delta\text{POA}/\Delta\text{CO}$ does not change significantly at the Pasadena ground site with
227 observed photochemical age indicating that the ratio is insensitive to the extent of photochemical
228 oxidation. Furthermore, it was calculated that the ratio would increase by 28% for an increase of OA
229 concentration from 5 to 15 $\mu\text{g m}^{-3}$, concentrations that are representative of this study. This possible
230 source of error is substantially smaller than current errors suggested for P-S/IVOC emission inventories
231 in 3-D models, where current schemes are based on scaling POA emission inventories with scaling
232 factors that are not well constrained (Woody et al. 2016).”***

233 **R1.2.2** At the end of 2.2.2 (P10) we read that the important ratios of IVOC or VOC to CO are derived
234 from measurements made between 00:00 and 06:00 local time in Pasadena, 'when the amount of
235 photochemical ageing was very low'. There are several problems here, associated with the reliability of
236 such ratios for daytime modelling, and the assumption that other ageing processes are negligible. My
237 guess would be that CO concentrations have a larger component of long-range transport than IVOC for
238 example, and also that night-time chemistry would be more important than assumed here.

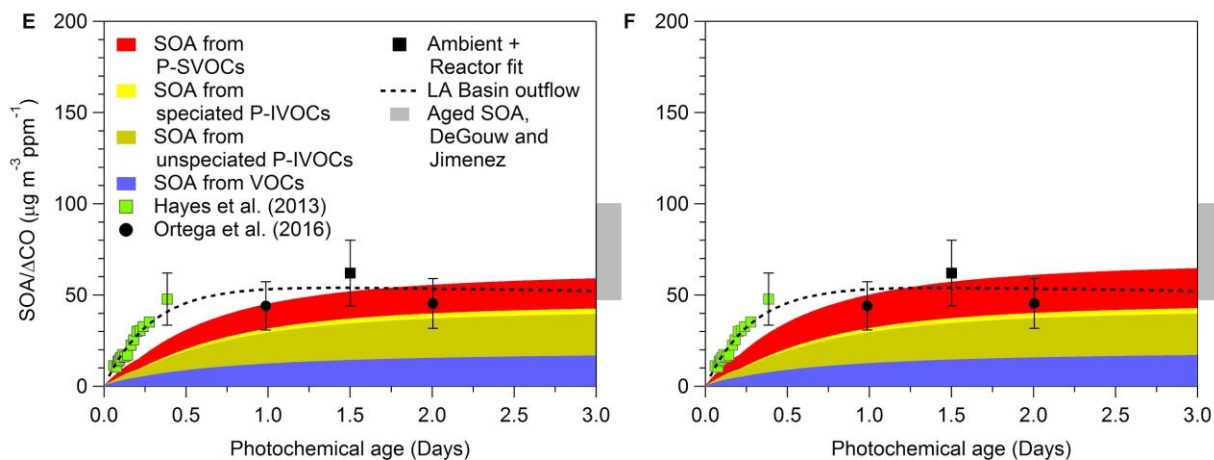
239 CO is well-known to have a background from long-range transport, which is estimated and always
240 subtracted before taking ratios, as described in Hayes et al. (2013) and references therein. Thus ΔCO
241 represents the urban contribution to CO and is the appropriate quantity to use here. For clarity, we
242 update the sentence below in the submitted manuscript (p. 10, L345-346):

243 ***“During the regression analyses the x-intercept was fixed at 105 ppbv CO to account for the
244 background concentration of CO determined in our previous work (Hayes et al., 2013). Thus, the slope
245 of the resulting line corresponds to the estimated emission ratio ($\Delta\text{IVOC}/\Delta\text{CO}$).”***

246 We further address the potential uncertainty in IVOCs suggested by this comment by running a
247 sensitivity case in which the IVOC initial concentration is calculated using the observed photochemical
248 age, the IVOC measurements at Pasadena, and the estimated IVOC oxidation rate constants following
249 Zhao et al. (2014). This alternate approach does not rely on the nighttime ratios of IVOC to CO.

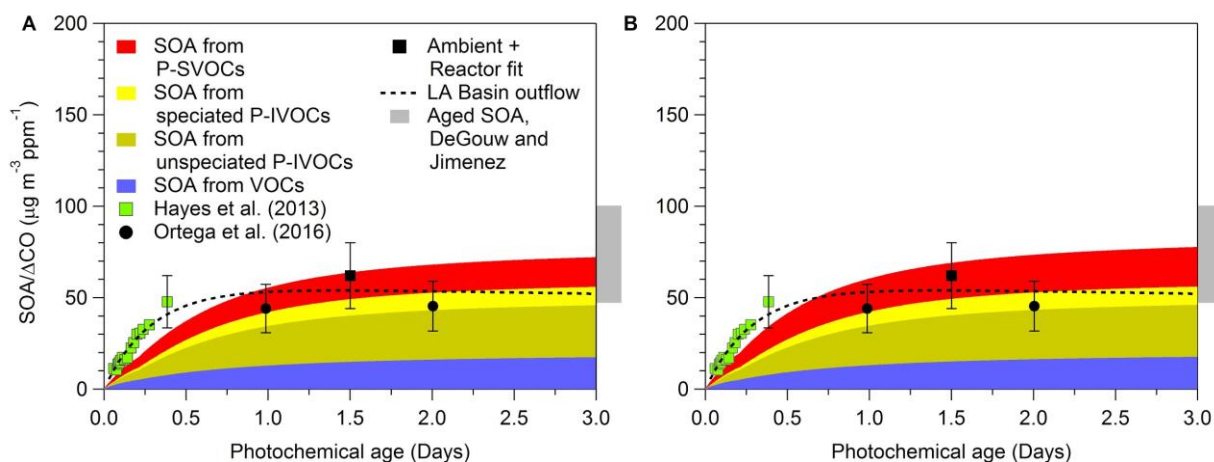
250

251 For comparison, we also include here the SOA formation results before running this sensitivity study
252 that are in the manuscript.



253
254 Figure 3. Predicted urban SOA mass for the E) ROB + ZHAO + MA and F) WOR + ZHAO + MA cases with
255 the original model set-up for this work.

256 The figure below represents the SOA formation for the same two cases as above but for initial IVOC
257 concentrations calculated without using the IVOC to CO ratios (as described above).



258
259 Figure S10. Predicted urban SOA mass for the A) ROB + ZHAO + MA and B) WOR + ZHAO + MA cases
260 when using IVOC initial concentrations determined using photochemical age, the Pasadena IVOC
261 concentrations, and the estimated IVOC oxidation rate constants.

262

263

264 To summarize these findings, we have added the paragraph below in the manuscript in section 3.3 and
265 included Figure S10 in the supporting information.

266 *“To further explore the impact of potential errors in the initial IVOC concentrations, a*
267 *sensitivity study has been carried out using initial concentrations calculated based on the observed*
268 *photochemical age and measured IVOC concentrations at Pasadena as well as the estimated IVOC*
269 *oxidation rate constants (Zhao et al., 2014). This alternate approach is implemented for the ROB +*
270 *ZHAO + MA and WOR + ZHAO + MA cases and does not use nighttime IVOC-to-CO ratios. The results*
271 *when using this alternative approach are shown in the supporting information (Figure S10). When*
272 *comparing Fig. S10 with Fig. 3, differences are minor. The model/measurement agreement improves*
273 *slightly at shorter photochemical ages (less than 1 day). At the same time a slightly larger over-*
274 *prediction is observed at longer photochemical ages. However, the formation of SOA modeled in this*
275 *sensitivity test is similar to the original cases from Fig. 3 with an average difference of only 21 %,*
276 *which represent a relatively small error compared to other uncertainties in SOA modeling. The IVOC*
277 *initial concentrations used in this sensitivity test are slightly higher than those calculated using the*
278 *IVOC-to-CO ratio, which explain the small increase of modeled SOA/ Δ CO. Ultimately, the different*
279 *approaches for determining the initial IVOC concentration in the model are reasonably consistent, and*
280 *both approaches perform similarly given the model and measurement uncertainties.”*

281 **R1.2.3** Thirdly, it is usually a good idea to change one aspect at a time of model simulations, in order to
282 investigate the effect of that one change. Here though the authors move from a set of ‘Tsimpidi’ cases
283 to cases where wall-loss are accounted for. At the same time they switch off the ageing of secondary
284 SVOCs. Thus, one cannot evaluate the importance of the ageing effect alone. This would have been a
285 useful step between the TSI and the various wall-loss cases.

286 We address this comment by kindly referring the reviewer to the updated texts below, which are copied
287 from the revised manuscript (page and line numbers written next to each section) where we discuss the
288 inclusion of the “aging” mechanisms in the model.

289 From the Introduction (text added at p. 4, L125 in original manuscript):

290 *“These “aging” mechanisms increase VOC yields to levels much higher than those observed in*
291 *chamber studies since it was perceived that the yields may be too low in chambers compared to the*
292 *real atmosphere. The “aging” mechanisms were added to chamber yields that were obtained without*
293 *using aging as part of the fits of the chamber data. In some model applications they improve model*
294 *agreement with field measurements (Ahmadov et al., 2012), while at long photochemical ages they*
295 *lead to model SOA formation that is substantially larger than observed (e.g. Hayes et al., 2015;*
296 *Dzepina et al., 2011).”*

297 From section 2.2 (text added at p. 8, L289 in original manuscript):

298 *“The three model cases accounting for wall losses of organic vapors are named ROB + MA,*
299 *ROB + ZHAO + MA, and WOR + ZHAO + MA. For these cases, the aging of the secondary SVOCs formed*
300 *from the oxidation of VOCs was not included, since multi-generation oxidation is not well-constrained*

301 using data from chamber studies that are run over relatively short time-scales (i.e. hours). In addition,
302 aging and correcting for wall-losses of organic vapors have been separately proposed to close the gap
303 between observed and predicted SOA concentration from pre-2007 models, *and are thought to*
304 *represent the same “missing SOA mass.” Therefore, we run the model with one of these options at a*
305 *time, as they are conceptually different representations of the same phenomenology.* The aging of
306 secondary SVOCs formed from the oxidation of P-IVOCs (and P-SVOCs) has been kept for all of the MA
307 cases, however. *To our knowledge, P-IVOC and P-SVOC mechanisms proposed in the literature have*
308 *always included aging.”*

309 As discussed in the submitted manuscript, the use of “aging” mechanisms were introduced to represent
310 processes that increase SOA yields in the real world compared to chambers, and that are now known to
311 be mostly due to vapor losses to chamber walls.

312 **R1.2.4** Further, on p8-9, we read that ageing of secondary SVOC from ‘VOC’ is not included, partly
313 because of poorly-constrained chamber data, but ageing of secondary SVOC from P-IVOCs and P-SVOCs
314 is included for the MA cases. These choices feel rather random, and indeed seem like tweaks to give the
315 model a decent chance of fitting the observations.

316 We address to this comment by clarifying that the choices are not random and we kindly refer the
317 reviewer to our response in R1.2.3. As discussed in our previous response, the VOC aging is conceptually
318 replaced by the correction for vapor wall losses on chamber walls. Therefore our choices are self-
319 consistent, and they are the simplest choices that can be made based on the literature.

320 **R1.2.5** Finally, the text on p9, L301-304 anyway seems to confirm that the refit was not able to
321 reproduce the chamber data. Although non-equilibrium reasons are given for this, I am a little confused
322 about the benefit of a refit that cannot reproduce the data.

323 To clarify, the refit *was able* to reproduce chamber data very well for the oxidation of VOCs. Therefore,
324 it seems reasonable to conclude that refitting the data for the VOCs is beneficial, since wall-losses appear
325 to be an important process that should be accounted for as best as possible. The refitting procedure was
326 unsuccessful only in the case of the IVOCs. We have updated the text to more clearly explain these
327 results.

328 *“Indeed, when trying to refit the VOC and IVOC yield curves, the model assuming equilibrium*
329 *partitioning between particles, the gas phase, and the walls was able to reproduce the yield curves for*
330 *VOCs, but not for IVOCs. This difference in the results is consistent with equilibrium not having been*
331 *reached during the chamber studies on the IVOCs, which produce a greater amount of lower volatility*
332 *SVOCs when compared to VOCs during oxidation. These lower volatility SVOCs have relatively slow*
333 *evaporation rates from the particles, which prevents the chamber system from reaching equilibrium*
334 *(Ye et al. 2016).”*

335

336 **Yield data?**

337 **R1.3.** Can the yields in Table S4 be correct? According to the manuscript (p8,L277-), this Table presents
338 the upper limits of the SOA yields, but the numbers look rather odd compared to Table S1 which is
339 supposed to be the lower limit. For isoprene the total yield is 0.039 in both Tables, and for other
340 compounds the differences are sec are quite small (0.194 vs 0.200 for Ole1, 0.382 vs 0.392 for Ole2,
341 0.932 vs 0.939 for Aro2, 0.835 vs 0.855 for Terp). The main difference seems to be that Table S4 has
342 mainly 0.0 for the 19 ug/m3 bin. A mistake maybe?

343 Firstly, we confirm that the SOA yields in Table S4 are indeed correct given our methodology.

344 Second, it is important to distinguish between total SOA yield , Y (particle-phase only), and the lumped
345 SVOC yields, α_i (gas plus particle phases in a single volatility bin), which are related by the equation
346 below (in the absence of wall-losses), and where C_{OA} is the particle concentration.

347
$$Y = \alpha_1 \left(1 + \frac{1}{C_{OA}}\right)^{-1} + \alpha_{10} \left(1 + \frac{10}{C_{OA}}\right)^{-1} + \alpha_{100} \left(1 + \frac{100}{C_{OA}}\right)^{-1} + \alpha_{1000} \left(1 + \frac{1000}{C_{OA}}\right)^{-1} \quad (1)$$

348 The equation above can be modified as discussed in our manuscript to include the partitioning of the
349 organics to the wall where C_w is the effective wall mass concentration.

350
$$Y = \alpha_1 \left(1 + \frac{1}{C_{OA}} + \frac{C_{w,1}}{C_{OA}}\right)^{-1} + \alpha_{10} \left(1 + \frac{10}{C_{OA}} + \frac{C_{w,10}}{C_{OA}}\right)^{-1}$$

351
$$+ \alpha_{100} \left(1 + \frac{100}{C_{OA}} + \frac{C_{w,100}}{C_{OA}}\right)^{-1} + \alpha_{1000} \left(1 + \frac{1000}{C_{OA}} + \frac{C_{w,1000}}{C_{OA}}\right)^{-1} \quad (2)$$

352 According to equations 1 and 2, at low C_{OA} the observed Y will be lower than that observed in the
353 absence of wall losses. On the other hand, when C_{OA} is much higher than C_w , the term $C_{w,i}/C_{OA}$
354 converges to 0 and equation 2 becomes identical to equation 1. Furthermore, at very high C_{OA} , Y is
355 simply the sum of the α_i values. Therefore, Y at very high C_{OA} concentrations is the same with or
356 without wall losses and thus the sum of α_i is also the same with or without wall losses. Therefore, the
357 observation that the total SVOC yields are quite similar between Table S1 and S4 is not surprising, and
358 actually expected. However, the difference in the volatility distribution of the yields, with a shift towards
359 lower volatility when wall losses of organic vapors are accounted for, means that Y will be higher for low
360 OA concentrations (typical of ambient conditions) and thus OA will have a tendency to form faster at
361 low photochemical aging.

362

363 To clarify this point we have added the following text to the manuscript in section 2.2.

364 *“Furthermore, as described in the supporting information, the updated SOA yields for VOC*
365 *oxidation result in distribution of SVOC mass into lower volatility bins compared to the original*
366 *parameterization, although the sum for the SVOC yields (α_i) remains similar. In the absence of aging,*
367 *the SOA yields, Y , resulting from the wall-loss correction should be considered upper limits (MA*
368 *parameterization), whereas the original yields serve as lower limits due to the considerations*
369 *discussed above (TSI parameterization without aging). As shown in the supporting information*
370 *(Figures S1 - S7) when aging (TSI parameterization with aging) is included the SOA yields increase*
371 *beyond those observed when applying the wall loss correction for most of the VOC classes at longer*
372 *photochemical ages. (It should be noted that SOA masses in Figures S1 – S7 were calculated using the*
373 *same background as for the other model cases, $2.1 \mu\text{g m}^{-3}$.) This feature of the aging parameterization*
374 *is likely to blame for SOA over-predictions observed at long aging times when comparing with*
375 *ambient data (e.g. Dzepina et al., 2011; Hayes et al., 2015).”*

376 **3-day simulations?**

377 **R1.4.** As noted above, I have grave reservations about the use of a box model for this study, and the
378 extension of the simulations to 3-days in Sect. 3.1. seems hard to defend. The authors suggest that they
379 limited the runs to 3-days to minimize the importance of missing processes such as deposition, but a box
380 model misses all processes of dispersion, transport and even chemistry in the correct photochemical
381 regimes when run over such a long time. I simply do not believe that such long runs with such an
382 artificial setup can be compared with measurements in other than a superficial way.

383 In any case, many SVOC species will show substantial deposition over 3-days (Karl et al, 2010, Hodzic et
384 al, 2016), as indeed would ozone and various NO_y species (e.g. N₂O₅).

385 We refer the reviewer to our response to comment R1.1.4. In addition, we have clarified the manuscript
386 in order to focus on the comparison of our results with the OFR measurements, which are completely
387 consistent with the model set-up, where deposition is also not important. We note that the box model is
388 run for the conditions of the OFR itself, which is not problematic. The consistency of the OFR and aircraft
389 results indicates that deposition does not have a major influence on the model results over short
390 timescales.

391

392 **Some other questions**

393 **R1.5.1** p3, L86 and generally. Actually VOCs are the only precursor of SOA (though of course other
394 precursors such as NO_x can be involved). VOC is a general term (defined here on L80-81) which includes
395 SVOC and IVOC. If the authors want to use the term VOC for volatile organic compounds which are not
396 S/IVOC then they need to refine and clarify their notation.

397 This is a semantic difference. In our work we use the term VOC as separate from S/IVOCs, while other
398 authors (and reviewer 1) include S/IVOCs as part of the term VOCs. Different definitions are often used
399 in the scientific literature for many terms, which is fine as long as each paper is clear on which definition
400 is used. Thus, we address this comment by adding the following sentences in the introduction section.

401 *“The notation used when discussing SOA precursors in this paper is similar to Hayes et al.*
402 *(2015). We differentiate VOCs, IVOCs and SVOCs by their effective saturation concentration (c^*).*
403 *Therefore, SVOCs and IVOCs have volatilities ranging from $c^* = 10^{-2}$ to 10^2 and 10^3 to $10^6 \mu\text{g m}^{-3}$*
404 *respectively, while VOCs are in the bins of $c^* \geq 10^7 \mu\text{g m}^{-3}$.”*

405 **R1.5.2** p3, L99. I was surprised not to see some more recent references here, since much has been done
406 in the last years. For example, Hodzic et al 2016 seem to cover some of the same themes (wall-loss
407 corrected VBS) as this paper, with an evaluation at global scale. Another relevant work would be that of
408 Dunmore et al 2015 and Ots et al. 2016, where IVOC emissions from diesel were suggested to be a major
409 source of ambient SOA.

410 We add the references Dunmore et al. 2015 and Ots et al. 2016 in the introduction section when
411 discussing P-S/IVOCs as important precursors to SOA.

412 We also added the following sentences in the experimental section (at p. 7, L237 in the original text)
413 when describing the way which the IVOC parameters were estimated.

414 *“In particular, the measured concentrations of speciated and unspeciated IVOCs and their*
415 *estimated volatility are used to constrain the initial concentration of these species (as discussed in*
416 *Section 2.2.2 below) as well as to estimate their yields (Zhao et al., 2014). Hodzic et al. (2016) have*
417 *also estimated the IVOC yields while accounting for wall-losses using recent laboratory studies.*
418 *However, the yields reported in that study are for a single lumped species, whereas in our work we*
419 *estimate the yields using 40 IVOC categories, each representing a single compound or a group of*
420 *compounds of similar structure and volatility. This method allows a more precise representation of*
421 *IVOC yields and rate constants in the SOA model.”*

422

423 **R1.5.3** p4, L105-107. If discussing VBS as a conceptual model, the 2-D version (Jimenez et al., 2009)
424 deserves a mention. Actually, why was this version not used? Box/Lagrangian models have few
425 restrictions on CPU usage, so would be a natural place to test 2-D VBS schemes.

426 We address this comment by adding the following paragraph at the end of section 2.2:

427 *“Simulations of O:C have been previously evaluated in Hayes et al. (2015) using laboratory*
428 *and field data from CalNex to constrain the predicted O:C. It was concluded in that work that it was*
429 *not possible to identify one parameterization that performed better than the other parameterizations*
430 *evaluated, because of the lack of constraints on the different parameters used (e.g. oxidation rate*
431 *constant, oxygen mass in the initial generation of products and that added in later oxidation*
432 *generations, SOA yields, and emissions). Therefore, incorporating O:C predictions into the current box*
433 *model and using those results in the evaluation discussed here would not provide useful additional*
434 *constraints.”*

435 We also want to mention that such a discussion would add length to the manuscript, which
436 might be undesirable as suggested by the reviewers. Not every available parameterization can be tested
437 in each manuscript, and we have chosen to focus on the 1D VBS parameterizations that are most
438 commonly used in regional and global models.

439 **R1.5.4** p4, L118. loses should be losses. (There are other some small typos/English problems throughout,
440 which should be checked.)

441 We correct “loses” to “losses” as suggested and have carefully proofread the revised manuscript.

442 **R1.5.5** p6, L185-189. The text states that the potential source of error from omission if cold-starts does
443 not apply to the total amount of vehicular POA emissions. This may be true if the absolute emission
444 rates are not used, but surely the volatility distribution of cold-start VOC is different to that of warm-
445 running engines?

446 We agree with the reviewer that the volatility distribution of POA emissions during cold-starts could be
447 potentially different from that of warm-running engines, although no information on that comparison
448 has been published to our knowledge. We have added the sentences below to the text in Section 2.2.2
449 to clarify this point.

450 *“It should be noted that the tunnel measurements do not include emissions due to cold starts*
451 *of vehicles. In the box model, only the relative volatility distribution of vehicular POA measured during*
452 *the tunnel study is used, and thus this potential source of error does not apply to the total amount of*
453 *vehicular POA emissions in the model. However, it is still possible that the volatility distribution of POA*
454 *is different during cold-starts compared to that of POA emitted from warm-running engines. To our*
455 *knowledge, measurements of the volatility distribution of POA during cold-starts are not available at*
456 *this time. By comparing the SOA model results using two different POA volatility distributions*
457 *(Robinson et al. 2007; Worton et al. 2014), we can evaluate to a certain extent the sensitivity of the*
458 *simulated SOA concentration to the initial POA volatility distribution.”*

459 **R1.5.6** On the same paragraph though, presumably the Worton et al data could be used to produce a
460 new estimate of total vehicle (S/I)VOC emissions. Why wasn't this done?

461 It is possible to calculate the P-S/IVOC emissions from the Worton et al. data in the following manner.
462 The emission ratios (in g C L^{-1}) for both diesel and gasoline are multiplied by the volume of each fuel sold
463 in Los Angeles county [Gentner et al. Proc. Natl. Acad. Sci. U.S.A. 109, 18318-18323, 2012] to obtain the
464 total emission (in g C) for each of the fuel types. To then implement these total emissions into the box
465 model framework, they are summed and divided by the total CO emissions [Gentner et al. Environ. Sci.
466 Technol. 47, 11837-11848, 2013], which are calculated in a manner analogous to that used for the P-
467 S/IVOCs. A POA/ Δ CO ratio of $3 \mu\text{g m}^{-3} \text{ppm}^{-1}$ is obtained, which is lower than the ratio currently used in
468 the box model, $6 \mu\text{g m}^{-3} \text{ppm}^{-1}$. The difference could be due to a greater influence of diesel emissions at
469 the Pasadena site than is indicated by the fuel sales data or cold starts. These possible sources of error
470 are the reason that the observed POA/ Δ CO ratio was chosen for constraining the P-S/IVOC emissions
471 rather than the approach suggested in this comment.

472 **R1.5.7** p8,L276-279, 281-288. Quantify these time-scales for the reader.

473 We have modified the text as follows in Section 2.2.

474 *“Specifically, at lower volatilities ($c^* \leq 1 \mu\text{g m}^{-3}$), the partitioning kinetics of the organic mass*
475 *from the particles to the chamber walls have an effective timescale of more than an hour, which is*
476 *similar or longer than typical chamber experiments (Ye et al., 2016). The limiting step in the*
477 *partitioning kinetics is evaporation of SVOCs from the particles to the gas phase, and therefore the*
478 *exact rate of evaporation depends on the OA concentration in the chamber.”*

479 *“According to Krechmer et al. (2016) and other chamber experiments (Matsunaga and*
480 *Ziemann, 2010), the gas-wall equilibrium timescale doesn't vary strongly with the chamber size. The*
481 *timescale for gas-wall equilibrium reported in these previous studies was 7 - 13 minutes.”*

482 **R1.5.8** P11, L370 and elsewhere. Define whether mass or volume fractions and stoichiometry are used.
483 This can be an easy error, especially when the cited Donahue paper redefined Raoult's law in terms of
484 mass rather than mole fractions.

485 We have updated the text as shown below.

486 *“Where $x_{p,i}$ is the particle phase fraction of lumped species i (expressed as a mass fraction); C_i*
487 *is the effective saturation concentration, and C_{OA} is the total mass of organic aerosol available for*
488 *partitioning ($\mu\text{g m}^{-3}$).”*

489 **R1.5.9** P11, L396. 'shorter' ... than what?

490 We now specify exactly the photochemical age in the text.

491 *“The ambient urban SOA mass at the Pasadena ground site is generally measured under*
492 *conditions corresponding to photochemical ages of 0.5 days or less (Hayes et al., 2013).”*

493 **R1.5.10** P15, L519-523. Too wordy and repetitive.

494 We address this comment by updating the text below in the submitted manuscript (at p. 15, L517 in the
495 original text):

496 ***“To make this comparison, the simulated SOA is apportioned between fossil S-SOA, fossil I-
497 SOA, fossil V-SOA, cooking S-SOA, and biogenic V-SOA. The last two apportionments correspond to
498 non-fossil carbon. This evaluation is possible following an approach similar to Hayes et al. (2015)
499 where the identity of the precursor is used to apportion SOA.”***

500 **R1.5.11** P15, L531. The work of Dunmore and Ots mentioned above would support this statement.

501 As suggested, we have added references to Dunmore et al. 2015 and Ots et al. 2016 in the line indicated
502 by the reviewer.

503 **R1.5.12** P15, L543 on. This paragraph is a good example where the authors attribute all problems to SOA
504 mechanisms. It may well be that the box model setup is responsible for the problems.

505 We address this comment by updating the conclusions about our results. We kindly refer the reviewer
506 to our updated texts below, which are copied from the updated manuscript.

507 **From Section 3.1**

508 ***“Finally, the ROB + ZHAO + MA and the WOR + ZHAO + MA cases both better represent SOA
509 formation and exhibit better model/measurement agreement among the different cases used in this
510 work. They are both consistent with the OFR reactor data at longer photochemical ages as shown in
511 Figs. 3 and 4 compared with the other cases. At a qualitative level, the MA parameterization
512 simulations are more consistent with the fit of the OFR measurements in which the SOA mass remains
513 nearly constant at longer photochemical ages. In contrast, the cases with the TSI parameterization do
514 not follow this trend as the SOA mass keeps increasing between 2 and 3 days age, which is not
515 observed in the measurements. As already mentioned, the model used for this work does not include
516 fragmentation reactions, and including these reactions, in particular branching between
517 functionalization and fragmentation during gas-phase SVOC oxidation, may improve the cases using a
518 potential update of the TSI parameterization as discussed below. Fig. 4F indicates that including
519 additional P-SVOC mass in the model and accounting for gas-phase wall losses in chamber studies
520 improves SOA mass concentration simulations with respect to the measurements. However, in the
521 WOR + ZHAO + MA case there is still a slight under-prediction of SOA formed at shorter photochemical
522 ages (between 0.05 and 0.5 days), and this discrepancy is observed in all the other model cases. Given
523 the uncertainties in the model set-up discussed in the experimental section, it is not possible to
524 conclude if one of the four cases (i.e. ROB + ZHAO + TSI, WOR + ZHAO + TSI, ROB + ZHAO + MA, WOR +
525 ZHAO + MA) more accurately represents SOA formation in the atmosphere.”***

526 We also want to mention that we explain the importance of fragmentation reactions as a response to
527 comment R2.2.1.

528 From Conclusions:

529 *“Therefore, the model cases with updated VOC yields that account for chamber wall-losses*
530 *best reproduce the ambient and OFR data. However, while the WOR + ZHAO + MA case appears to*
531 *represent a slight improvement over the ROB + ZHAO + MA case, as well as over the ROB + ZHAO + TSI*
532 *and WOR + ZHAO + TSI cases, it is not possible to conclude that one set of parameters is better than*
533 *the other since the difference in the predictions for these 4 cases (15 % on average) is likely smaller*
534 *than the uncertainties due to the model setup as well as the lack of a gas-phase fragmentation*
535 *pathway during aging.”*

536 **R1.5.13** P17, Sect. 3.2. Given my reservations about the validity of the box-model, and its obvious lack of
537 treatment of VOC degradation with transport time, I wasn’t convinced that this section had a good basis.
538 In addition, the manuscript is already quite long, and this section feels like a side-issue.

539 The model includes in fact a detailed treatment of VOC degradation in which the reduction in
540 concentration with photochemical age is simulated. In fact, the treatment of VOC degradation in the box
541 model is more rigorous than in 3-D gridded models in that there is no lumping of VOCs and the IVOCs
542 are speciated, which allows the use of more precise oxidation rate constants. To respond to the concern
543 regarding manuscript length, we have shortened this section to one paragraph.

544

545 **Referee 2 Comments**

546 **General Comments:**

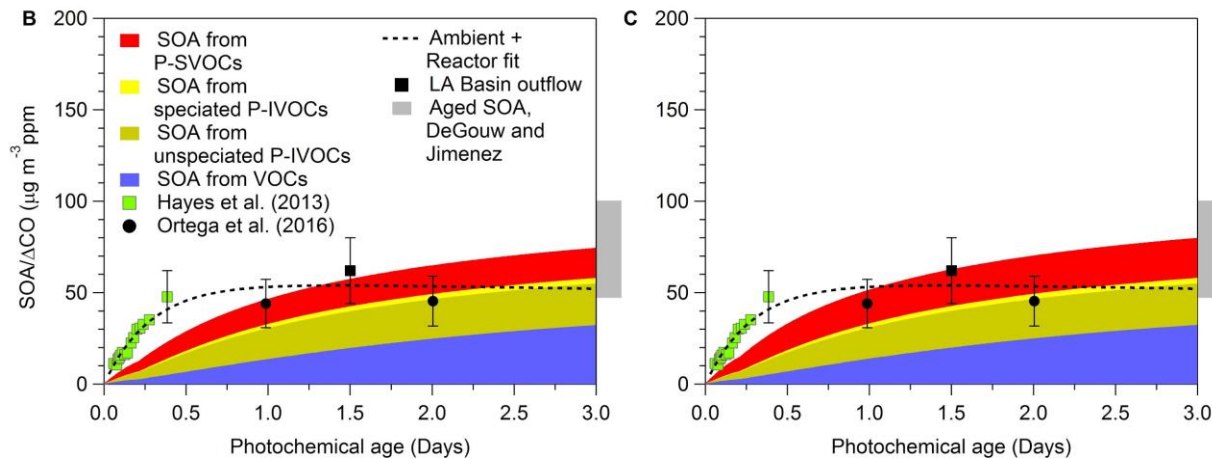
547 **R2.1** Ma and coauthors present a follow-up to the work in Hayes et al. (2015), adding more recent
548 parameterizations for I/S-VOC emissions and yields as well as very recent approaches to correcting
549 chamber yields for wall losses. I am satisfied with the application of the box model to the Pasadena data
550 given the lack of quantitative statistics presented. The important limitations of the aging mechanisms
551 and over-exuberant IVOC formation pathways is demonstrated more qualitatively than quantitatively.
552 Also, the authors are careful to avoid strong conclusions about the dominance of SOA from IVOCs over
553 SVOCs or vice-versa. I do urge the authors to move toward a 3D-CTM analysis in the future, particularly
554 since I'm pretty sure input datasets exist for all the major CTMs. Although the conclusions are not
555 exactly novel (other studies have shown that the VBS functionalization mechanisms overpredict at long
556 photochemical lifetimes), I appreciate the demonstration of the improved parameterizations,
557 particularly the chamber wall-loss correction. I found some aspects of the experimental design to have
558 unnecessary limitations. Moreover, I encourage the authors to consider improving several aspects of the
559 presentation before I recommend publication of this manuscript.

560 We thank the reviewer for their thoughtful comments, and have provided point-by-point responses
561 below. As discussed in response to, e.g., R1.1.1, we disagree with the notion that a 3D-CTM is superior in
562 all cases. In some cases a box model can be complementary and even superior to a 3D-CTM for some
563 applications.

564 **Specific Comments:**

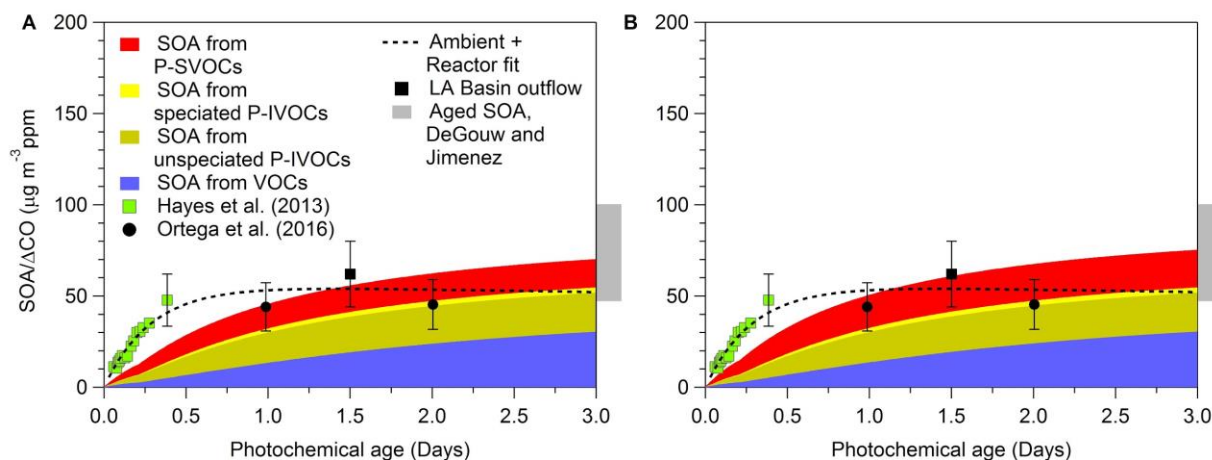
565 **R2.2.1** My primary question/criticism is why do the authors not investigate aging mechanisms with
566 fragmentation given the emerging global/regional model implementations of these pathways and the
567 low computational overhead of their own box model? This would seem like an ideal application given
568 the experimental data available to them from CalNex. Why not use measured AMS elemental ratios to
569 help constrain the configuration choices here? Potentially, that analysis could give complementary
570 information to the analysis in Section 3.2 and Fig. 6.

571 We address to this comment by running two model cases and including a fragmentation process due to
572 heterogeneous oxidation of the particles. The fragmentation is parameterized as an exponential decay
573 of OA concentration with a lifetime of 50 days as reported in Ortega et al. 2016.



574

575 Figure 3. Predicted urban SOA mass for the B) ROB + ZHAO + TSI and C) WOR + ZHAO + TSI cases with
 576 the original model set-up for this work.



577

578 Figure R1. Predicted urban SOA mass by the A) ROB + ZHAO + TSI and B) WOR + ZHAO + TSI cases when
 579 including fragmentation.

580 To summarize these findings, we have updated the text in the manuscript and added a discussion of the
 581 different fragmentation mechanisms. We only show results for two cases (those above), but all six
 582 model cases give similar results when including fragmentation.

583 *“According to the OFR data from Ortega et al. (2016), the mass of OA starts to decay due to*
 584 *fragmentation after heterogeneous oxidation at approximately 10 days of photochemical aging. The*
 585 *results are consistent with other OFR field measurements (George and Abbatt, 2010; Hu et al., 2016;*
 586 *Palm et al., 2016). In this work, the model is run only up to 3 days, which is much shorter than the age*
 587 *when heterogeneous oxidation appears to become important. In fact, when including a fragmentation*
 588 *pathway for each of the model cases, a reduction of OA of only 6 % is observed compared to the cases*
 589 *without fragmentation at 3 days of photochemical aging. In this sensitivity study, the fragmentation is*
 590 *parameterized as an exponential decrease in OA concentration that has a lifetime of 50 days following*

591 *Ortega et al. (2016). Given the results, the inclusion of fragmentation due to heterogeneous oxidation*
592 *in the model does not significantly change the model results or the conclusions made in this work.*

593 *More generally, there are at least three different fragmentation mechanisms that could be*
594 *responsible for the decrease of SOA formation at very high photochemical ages. The first mechanism is*
595 *the reaction of oxidants (e.g. OH) with the surface of an aerosol particle and decomposition to form*
596 *products with higher volatility, i.e. due to the heterogeneous oxidation just described. The second type*
597 *of fragmentation that may be important for very high photochemical ages in the OFR (Palm et al.,*
598 *2016) is due to the high concentration of OH. Most of the molecules in the gas phase will react*
599 *multiple times with the available oxidants before having a chance to condense, which will lead to the*
600 *formation of smaller products too volatile to form SOA. However, this is only important at very high*
601 *photochemical ages in the OFR, which are not used in this work. A third type of fragmentation can*
602 *occur during the aging of gas-phase SVOCs (Shrivastava et al., 2013; 2015). The TSI parameterization*
603 *used in the model from this work and from previous modeling works (Robinson et al., 2007; Hodzic et*
604 *al., 2010; Shrivastava et al., 2011) only includes the functionalization of the SVOCs and neglects*
605 *fragmentation reactions. More recently, Shrivastava et al. (2013) have modified the VBS approach in a*
606 *box model by incorporating both pathways and performed several sensitivity studies. The results*
607 *when including fragmentation generally exhibit better agreement with field observations, but as*
608 *noted in that work the agreement may be fortuitous given that both the emissions as well as the*
609 *parameters representing oxidation in the model are uncertain. This third type of fragmentation is not*
610 *simulated in our sensitivity study using the approach above, and it remains poorly characterized due*
611 *to the complexity of the chemical pathways and the number of compounds contributing to SOA*
612 *formation as described in Shrivastava et al. (2013)."*

613 **R2.2.2** The authors discuss extensively the problems with aging VOC oxidation products and the
614 tendency for mechanisms to accumulate mass at long photochemical lifetimes. It is important that they
615 emphasize (stronger than they already do) that this aging approach is likely problematic precisely
616 because it does not consider fragmentation. One of the main conclusions I read from the paper is that
617 wall-loss corrected VOC yields should be used and aging mechanisms turned off. Conceivably, a future
618 study will conclude that turning off aging is a bad idea because even though the OA mass is better
619 predicted at long time, the O:C is underpredicted. The models of the future will hopefully have both
620 more accurate yields and probably aging with both functionalization and fragmentation adequately
621 described. To avoid confusion in the meantime, I recommend the authors refer everywhere to the TSI
622 aging as "aging by functionalization only" or something similar, with an appropriate acronym for
623 readability.

624 We have addressed this comment in our responses to comments R2.2.1 and R1.5.12. We have not
625 changed the abbreviations in the text to "TSI with aging by functionalization only", since that would be
626 very cumbersome terminology. Instead we very clearly address this important issue in the abstract and
627 the conclusions as well as in new text quoted in our responses to R2.2.1 and R1.5.12.

628

629 **R2.2.3** L390-394 and L480-483: The authors repeatedly refer to the OFR work of Ortega et al. (2016) to
630 justify not including fragmentation in any model case. This argument relies on the assertion that
631 fragmentation only played a dominant role when the OA mass began to decrease after it had plateaued
632 for a couple of days in photochemical age space. But the OA concentrations started leveling off in that
633 study at about 1 day. As with any competition, the manifestation of a plateau indicates to me that
634 fragmentation is playing a role equal to that of functionalization. So sentences like L477-480 and L482-
635 483 are pretty confusing, if not misleading.

636 We completely agree with the reviewer and have modified the text to clarify the manuscript.

637 At L390 - 394, the new text reads as follows:

638 ***“Since fragmentation and dry deposition are not included in the model, it has only been run to***
639 ***3 days in order to minimize the importance of these processes with respect to SOA concentrations***
640 ***(Ortega et al., 2016). Nevertheless, it is very likely that gas-phase fragmentation of SVOCs (e.g.***
641 ***branching between functionalization and fragmentation) occurs during oxidative aging over these***
642 ***photochemical ages as is discussed in further detail below.”***

643 At L480 - 483, the text has been changed already in response to comment R1.5.12 and can be viewed in
644 our response to that comment.

645 **R2.2.4** The application of the wall-loss corrected chamber yields seems problematic to me. First of all,
646 many of the studies used to inform the Tsimpidi et al. (2010) yield set included seed aerosol in their
647 experiment. As the authors point out multiple times, the data they have included in Table S4 should be
648 considered an upper bound. However, I fear that their demonstration of this approach will encourage
649 others to blanket apply the parameters of Krechmer et al. (2016) to historical chamber yields without
650 considering the details and possible interferences. I encourage the authors to describe in detail the
651 problems with applying the narrowly defined Krechmer Cw’s to existing data and repeat that paper’s call
652 for more detailed analysis of chamber data before the community gobbles this simple approach and
653 then moves on to the next hot SOA formation topic.

654 We are aware of multiple groups that are working on further characterizing vapor wall losses and their
655 impact on SOA formation experiments. In that context, it seems very unlikely that our simple approach
656 would become “dominant” in the SOA modeling field. We still believe that it provides one useful
657 sensitivity study about the impact of the vapor loss problem. We address this comment by adding the
658 following sentence in the conclusion section of the manuscript.

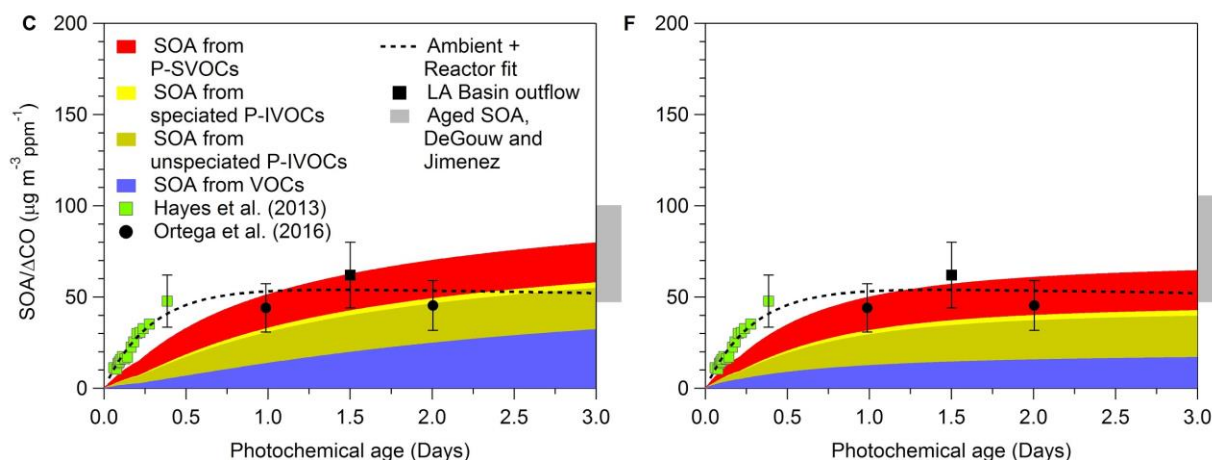
659 ***“Moreover, uncertainties in the vapor wall-loss corrected yields remain, and the correction of***
660 ***the yields has been performed here using data from a limited number of laboratory studies. In***
661 ***particular, the effect of temperature and humidity on gas-wall partitioning needs to be characterized.***
662 ***The results obtained in our work motivate future studies by showing that SOA models using wall-loss***
663 ***corrected yields reproduce observations for a range of photochemical ages at a level of accuracy that***
664 ***it is as good as or better than parameterizations with the uncorrected yields.”***

665 **R2.2.5** Why is the SOA mass in Fig. 5 not also divided by CO concentrations to correct for dilution?

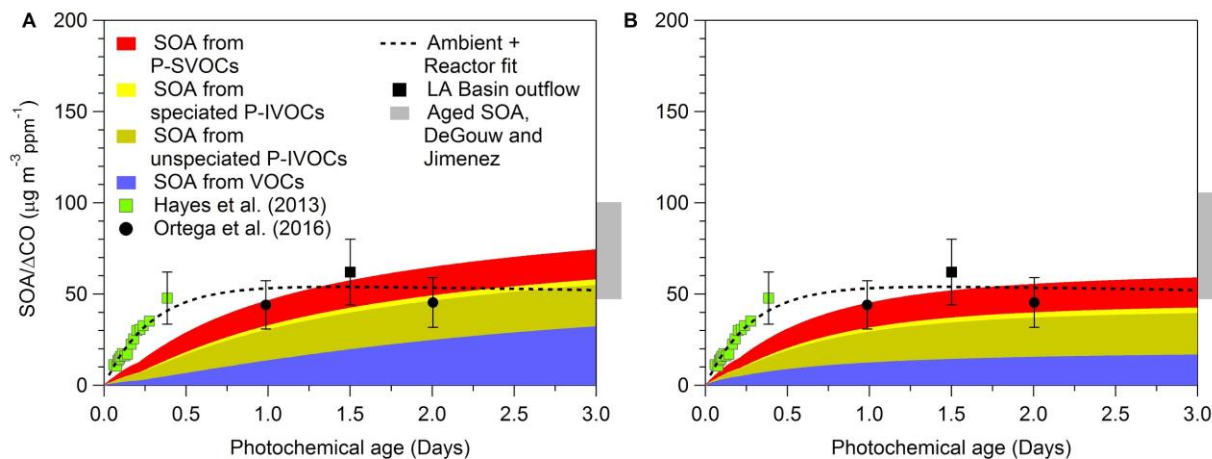
666 As suggested, we have included a right-side axis in the Fig. 5A bar graph representing the SOA mass to
667 ΔCO concentration ratios.

668 **R2.2.6** L257-258: Woody et al. (2016) proposed a meat cooking volatility distribution. Why not try this
669 one in a sensitivity test?

670 We performed a sensitivity study running the model using the meat cooking volatility distribution
671 proposed by Woody et al. (2016) as suggested by the reviewer. For ease of comparison, we include here
672 the original results obtained before the sensitivity study and taken from the submitted manuscript.



673
674 Figure 3. Predicted urban SOA mass for the C) WOR + ZHAO + TSI and F) WOR + ZHAO + MA cases with
675 the original model set-up for this work.



676
677 Figure S8. Predicted urban SOA mass for the A) WOR + ZHAO + TSI and B) WOR + ZHAO + MA cases when
678 using the meat cooking volatility distribution + reported in Woody et al. (2016).

679

680 We have added the figure above in the supporting information and the paragraph below in the
681 manuscript to summarize the findings.

682 *“Finally, Woody et al. (2016) recently proposed a meat cooking volatility distribution and*
683 *therefore we perform a sensitivity study by using this distribution in our model for P-SVOCs coming*
684 *from cooking sources. The results are displayed in the supporting information (Figure S8), where this*
685 *alternate approach has been implemented for the WOR + ZHAO + TSI and WOR + ZHAO + MA cases. By*
686 *comparing the results obtained from this sensitivity study with Fig. 3, the two cases in the sensitivity*
687 *study display a slight decrease of SOA/ Δ CO values over 3 days of photochemical aging with a*
688 *difference of approximately 8% at 3 days. Thus, the model-measurement comparison does not change*
689 *significantly relative to the base case. Given the similarities between the sensitivity study and Fig. 3,*
690 *as well as the possibility of cooking SOA sources other than meat-cooking (i.e. heated cooking oils, Liu*
691 *et al. (2017)), the remainder of our work uses the Robinson et al. volatility distribution for P-SVOCs*
692 *from cooking sources.”*

693 **R2.2.7** Can the authors clarify more directly why the model with the Worton parameters for SVOCs gives
694 more OA than that with the Robinson parameters? The volatility distribution and Fig. 2 show pretty
695 clearly that the emissions are substantially higher in volatility. Is the difference really from the added
696 7.5% mass that comes with the 1-bin aging mechanism? If that’s the case, please emphasize more
697 clearly the uncertainty in this parameter/approach to put the differences in these two model runs into
698 context.

699 We want to clarify that the difference between the results for the Worton and Robinson parameters is
700 not due to the added 7.5% mass during aging but rather the ratio of SVOC/POA at the beginning of the
701 SOA formation. We kindly refer the reviewer to the paragraph below from the submitted manuscript (p.
702 12, L439). For clarity, we have updated the text.

703 *“The more rapid SOA formation is due to the updated SVOC volatility distribution in this*
704 *model case compared to the cases that use the Robinson et al. (2007) distribution. Specifically, as*
705 *shown in Fig. 2F, there is a higher relative concentration of gas phase SVOCs in the $c^* = 10^2$ bin and*
706 *thus a higher ratio of P-SVOC to POA. Given that in the box model (and in most air quality models) the*
707 *P-SVOC emissions are determined by scaling the POA emissions according to their volatility*
708 *distribution, a higher P-SVOC to POA ratio will then result in a higher initial P-SVOCs concentration.*
709 *Furthermore, SOA formation from P-SVOCs is relatively fast. Together these changes lead to increases*
710 *in SOA formation during the first hours of photochemical aging when using the Worton et al. volatility*
711 *distribution.”*

712

713 **R2.2.8** Section 3.2 and Fig. 6: This analysis is an interesting idea but I don't think the slight differences
714 among the model cases warrant such a long-winded discussion and detailed figure. It would be enough
715 to add a comment to section 3.1 that the WOR cases give more SOA from precursors with KOH in the
716 range identified by Ortega et al. (2016). The abstract and conclusions would need to be correspondingly
717 reduced.

718 We have shortened the discussion in Section 3.2 as suggested to one paragraph. We have also reduced
719 the relevant paragraph in the conclusions.

720 **R2.2.9** L716-718 and L796-797: Why do the authors not discuss the limitations of their aging
721 mechanisms that only reduce volatility by one bin at a time? It is possible that a compound can shift
722 more than one generation in volatility upon oxidation; the more recent 2D-VBS approaches and the
723 SOM methods allow for multi-decadal shifts in volatility. Approaches like these might push the products
724 below the "oxidation-partitioning barrier" manifested when compounds are protected from gas-phase
725 oxidation.

726 We address this comment by kindly referring the reviewer to the paragraph below in the submitted
727 manuscript (p. 20, L712). We have also updated this paragraph for clarity.

728 **"With these considerations in mind, the volatility distribution of the SVOCs is somewhat**
729 **different in the model compared to the measurements. Most notably, the model does not form a**
730 **significant amount of lower volatility SOA in the 10^{-2} $\mu\text{g m}^{-3}$ bin, whereas the measurements have a**
731 **much higher concentrations in this bin. A factor that may explain this difference between the volatility**
732 **distributions is the lack of particle phase reactions that continue to transform SOA into lower volatility**
733 **products, a process which is not considered in the model. *One example of a particle phase reaction is***
734 ***the formation of SOA within deliquesced particles, including the partitioning of glyoxal to the aqueous***
735 ***phase to produce oligomers as discussed in Ervens and Volkamer (2010), although that specific***
736 ***mechanism was of little significance during CalNex (Washenfelder et al., 2011; Knote et al., 2014).***
737 ***Alternatively, the use of an aging parameterization where the volatility may decrease by more than***
738 ***one order of magnitude per oxidation reaction would also distribute some SOA mass into lower c^****
739 ***bins. Hayes et al. (2015) previously evaluated different parameters for aging. However, the results***
740 ***from this previous study showed that substantial over-prediction of SOA was observed when using the***
741 ***Grieshop et al. (2009) parameterization in which each oxidation reaction reduced volatility by two***
742 ***orders of magnitude. New parameterizations may be necessary to produce the observed SOA volatility***
743 ***and concentration simultaneously (Cappa et al. 2012). However, we note that the additional low***
744 ***volatility organic mass will not significantly change SOA predictions in urban regions where OA***
745 ***concentrations are relatively high.*"**

746

747 **R2.2.10** L760-762: How do these reaction rate constants compare to estimation methods developed for
748 the 2D-VBS? If you used those approximations (based on C* and assumed O:C) would you do better?

749 We are not sure exactly what version of the 2-D VBS the reviewer is referring to, but 2-D VBS
750 parameterizations have used a single rate constant of $4 \times 10^{-11} \text{ cm}^3 \text{ molec}^{-1} \text{ s}^{-1}$ for oxidation and aging of
751 IVOCs [Murphy et al. Atmos. Chem. Phys. 12, 10797-10816, 2012]. This rate constant is generally higher
752 than that used in our own work for the initial oxidation reaction, and thus would be expected to
753 improve the model/measurement agreement at short photochemical age. At the same time, such a
754 result is not surprising given that the rate constant used in the 2-D VBS was tuned to best match
755 laboratory and field observations. In contrast, the rate constants from our work are estimated based on
756 the precursor structure as described in the manuscript as well as in Zhao et al. (2014), and thus they are
757 better constrained. Furthermore, it should be noted that the aging rate constant used in the box model
758 for subsequent oxidation reactions is the same as that used in the reference above ($4 \times 10^{-11} \text{ cm}^3 \text{ molec}^{-1}$
759 s^{-1}).

760 Furthermore, in the statistical oxidation mode (SOM) [Cappa et al. Atmos. Chem. Phys. 12, 9505-9528,
761 2012] the reaction rates constants are parameterized using both carbon and oxygen number. When
762 comparing our rate constants in the supporting information against those summarized in Figure S1 of
763 the supporting information of Cappa et al., the rate constants are very similar. This result is not
764 surprising given that both are based on the same structure-activity relationship [Kwok and Atkinson
765 Atmos. Environ. 29, 1685-1695, 1995].

766 **Minor Changes/Typos:**

767 **R2.3.1** L48-50: This sentence should say something about how the two methods predict similar mass at
768 short to moderate photochemical ages.

769 We address to this comment by updating the sentence below in the manuscript.

770 *“The model predicts similar SOA mass at short to moderate photochemical ages when the*
771 *“aging” mechanisms or the updated version of the yields for VOC oxidation are implemented.”*

772 **R2.3.2** L82: Consider replacing “nucleate” with “form”.

773 We replace “nucleate” by “form” in the text as suggested by the reviewer.

774 **R2.3.3** L742-743: Make sure to also mention that Woody et al. (2016) cited excessive model dispersion
775 as a potential complicating factor.

776 This is an excellent suggestion and we have updated the sentence below in the manuscript.

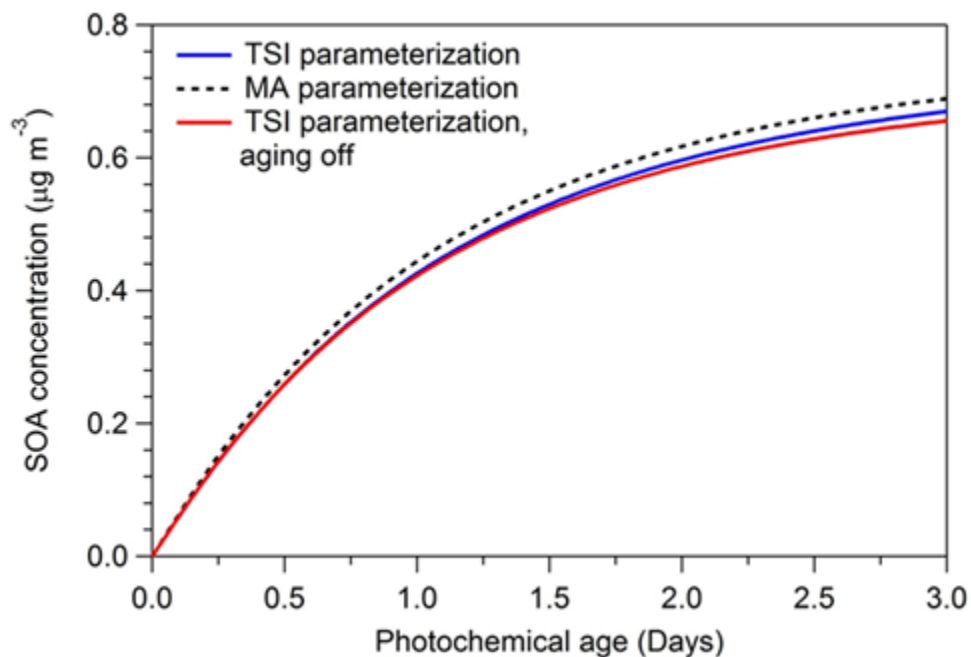
777 *“As stated in Woody et al. (2016), the higher ratio may compensate for other missing (or*
778 *underrepresented) formation pathways in SOA models or excessive dispersion of SOA in their model.”*

779

780

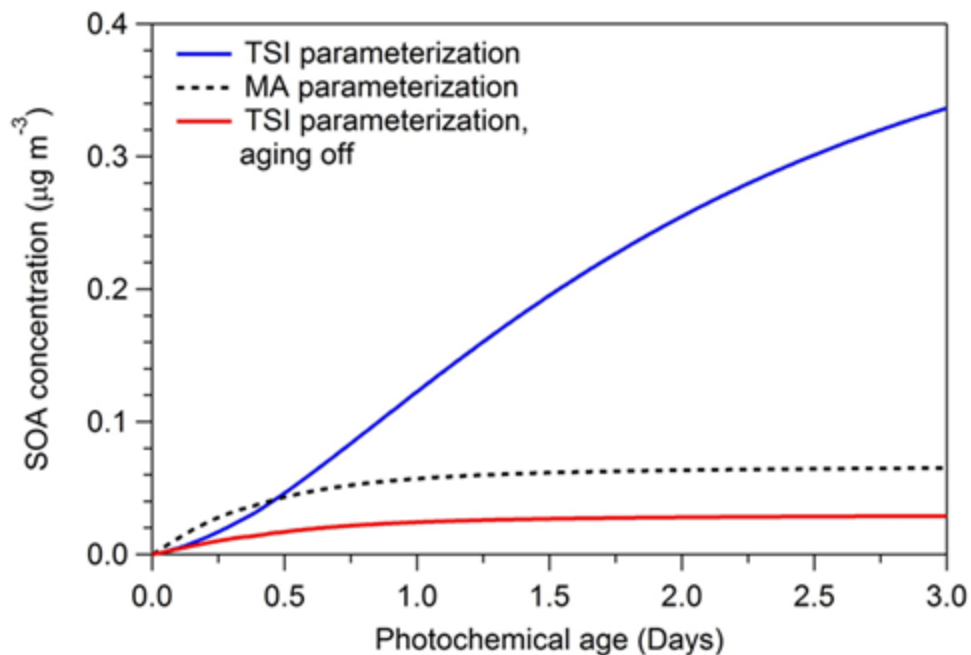
781 **R2.3.4** I recommend adding figures with SOA mass curves (not just the yields) for each of the VOC
782 product species to the supporting information, thereby visually demonstrating the effects of the upper-
783 and lower-bound yield parameterizations. It would be a good idea to assume a background
784 concentration equal to $2.1 \mu\text{g m}^{-3}$ (or greater if you just want to take an average of your total OA, model
785 wide) like in the model so that you get relevant partitioning.

786 We address this comment by adding figures with SOA mass curves for each of the VOC classes in the
787 supporting information as suggested. These figures are also displayed below.



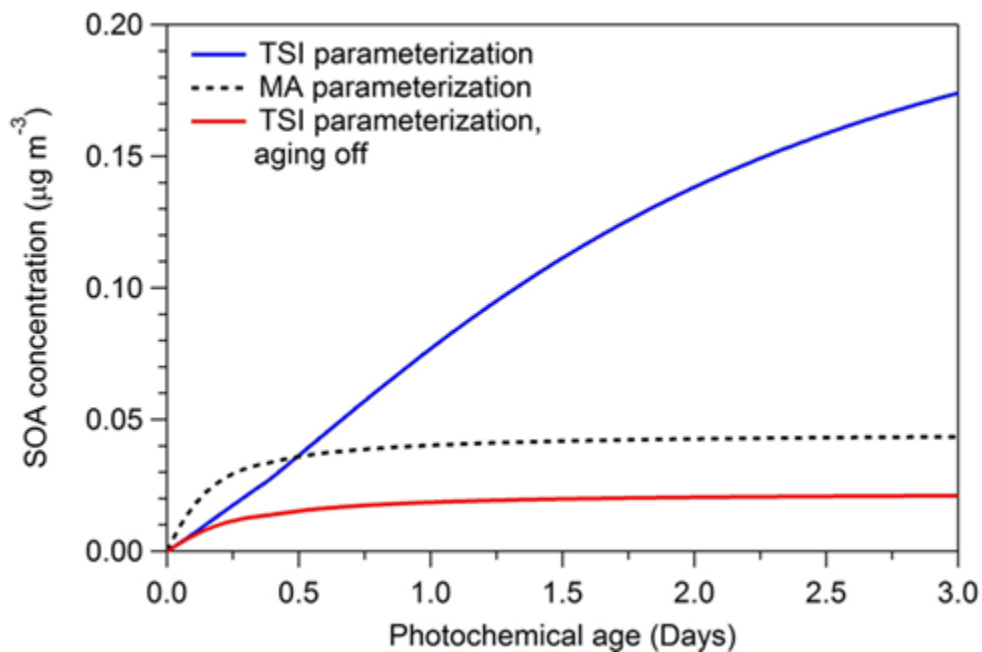
788

789 Figure S1. Predicted urban SOA mass from the alkane VOCs (Alk5) for different SOA formation
790 parameterizations.



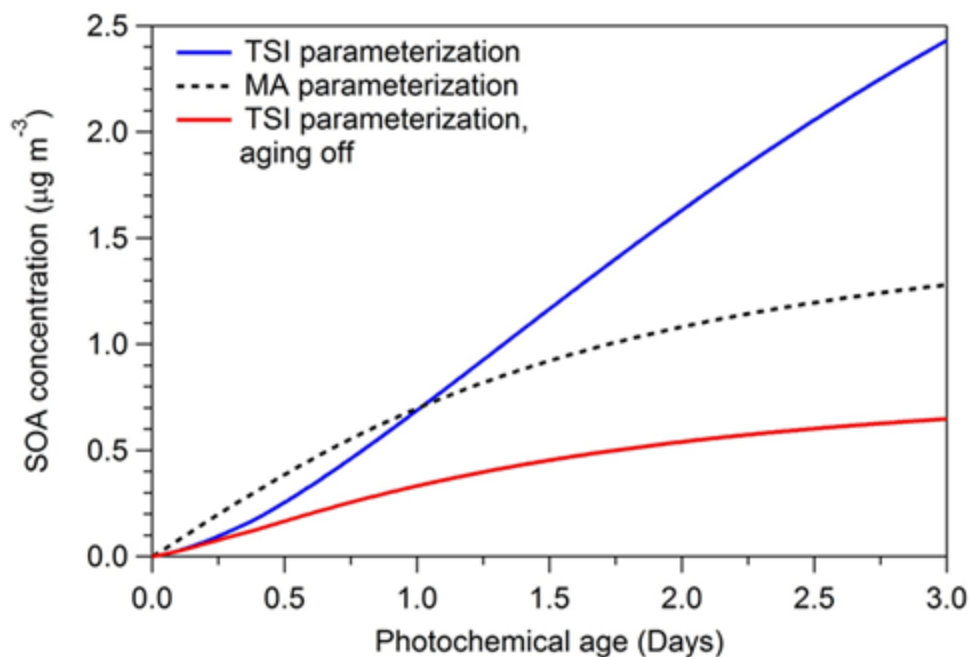
791

792 Figure S2. Predicted urban SOA mass from the olefin VOCs (Ole1) for different SOA formation
 793 parameterizations.



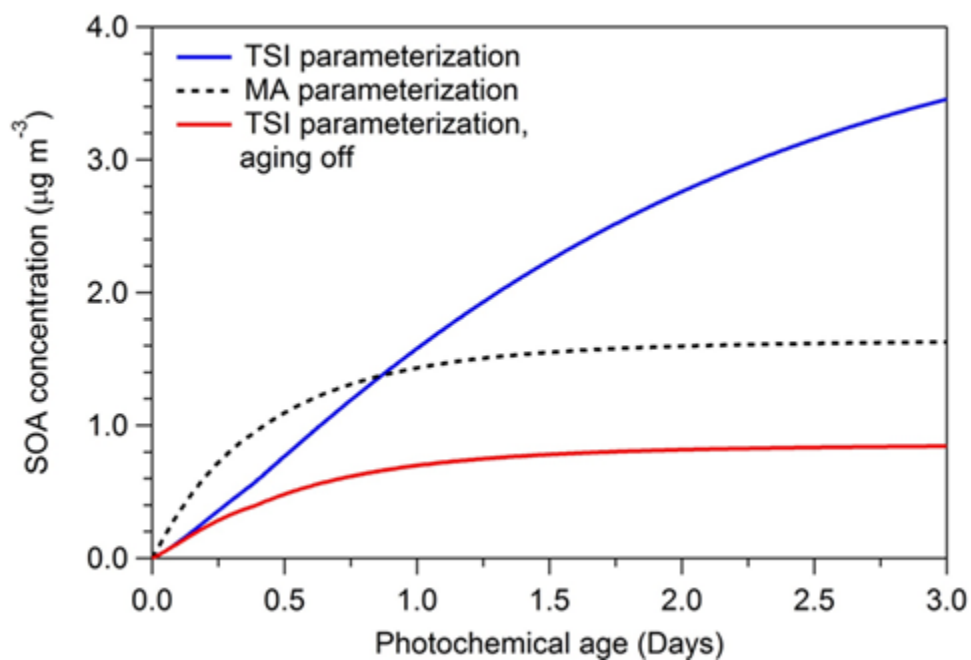
794

795 Figure S3. Predicted urban SOA mass from the olefin VOCs (Ole2) for different SOA formation
 796 parameterizations.



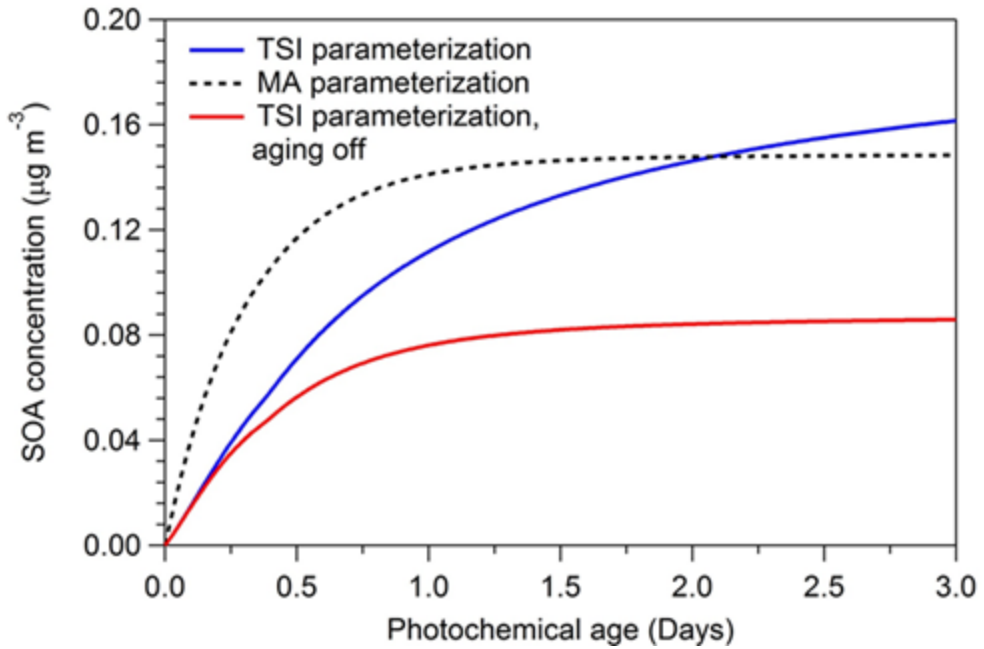
797

798 Figure S4. Predicted urban SOA mass from the aromatic VOCs (Aro1) for different SOA formation
 799 parameterizations.



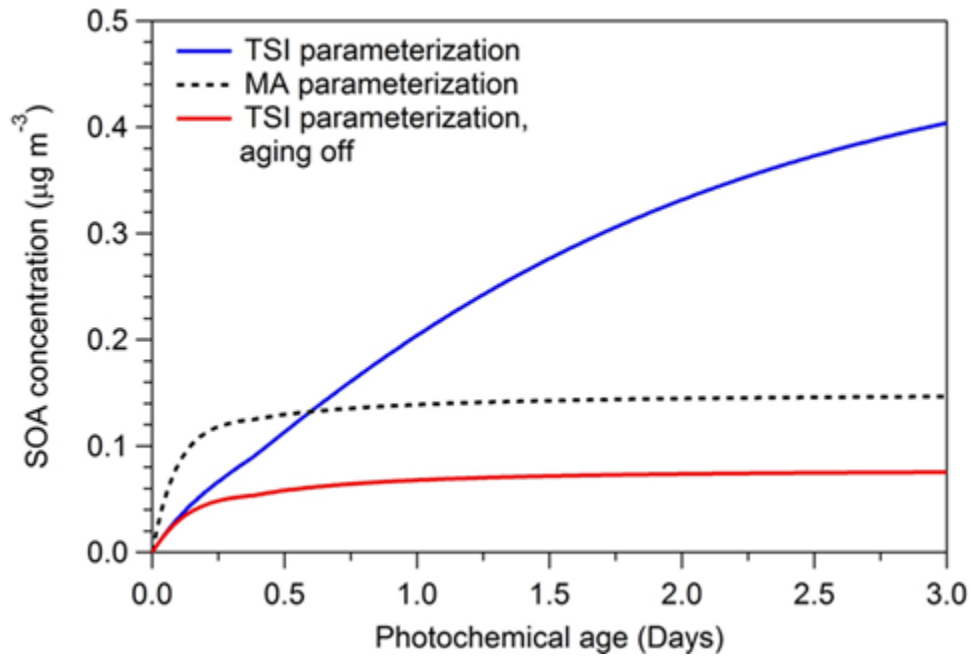
800

801 Figure S5. Predicted urban SOA mass from the aromatic VOCs (Aro2) for different SOA formation
 802 parameterizations.



803

804 Figure S6. Predicted urban SOA mass from isoprene (Isop) for different SOA formation
 805 parameterizations.



806

807 Figure S7. Predicted urban SOA mass from terpenes (Terp) for different SOA formation
 808 parameterizations.

809

810 To summarize these findings, we have added the paragraph below in the manuscript in section 2.2 and
811 include the Figures S1 to S7 in the supporting information.

812 *“Furthermore, as described in the supporting information, the updated SOA yields for VOC*
813 *oxidation result in distribution of SVOC mass into lower volatility bins compared to the original*
814 *parameterization, although the sum for the SVOC yields (α_i) remains similar. In the absence of aging,*
815 *the SOA yields, Y , resulting from the wall-loss correction should be considered upper limits (MA*
816 *parameterization), whereas the original yields serve as lower limits due to the considerations*
817 *discussed above (TSI parameterization without aging). As shown in the supporting information*
818 *(Figures S1 - S7) when aging (TSI parameterization with aging) is included the SOA yields increase*
819 *beyond those observed when applying the wall loss correction for most of the VOC classes at longer*
820 *photochemical ages (it should be noted that SOA masses in Figures S1 - S7 were calculated using the*
821 *same background as for the other model cases, $2.1 \mu\text{g m}^{-3}$). This feature of the aging parameterization*
822 *is likely to blame for SOA over-predictions observed at long aging times when comparing with*
823 *ambient data (e.g. Dzepina et al., 2011; Hayes et al., 2015).”*

824 **R2.3.5** SI, L6-22: I found the derivation of the wall-loss correction confusing. First, the quantity in
825 parentheses in equations 5 and 6 should be the reciprocal. I assume they used the correct form for the
826 calculation because I calculated the adjusted ARO2 and it would have been way off using the equation
827 as it is written. Also, [VOC] should be replaced with something more accurate like $[\Delta\text{ROG}]$ or $[\Delta\text{VOC}]$. It
828 would be helpful to explain briefly why the mass of compounds on the walls, C_w , is a function of C^*
829 alone and not C_{tot} , C_g or C_p . This is essentially a consequence of the equilibrium assumption in the
830 chamber analysis, as I understand it.

831 We have corrected equations 5 and 6. We also replace [VOC] by $[\Delta\text{VOC}]$ as suggested. We also address
832 this comment by clarifying that c_w is the equivalent organic mass concentration of the walls. The
833 notation c_w is used by Krechmer et al. (2016) and we have kept it for consistency. We add the text below
834 in the supporting information for clarity.

835 *“For clarity, c_w is the equivalent organic mass concentration of the walls, and it is an*
836 *empirically determined value. Equations 2 and 3 are the partitioning equations that describe either*
837 *the partitioning between the gas phase and walls or the gas phase and the particles, which both*
838 *depend on the volatility of the organic vapors, c^* . The significance of c_w can be understood by*
839 *comparing equations 2 and 3. In equation 3, the partitioning is dependent on the total particle phase,*
840 *c_{OA} . Similarly, the parameter c_w is the amount of mass in the chamber walls available for partitioning*
841 *expressed as an effective mass concentration based on the work of Krechmer et al. (2016). However,*
842 *the value of c_w is a function of c^* as shown in equation 1.”*

1 **Evaluating the impact of new observational constraints on P-**
2 **S/IVOC emissions, multi-generation oxidation, and chamber**
3 **wall losses on SOA modeling for Los Angeles, CA**

4

5 Prettiny K. Ma,¹ Yunliang Zhao,² Allen L. Robinson,² David R. Worton,^{3,a} Allen H.
6 Goldstein,^{3,4} Amber M. Ortega,^{5,b} Jose L. Jimenez,⁵ Peter Zotter,^{6,c} André S. H. Prévôt,⁶
7 Sönke Szidat,⁷ and Patrick L. Hayes¹

8

9 ¹Department of Chemistry, Université de Montréal, Montréal, QC, Canada

10 ²Center for Atmospheric Particle Studies, Carnegie Mellon University, Pittsburgh, PA,
11 USA

12 ³Department of Civil and Environmental Engineering, University of California, Berkeley,
13 CA, USA

14 ⁴Department of Environmental Science, Policy and Management, University of
15 California, Berkeley, CA, USA

16 ⁵Cooperative Institute for Research in the Environmental Sciences and Dept. of
17 Chemistry and Biochemistry, University of Colorado, Boulder, CO, USA

18 ⁶Laboratory of Atmospheric Chemistry, Paul Scherrer Institute, Villigen, Switzerland

19 ⁷Department of Chemistry and Biochemistry & Oeschger Centre for Climate Change,
20 University of Bern, Bern, Switzerland

21 ^anow at: Gas and Particle Metrology, National Physical Laboratory, Hampton Rd,
22 Teddington, Middlesex, UK

23 ^bnow at: Air Pollution Control Division, Colorado Department of Public Health and
24 Environment, Denver, CO, USA

25 ^cnow at: Lucerne University of Applied Sciences and Arts, School of Engineering and
26 Architecture, Bioenergy Research, Technikumstrasse 21, CH-6048 Horw, Switzerland

27 *Correspondence to:* Patrick L. Hayes (patrick.hayes@umontreal.ca)

28

29 **ABSTRACT**

30 Secondary Organic Aerosols (SOA) are important contributors to fine PM mass in
31 polluted regions, and their modeling remains poorly constrained. A box model is
32 developed that uses recently published literature parameterizations and data sets to better
33 constrain and evaluate the formation pathways and precursors of urban SOA during the
34 CalNex 2010 campaign in Los Angeles. When using the measurements of IVOCs
35 reported in Zhao et al. (2014) and of SVOCs reported in Worton et al. (2014) the model
36 is biased high at longer photochemical ages whereas at shorter photochemical ages it is
37 biased low, if the yields for VOC oxidation are not updated. The parameterizations using
38 an updated version of the yields, which takes into account the effect of gas phase wall-
39 losses in environmental chambers, show model/measurement agreement at longer
40 photochemical ages, even though some low bias at short photochemical ages still
41 remains. Furthermore, the fossil/non-fossil carbon split of urban SOA simulated by the
42 model is consistent with measurements at the Pasadena ground site.

43 Multi-generation oxidation mechanisms are often employed in SOA models to
44 increase the SOA yields derived from environmental chamber experiments in order to
45 obtain better model/measurement agreement. However, there are many uncertainties
46 associated with these “aging” mechanisms. Thus, SOA formation in the model is
47 compared against data from an oxidation flow reactor (OFR) in order to constrain SOA
48 formation at longer photochemical ages than observed in urban air. The model predicts
49 similar SOA mass at short to moderate photochemical ages when the “aging”
50 mechanisms or the updated version of the yields for VOC oxidation are implemented.
51 The latter case though has SOA formation rates that are more consistent with
52 observations from the OFR. Aging mechanisms may still play an important role in SOA
53 chemistry, but the additional mass formed by functionalization reactions during aging
54 would need to be offset by gas-phase fragmentation of SVOCs.

55 All the model cases evaluated in this work have a large majority of the urban SOA
56 (69 – 83 %) at Pasadena coming from the oxidation of P-SVOCs and P-IVOCs. The
57 importance of these two types of precursors is further supported by analyzing the
58 percentage of SOA formed at long photochemical ages (1.5 days) as a function of the
59 precursor rate constant. The P-SVOCs and P-IVOCs have rate constants that are similar
60 to highly reactive VOCs that have been previously found to strongly correlate with SOA
61 formation potential measured by the OFR.

62 Finally, the volatility distribution of the total organic mass (gas and particle
63 phase) in the model is compared against measurements. The total SVOC mass simulated
64 is similar to the measurements, but there are important differences in the measured and
65 modeled volatility distributions. A likely reason for the difference is the lack of particle-
66 phase reactions in the model that can oligomerize and/or continue to oxidize organic
67 compounds even after they partition to the particle phase.

68 1. INTRODUCTION

69 Atmospheric aerosols are important climate forcing agents (Christensen et al.,
70 2013), negatively impact human health (Dockery and Pope, 1994) and reduce visibility
71 by scattering and absorbing light (Watson, 2002). However, predicting quantitatively the
72 composition and concentrations of aerosols is challenging, in part because of their
73 complex composition and the variety of emission sources and chemical pathways that
74 contribute to aerosol loadings in the atmosphere (Heald et al., 2011; Spracklen et al.,
75 2011). Atmospheric aerosols are composed of black carbon, inorganic, and organic
76 matter, and the latter is a mixture of hundreds to thousands of compounds (Gentner et al.,
77 2012).

78 Due to this complexity, organic aerosol is often categorized into two groups.
79 Primary organic aerosol (POA) is directly emitted into the atmosphere from sources such
80 as motor vehicles, food cooking, and biomass burning (Hallquist et al., 2009). On the
81 other hand, secondary organic aerosol (SOA) is the product of diverse chemical reactions
82 occurring in the atmosphere that transform more-volatile precursors such as volatile
83 organic compounds (VOCs) into lower volatility products that are either incorporated
84 into existing particles or **form** new particles. Many previous studies have shown that SOA
85 is an important fraction of OA globally often representing more than half the total OA
86 concentration (Zhang et al., 2007; Jimenez et al., 2009).

87 In SOA parameterizations for use in regional and global models, a semi-empirical
88 approach is used in which VOCs, often the only SOA precursors considered, react with
89 OH radicals and other oxidants to form secondary products with lower volatility at a
90 given mass yield. These secondary semi-volatile organic compounds (SVOCs) can
91 partition to the particle phase to form SOA (Pankow, 1994; Odum et al., 1996; Donahue
92 et al., 2006). The parameters used in the models for the VOCs, such as the yields and
93 product volatilities, are often determined from published chambers studies (e.g. Kroll et
94 al., 2006; Chan et al., 2009; Hallquist et al., 2009; Presto et al., 2010). Over the past
95 decade a number of studies have shown that traditional models that consider only the
96 oxidation of VOCs alone predict SOA concentrations much lower than those observed in
97 polluted urban regions (Volkamer et al., 2006; Dzepina et al., 2009; Hodzic and Jimenez,
98 2011; Hayes et al., 2015). As a result, several updates have been proposed in the
99 literature to improve SOA models including new pathways for SOA formation, new SOA
100 precursors, and increased yields for known precursors (e.g. Ng et al., 2007; Robinson et
101 al., 2007; Ervens and Volkamer, 2010).

102 The volatility basis-set (VBS) approach (Donahue et al., 2006) has been used in
103 most recent parameterizations of SOA yields. In this approach, the organic mass is
104 distributed in logarithmically spaced volatility bins, and the SOA forming reactions then
105 redistribute the mass from precursors such as anthropogenic and biogenic VOCs, into

106 bins with generally lower volatility (except for fragmentation reactions) leading to
107 increased OA concentrations (Robinson et al., 2007; Tsimpidi et al., 2010). While the
108 VBS provides a valuable conceptual framework for SOA modeling, substantial
109 uncertainties remain in the correct parameters for different precursors and conditions.

110 In this paper we focus on investigating three interrelated questions that are
111 responsible for important uncertainties in urban SOA modeling. The first is how to best
112 incorporate SOA from primary semi- and intermediate volatility compounds (P-
113 S/IVOCs), two recently-proposed types of SOA precursors. While there is now ample
114 evidence that P-S/IVOCs are important contributors to SOA (Robinson et al., 2007; Zhao
115 et al., 2014; Dunmore et al., 2015; Ots et al., 2016), the emissions of these precursors as
116 well as the parameters that govern their oxidation and SOA formation are not well
117 constrained. Also, it is well known that models of SOA that incorporate P-S/IVOCs often
118 do not agree with measurements across a range of photochemical ages, although the
119 modeled SOA mass varies substantially with the parameterization used (Dzepina et al.,
120 2009; Hayes et al., 2015; Fountoukis et al., 2016; Woody et al., 2016). The second
121 question is whether losses of semi-volatile gases to the walls of environmental chambers
122 (Matsunaga and Ziemann, 2010; Krechmer et al., 2016) have resulted in low biases for
123 the yields of some or all precursors, especially VOCs, as has been recently reported
124 (Zhang et al., 2014). The third question is the appropriateness of including “aging”
125 mechanisms in the VBS parameterization of SOA from VOCs, in which the initial
126 oxidation reaction is followed by subsequent oxidation reactions of the first and later
127 generation products, with each reaction resulting in a reduction of the organic volatility
128 by, for example, an order of magnitude. These “aging” mechanisms increase VOC yields
129 to levels much higher than those observed in chamber studies since it was perceived that
130 the yields may be too low in chambers compared to the real atmosphere. The “aging”
131 mechanisms were added to chamber yields that were obtained without using aging as part
132 of the fits of the chamber data. In some model applications they improve model
133 agreement with field measurements (Ahmadov et al., 2012), while at long photochemical
134 ages they lead to model SOA formation that is substantially larger than observed (e.g.
135 Dzepina et al., 2011; Hayes et al., 2015). While the inclusion of some of these new SOA
136 precursors, updated yields, and aging can provide in some cases better agreement with
137 measurements, the relative amount of SOA formed from VOCs (V-SOA), P-IVOCs (I-
138 SOA), and P-SVOCs (S-SOA) is highly uncertain, and changes strongly depending on
139 which of the above updates are implemented in a specific model. In addition, the fact that
140 different subsets and variants of these updates can allow specific models to match SOA
141 measurements raises important questions regarding whether or not the model mechanisms
142 are representative of actual SOA forming processes in the atmosphere.

143 The notation used when discussing SOA precursors in this paper is similar to
144 Hayes et al. (2015). We differentiate VOCs, IVOCs and SVOCs by their effective

145 saturation concentration (c^*). Therefore, SVOCs and IVOCs have volatilities ranging
146 from $c^* = 10^{-2}$ to 10^2 and 10^3 to 10^6 $\mu\text{g m}^{-3}$ respectively, while VOCs are in the bins of c^*
147 $\geq 10^7$ $\mu\text{g m}^{-3}$.

148 Recently, we evaluated three parameterizations for the formation of S-SOA and I-
149 SOA using a constrained 0-D box model that represents the South Coast Air Basin during
150 the California Research at the Nexus of Air Quality and Climate Change (CalNex)
151 campaign (Hayes et al., 2015). Box models are often used to compare with ambient
152 measurements, and have been shown to be of similar usefulness or even superior to 3-D
153 models if the emissions and atmospheric transport affecting a given case study are well
154 constrained, and if the use of ratios to tracers can be used to approximately account for
155 dispersion (e.g. Volkamer et al., 2006; Dzepina et al., 2009; Hayes et al., 2015; Yuan et
156 al., 2015). A box model allows the evaluation of multiple model parameterizations either
157 previously proposed in the literature or developed from recent field and laboratory data
158 sets, as well as the performance of sensitivity studies, all of which would be difficult to
159 carry-out in more computationally demanding gridded 3-D models. There are six model
160 cases presented in this paper that are described in further detail below. Given the number
161 of model cases (including three additional model cases from Hayes et al. (2015)), it
162 would be very computationally expensive to use a 3-D model to evaluate all the cases.

163 Moreover, there are important limitations to traditional comparisons of 3-D
164 models' predicted concentrations against measurements, as for example discussed for the
165 Pasadena ground site in Woody et al. (2016). In that study, the SOA predicted by the
166 Community Multiscale Air Quality (CMAQ) model with a VBS treatment of OA is a
167 factor of 5.4 lower than the measurements during the midday peak in SOA
168 concentrations. This underestimation was attributed to several different factors. First, the
169 model photochemical age for the site was too low by a factor of 1.5. In the box model
170 presented in this current work, that problem is eliminated as the photochemical aging of
171 the urban emissions in the model is instead determined from the measured ratio of 1,2,4-
172 trimethylbenzene to benzene as described previously (Parrish et al., 2007; Hayes et al.,
173 2013). Second, it is difficult to distinguish errors due to model dispersion from those due
174 to emission inventories and photochemical age. Woody et al. (2016) conclude that
175 excessive dispersion or low emissions account for an error of about a factor of 2. Those
176 errors are also eliminated by the use of emission ratios in this work. After those errors are
177 accounted for, by analyzing the 3-D model output using similar techniques as in our box
178 model, the real under-prediction of SOA formation efficiency by a factor of 1.8 emerged,
179 compared to the initial value of 5.4 from the concentration comparisons. These errors (of
180 approximately 300%) in the interpretation of 3-D model comparisons, which are ignored
181 in most 3-D model studies, are far larger than the uncertainties due to emission ratios or
182 dispersion in our box model (about 10 - 20%), as demonstrated in section 2.4.

183 In addition, there are uncertainties in the P-S/IVOC emissions inventories used in
184 3-D models and in the methods used to estimate P-S/IVOC emissions from the traditional
185 POA inventories. In our box model, as described in further detail below, we incorporated
186 recently published field measurements of P-S/IVOCs to better constrain the concentration
187 of these species. Thus, while 3-D models are essential for simulating spatially and
188 temporally complex environments under the influence of many sources, in cases where
189 transport is relatively simple and there is a well-defined urban plume such in Pasadena
190 during the CalNex campaign, the box model is a valuable complementary or even
191 superior approach that is less susceptible to the convoluted uncertainties in 3-D models
192 discussed above. Another reason to use a box model is that it allows a direct comparison
193 against OFR measurements taken in the field (Ortega et al., 2016). The OFR provided
194 (every 20 minutes at the Pasadena ground site) a measure of SOA formation potential for
195 a photochemical age of up to two weeks. To the best of our knowledge, 3-D models have
196 not yet been adapted for comparison against OFR data. Finally, box models are more
197 widely usable by experimental groups (such as ours) due to reduced complexity, while
198 3-D models are almost exclusively used by modeling-only groups, who tend to be more
199 distant from the availability, use, and interpretation of experimental constraints. Thus the
200 use of a range of models by a range of different groups is highly beneficial to scientific
201 progress.

202 The results obtained in our previous work (Hayes et al., 2015) using a box model
203 indicated that different combinations of parameterizations could reproduce the total SOA
204 equally well even though the amounts of V-SOA, I-SOA, and S-SOA were very different.
205 In addition, the model over-predicted SOA formed at longer photochemical ages (\approx 3
206 days) when compared to observations downwind of multiple urban sites. This
207 discrepancy suggests that the ratio of P-S/IVOCs-to-POA may have been too high in the
208 parameterizations evaluated. Also, as mentioned previously and discussed in Hayes et al.
209 (2015), the implementation of aging for VOC products remains uncertain.

210 The goal of this study is to use several recently published results to better evaluate
211 and constrain the box model introduced in our previous work, and thus facilitate the
212 identification of parameterizations that can be eventually incorporated into 3-D air
213 quality models to accurately predict SOA for the right reasons. It is important to note that
214 parameterizations used in the box model are based on several published measurements
215 taken from laboratory experiments and field studies that provide more realistic
216 constraints than in previous versions and that were not available to be implemented in
217 Hayes et al. (2015). In particular, our work here improves the box model by incorporating
218 recently published measurements of P-IVOCs and P-SVOCs that allow better
219 constraining of the concentration, reactivity, yields, and volatility of these precursors
220 (Worton et al., 2014; Zhao et al., 2014). In addition, given that experiments in
221 environmental chambers may underestimate SOA yields for the VOCs due to losses of

222 semi-volatile gases to the chamber walls (Zhang et al., 2014), the SOA yields from VOCs
223 have been re-estimated using a very recent parameterization of these wall-losses
224 (Krechmer et al., 2016). The wall-loss corrected yields obtained are then used in the
225 model in a sensitivity study to evaluate the corresponding change in the modeled SOA
226 concentrations. The model is modified based on these literature constraints. No model
227 tuning is performed with the goal of improving the agreement with the observations. The
228 results obtained from the new box model are compared against ambient ground site and
229 airborne measurements, and also against recently-published oxidation flow reactor (OFR)
230 measurements (Ortega et al., 2016). This combination of data sets allows the model to be
231 evaluated for photochemical ages ranging up to 3 equivalent days (at 1.5×10^6 molec OH
232 cm^{-3}) providing a means to evaluate the aging mechanisms of the VOCs in the VBS.

233 **2. EXPERIMENTAL SECTION**

234 **2.1 Measurement and sampling site**

235 The box model is constructed in order to represent the South Coast Air Basin
236 during CalNex in spring/summer 2010. The measurements of aerosols used in this study
237 were conducted in Pasadena, California (34.1406° N 118.1224° W), located to the
238 northeast of downtown Los Angeles (Hayes et al., 2015). An overview of CalNex has
239 been published previously (Ryerson et al., 2013). The location and the meteorology of the
240 ground site at Pasadena are described in further detail in Hayes et al. (2013). Pasadena is
241 a receptor site for pollution due to winds that transport emissions from the Ports of Los
242 Angeles and Long Beach and downtown Los Angeles. Airborne measurements of
243 aerosols were also carried out in the South Coast Air Basin as part of the CalNex project.
244 A detailed description of the airborne measurements is given in Bahreini et al. (2012).
245 Furthermore, measurements of POA composition and volatility taken at the Caldecott
246 Tunnel in the San Francisco Bay Area reported in previous work (Worton et al., 2014)
247 are also used to constrain the model as described below. The tunnel air samples were
248 collected during July 2010.

249 Two additional datasets are used to evaluate the model. In addition to sampling
250 ambient air, an aerosol mass spectrometer (AMS) sampled air that had been
251 photochemically aged using an oxidation flow reactor (OFR) (Ortega et al., 2016). The
252 OFR exposed ambient air to varying concentrations OH radicals in order to obtain
253 photochemical ages much higher than the ambient levels observed at the Pasadena site,
254 and the amount of SOA produced was quantified as a function of OH exposure.
255 Moreover, radiocarbon (^{14}C) analysis has been performed on filter samples and results
256 were combined with positive matrix factorization (PMF) data to determine fossil and
257 non-fossil fractions of the SOA components as reported in Zotter et al. (2014). The ^{14}C

258 results are used for subsequent comparison against the box model from which fossil and
259 non-fossil SOA mass can be estimated.

260 **2.2 Model set-up**

261 The SOA model is set-up to include 3 types of precursors: VOCs, P-IVOCs, and
262 P-SVOCs. The parameters used in the box model to simulate the formation of SOA from
263 these precursors are listed in Tables S1 to S3 of the supporting information. The box
264 model dynamically calculates the evolution of organic species in an air parcel as it
265 undergoes photochemical aging, hence producing SOA. The total SOA also includes
266 background SOA (BG-SOA) at a constant concentration of $2.1 \mu\text{g m}^{-3}$, as determined in
267 our previous work (Hayes et al., 2015). The model accounts for P-SVOC emissions from
268 vehicular exhaust and cooking and treats POA as semi-volatile (Robinson et al., 2007). **It**
269 **should be noted that the model uses CO and NO_x as inputs to constrain the model, and the**
270 **SOA yields for high-NO_x conditions are used, based on our previous work (Hayes et al.,**
271 **2013; 2015). Therefore, to verify model performance both predictions of VOC and POA**
272 **concentrations have been compared against field measurements and the model**
273 **performance appears to be satisfactory (Hayes et al., 2015).**

274 A schematic of the model is shown in Figure 1. All the model cases are listed in
275 Table 1, and all the parameterizations are shown schematically in Figure 2. The first
276 model case (ROB + TSI) incorporates the Robinson et al. (2007) parameterization for
277 SOA formation that models P-IVOCs and P-SVOCs (i.e. P-S/IVOCs) using a single
278 volatility distribution and oxidation rate constant. The ROB + TSI case also uses the
279 Tsimpidi et al. (2010) parameterization for SOA formation from VOCs. A detailed
280 description of the parameters used in ROB + TSI can be found in Hayes et al. (2015), and
281 the ROB + TSI model case used here is identical to the case of the same name used in
282 that paper. Briefly, as displayed in Fig. 2A, the Tsimpidi et al. (2010) parameterization
283 proposes that the VOCs undergo an initial oxidation step that will form four lumped
284 products with different volatilities ($c^* = 1, 10^1, 10^2, 10^3 \mu\text{g m}^{-3}$, where c^* is the effective
285 saturation concentration). The first-generation oxidation products can be further oxidized,
286 decreasing their volatility by one order of magnitude (i.e. aging). This “bin-hopping”
287 mechanism repeats until the lowest volatility product is reached ($c^* = 10^{-1} \mu\text{g m}^{-3}$ in this
288 study and $1 \mu\text{g m}^{-3}$ in other studies such as Tsimpidi et al. (2010) and Hayes et al. (2015).
289 The Robinson et al. (2007) parameterization proposes that the P-S/IVOCs are initially
290 distributed in logarithmically spaced volatility bins ranging from $c^* = 10^{-2}$ to $10^6 \mu\text{g m}^{-3}$.
291 Thereafter, the oxidation of P-S/IVOCs decreases their volatility by one order of
292 magnitude until the lowest volatility product is reached ($c^* = 10^{-2} \mu\text{g m}^{-3}$). The lowest
293 volatility product possible is not the same for the oxidation of VOCs versus the oxidation
294 of the P-S/IVOCs (10^{-1} vs. $10^{-2} \mu\text{g m}^{-3}$, respectively). However, whether the mass is

295 distributed into either bin has a negligible effect on the SOA mass simulated in the box
296 model because of the relatively high SOA concentrations during the case study.

297 In this work, 5 model parameterizations are tested that incorporate new
298 measurements of IVOCs and P-SVOC volatility as well as updated VOC yields that
299 account for wall-losses of vapors (Zhang et al., 2014; Krechmer et al., 2016). For the first
300 new case (ROB + ZHAO + TSI), we incorporate IVOC data measured in Pasadena
301 during the CalNex campaign as reported from Zhao et al. (2014). In particular, the
302 measured concentrations of speciated and unspeciated IVOCs and their estimated
303 volatility are used to constrain the initial concentration of these species (as discussed in
304 Section 2.2.2 below) as well as to estimate their yields (Zhao et al., 2014). Therefore, we
305 replace the inferred concentrations of IVOCs that were used in our previous work and
306 based on the volatility distribution of Robinson et al. (2007) with concentrations that are
307 directly constrained by measurements. In the ROB + ZHAO + TSI case the SOA
308 formation parameters used (e.g. yields, oxidation rate constants) are taken from Zhao et
309 al. (2014) for the IVOCs and from Hayes et al. (2015) for the VOCs and SVOCs.
310 Hodzic et al. (2016) have also estimated the IVOC yields while accounting for wall-
311 losses using recent laboratory studies. However, the yields reported in that study are for a
312 single lumped species, whereas in our work we estimate the yields using 40 IVOC
313 categories, each representing a single compound or a group of compounds of similar
314 structure and volatility. This method allows a more precise representation of IVOC yields
315 and rate constants in the SOA model.

316 For the second new case (WOR + ZHAO + TSI), the volatility distribution of P-
317 SVOCs is updated using measurements of POA performed at the Caldecott tunnel in the
318 California Bay Area (Worton et al., 2014). In the previous two cases described above, the
319 relative volatility distribution of P-SVOCs was taken from the work of Robinson et al.
320 (2007). In this distribution, the relative concentration of SVOCs increases monotonically
321 between the $c^* = 10^{-2}$ and $10^2 \mu\text{g m}^{-3}$ bins. The P-SVOC volatility distribution in the
322 WOR + ZHAO + TSI case increases monotonically as well, but the relative
323 concentrations in each bin are different and notably there is a much higher relative
324 concentration of SVOCs in the $c^* = 10^2 \mu\text{g m}^{-3}$ bin (see Fig. 2 and Table S3 in the
325 supporting information). In this model case, the updated P-SVOC volatility distribution is
326 only applied to vehicular P-S/IVOCs whereas the volatility distribution proposed by
327 Robinson et al. (2007) is still used for cooking emissions.

328 Several recently published papers have found that chamber experiments may
329 underestimate SOA yields due to the loss of semi-volatile vapors to chamber walls
330 (Matsunaga and Ziemann, 2010; Zhang et al., 2014; Krechmer et al., 2016). A sensitivity
331 study has been performed to explore this uncertainty by running the three model cases
332 described above (ROB + TSI, ROB + ZHAO + TSI, and WOR + ZHAO + TSI) with a

333 revised version of the SOA yields for VOCs that accounts for these wall losses. A
334 detailed description of how these updated yields were estimated is provided in the
335 supporting information and the values can be found in Table S4. Briefly, equilibrium
336 partitioning is assumed to hold for the organic mass found in the gas phase, particle
337 phase, or chamber walls. The SOA yields are then obtained by refitting SOA chamber
338 yield curves using a model that accounts for partitioning between the three compartments
339 (particle, gas, and wall) and incorporates the equivalent wall mass concentrations
340 published in Krechmer et al. (2016), which are volatility dependent. The SOA chamber
341 yield curves that were refitted were first calculated using the parameters published in
342 Tsimpidi et al. (2010). There are limits to the assumption that partitioning between the
343 three phases occurs on short enough timescales for all four VOC product volatilities that
344 equilibrium is reached during an SOA chamber study. Specifically, at lower volatilities
345 ($c^* \leq 1 \mu\text{g m}^{-3}$), the partitioning kinetics of the organic mass from the particles to the
346 chamber walls have an effective timescale of more than an hour, which is similar or
347 longer than typical chamber experiments (Ye et al., 2016). The limiting step in the
348 partitioning kinetics is evaporation of SVOCs from the particles to the gas phase, and
349 therefore the exact rate of evaporation depends on the OA concentration in the chamber.

350 Furthermore, as described in the supporting information, the updated SOA yields
351 for VOC oxidation result in distribution of SVOC mass into lower volatility bins
352 compared to the original parameterization, although the sum for the SVOC yields (α_i)
353 remains similar. In the absence of aging, the SOA yields, Y , resulting from the wall-loss
354 correction should be considered upper limits (MA parameterization), whereas the original
355 yields serve as lower limits due to the considerations discussed above (TSI
356 parameterization without aging). As shown in the supporting information (Figures S1 -
357 S7) when aging (TSI parameterization with aging) is included the SOA yields increase
358 beyond those observed when applying the wall loss correction for most of the VOC
359 classes at longer photochemical ages. (It should be noted that SOA masses in Figures S1 -
360 S7 were calculated using the same background as for the other model cases, $2.1 \mu\text{g m}^{-3}$.)
361 This feature of the aging parameterization is likely to blame for SOA over-predictions
362 observed at long aging times when comparing with ambient data (e.g. Dzepina et al.,
363 2009; Hayes et al., 2015).

364 According to Krechmer et al. (2016) and other chamber experiments (Matsunaga
365 and Ziemann, 2010), the gas-wall equilibrium timescale doesn't vary strongly with the
366 chamber size. The timescale for gas-wall equilibrium reported in these previous studies
367 was 7 - 13 minutes. Similar timescales have been calculated for a variety of
368 environmental chambers, including chambers that were used to determine many of the
369 yields used in this paper. In addition, Matsunaga and Ziemann found that partitioning was
370 nearly independent of chamber treatment, reversible, and obeyed Henry's law. Thus, the

371 effective wall concentrations determined from the chamber experiments reported in
372 Krechmer et al. (2016) are likely applicable to other chambers with different sizes.

373 The three model cases accounting for wall losses of organic vapors are named
374 ROB + MA, ROB + ZHAO + MA, and WOR + ZHAO + MA. For these cases, the aging
375 of the secondary SVOCs formed from the oxidation of VOCs was not included, since
376 multi-generation oxidation is not well-constrained using data from chamber studies that
377 are run over relatively short time-scales (i.e. hours). In addition, aging and correcting for
378 wall-losses of organic vapors have been separately proposed to close the gap between
379 observed and predicted SOA concentration from pre-2007 models, and are thought to
380 represent the same “missing SOA mass.” Therefore, we run the model with one of these
381 options at a time, as they are conceptually different representations of the same
382 phenomenology. The aging of secondary SVOCs formed from the oxidation of P-IVOCs
383 (and P-SVOCs) has been kept for all of the MA cases, however. To our knowledge, P-
384 IVOC and P-SVOC mechanisms proposed in the literature have always included aging. A
385 similar approach for correcting the yields as described above cannot be applied to P-
386 IVOCs because organics with low volatilities ($c^* < 10 \mu\text{g m}^{-3}$) will partition to chamber
387 walls very slowly, and SVOCs from P-IVOC oxidation tend to have lower volatilities
388 than the SVOCs formed from VOC oxidation (Tables S1 and S2). Indeed, when trying to
389 refit the VOC and IVOC yield curves, the model assuming equilibrium partitioning
390 between particles, the gas phase, and the walls was able to reproduce the yield curves for
391 VOCs, but not for IVOCs. This difference in the results is consistent with equilibrium not
392 having been reached during the chamber studies on the IVOCs, which produce a greater
393 amount of lower volatility SVOCs when compared to VOCs during oxidation. These
394 lower volatility SVOCs have relatively slow evaporation rates from the particles, which
395 prevents the chamber system from reaching equilibrium (Ye et al., 2016).

396 Simulations of O:C have been previously evaluated in Hayes et al. (2015) using
397 laboratory and field data from CalNex to constrain the predicted O:C. It was concluded in
398 that work that it was not possible to identify one parameterization that performed better
399 than the other parameterizations evaluated, because of the lack of constraints on the
400 different parameters used (e.g. oxidation rate constant, oxygen mass in the initial
401 generation of products and that added in later oxidation generations, SOA yields, and
402 emissions). Therefore, incorporating O:C predictions into the current box model and
403 using those results in the evaluation discussed here would not provide useful additional
404 constraints.

405 2.2.1 IVOC oxidation parameterizations

406 An important difference between the ROB + TSI and ROB + MA cases and the
407 other four cases that have been updated with the IVOC measurements of Zhao et al.
408 (2014) is that in the ZHAO cases, the first generation of IVOC oxidation distributes part

409 of the product mass into four different volatility bins ($c^* = 10^{-1}, 1, 10^1, 10^2 \mu\text{g m}^{-3}$) as is
410 displayed in Fig. 2E. This IVOC oxidation scheme is similar to that used for the first step
411 of VOC oxidation (Tsimplidi et al., 2010) as displayed in Fig. 2A and D, and has been
412 used to model chamber measurements of SOA from IVOCs (Presto et al., 2010).
413 Contrastingly, in the ROB + TSI and ROB + MA cases, a “bin-hopping” approach is used
414 for all P-S/IVOCs where oxidation lowers volatility by only one order of magnitude (see
415 Fig. 2B and C). The Robinson et al. (2007) parameters are still used for the formation of
416 SOA from P-SVOCs in the ROB + ZHAO + TSI and ROB + ZHAO + MA cases, but the
417 parameters are only applied to primary emissions in c^* bins between 10^{-2} and $10^2 \mu\text{g m}^{-3}$
418 inclusive (i.e. the volatilities corresponding to P-SVOCs).

419 **2.2.2. Determination of initial precursor concentrations**

420 In the ROB + TSI and ROB + MA cases, the initial concentration of P-S/IVOCs is
421 estimated as follows. The volatility distribution determined by Robinson et al. (2007) is
422 assumed to represent all P-S/IVOCs emitted (Dzepina et al., 2009). The total
423 concentration of P-S/IVOCs is then set so that the amount of P-S/IVOCs in the particle
424 phase is equal to the initial POA concentration. The initial POA concentration is
425 determined from the product of the background-subtracted CO concentration and the
426 $\Delta\text{POA}/\Delta\text{CO}$ emission ratio (Hayes et al., 2015). While this ratio may change due to
427 evaporation/condensation or photochemical oxidation of POA, our previous work (Hayes
428 et al., 2013) has shown that $\Delta\text{POA}/\Delta\text{CO}$ does not change significantly at the Pasadena
429 ground site with observed photochemical age indicating that the ratio is insensitive to the
430 extent of photochemical oxidation. Furthermore, it was calculated that the ratio would
431 increase by 28% for an increase of OA concentration from 5 to $15 \mu\text{g m}^{-3}$, concentrations
432 that are representative of this study. This possible source of error is substantially smaller
433 than current errors suggested for P-S/IVOC emission inventories in 3-D models, where
434 current schemes are based on scaling POA emission inventories with scaling factors that
435 are not well constrained (Woody et al., 2016). The same method is used for the other four
436 model cases, but only the initial concentration of P-SVOCs is estimated by this method
437 and the initial concentration of P-IVOCs is estimated separately as described in the next
438 paragraph. In addition, in the WOR + ZHAO + TSI and WOR + ZHAO + MA cases the
439 volatility distribution of vehicular P-SVOCs reported in Worton et al. (2014) is used for
440 estimating the initial concentration of vehicular P-SVOCs whereas the volatility
441 distribution of Robinson et al. (2007) is used for estimating the initial concentration of
442 cooking P-SVOCs.

443 It should be noted that the tunnel measurements do not include emissions due to
444 cold starts of vehicles. In the box model, only the relative volatility distribution of
445 vehicular POA measured during the tunnel study is used, and thus this potential source of
446 error does not apply to the total amount of vehicular POA emissions in the model.

447 However, it is still possible that the volatility distribution of POA is different during cold-
448 starts compared to that of POA emitted from warm-running engines. To our knowledge,
449 measurements of the volatility distribution of POA during cold-starts are not available at
450 this time. By comparing the SOA model results using two different POA volatility
451 distributions (Robinson et al., 2007; Worton et al., 2014), we can evaluate to a certain
452 extent the sensitivity of the simulated SOA concentration to the initial POA volatility
453 distribution.

454 The initial concentrations of VOCs and IVOCs are calculated by multiplying the
455 background-subtracted CO concentrations measured at Pasadena by the emission ratios
456 $\Delta\text{VOC}/\Delta\text{CO}$ or $\Delta\text{IVOC}/\Delta\text{CO}$. In the ROB + TSI and ROB + MA cases this method is
457 only applied to the VOCs. The initialization method for the concentrations of the VOCs
458 is the same for all six cases in this paper. For the biogenic VOCs, we follow the same
459 method as Hayes et al. (2015) to determine the initial concentrations since these
460 compounds are not co-emitted with CO. The emission ratios are taken from the literature
461 when available (Warneke et al., 2007; Borbon et al., 2013). For most of the IVOCs and
462 some VOCs, emission ratios are not available in the literature. The ratios are instead
463 determined by performing linear regression analyses on scatter plots of the IVOC or
464 VOC and CO concentrations measured in Pasadena between 00:00-06:00 local time when
465 the amount of photochemical aging was very low. During the regression analyses the x-
466 intercept was fixed at 105 ppbv CO to account for the background concentration of CO
467 determined in our previous work (Hayes et al., 2013). Thus, the slope of the resulting line
468 corresponds to the estimated emission ratio ($\Delta\text{IVOC}/\Delta\text{CO}$).

469 It should be noted that the use of VOC emission ratios to CO to estimate VOC
470 emissions does not assume that VOCs are always co-emitted with CO. Rather, it assumes
471 that VOC emission sources are individually small and finely dispersed in an urban area,
472 so that they are spatially intermingled with the sources of CO. Moreover, previous studies
473 have measured the emission ratios of anthropogenic VOCs with respect to CO and the
474 results show that vehicle exhaust is a major source of VOC and CO (Warneke et al.,
475 2007; Borbon et al., 2013). Furthermore, the ratios are consistent both temporally and
476 spatially. Thus, when thinking of the entire urban area as a source, the use of emission
477 ratios to CO is justified. As shown in Hayes et al. (2015) in the supporting information,
478 the modeled VOC concentrations are consistent with the measurements indicating that
479 major VOCs sources have not been omitted, and the smooth time variations of the VOC
480 concentrations support the use of a “global urban source”.

481 **2.3 SOA model**

482 The VOC yields are taken from Tsimpidi et al. (2010) or determined in this work
483 as described below. The estimation of the IVOC yields (based on values taken from
484 Presto et al. (2010) and of the OH reaction rate constants for IVOCs follows the same

485 approach used by Zhao et al. (2014). However, instead of using the total SOA yield, Y ,
486 for a fixed OA concentration as reported in Zhao et al. (2014), we use the SVOC yield, α ,
487 of each c^* bin. It is important to note here that the SOA yields taken from Tsimpidi et al.
488 and Presto et al. use a four-product basis set with $c^* = 10^0, 10^1, 10^2, 10^3 \mu\text{g m}^{-3}$ and $c^* =$
489 $10^{-1}, 10^0, 10^1, 10^2 \mu\text{g m}^{-3}$ respectively. For this box model, it is more appropriate to have
490 a uniform VBS in terms of the bin range utilised so a bin with a lower volatility ($c^* = 10^{-1}$
491 $\mu\text{g m}^{-3}$) has been added to the VBS distribution of Tsimpidi et al. (2010). The yield for
492 bin $c^* = 10^{-1} \mu\text{g m}^{-3}$ is 0 for VOC oxidation, but when aging occurs mass can be
493 transferred into this bin. However, the change in the total V-SOA mass is negligible
494 because for both bin $c^* = 10^{-1}$ and $10^0 \mu\text{g m}^{-3}$ the secondary products almost completely
495 partition to the particle phase.

496 The OH reaction rate constants are taken from the literature (Atkinson and Arey,
497 2003; Carter, 2010) as described previously in Hayes et al. (2015). During aging, the
498 oxidation products undergo subsequent reactions with OH radicals with a reaction rate
499 constant of $1 \times 10^{-11} \text{ cm}^3 \text{ molec}^{-1} \text{ s}^{-1}$ and $4 \times 10^{-11} \text{ cm}^3 \text{ molec}^{-1} \text{ s}^{-1}$ for the products of
500 VOC oxidation and P-S/IVOC oxidation respectively (Hayes et al., 2015). For each
501 oxidation step during aging, there is a mass increase of 7.5 % due to added oxygen.

502 The gas-particle partitioning is calculated in each bin by using the reformulation
503 of Pankow theory by Donahue et al. (2006).

$$x_{p,i} = \left(1 + \frac{C_i}{C_{OA}}\right)^{-1}; C_{OA} = \sum_i [\text{SVOC}]_i x_{p,i}$$

504 Where $\chi_{p,i}$ is the particle phase fraction of lumped species i (expressed as a mass
505 fraction); C_i is the effective saturation concentration, and C_{OA} is the total mass of organic
506 aerosol available for partitioning (in $\mu\text{g m}^{-3}$). Only species in the gas phase are allowed to
507 react with OH radicals in the model, since aerosol species react at much lower rates
508 (Donahue et al., 2013).

509 The simulated SOA mass from the model is compared against field measurements
510 of aerosol composition including results from PMF analysis of aerosol mass spectrometry
511 data (Hayes et al., 2013; 2015). Specifically, the model predictions of urban SOA (i.e.
512 SOA formed within the South Coast Air Basin) are compared against the semi-volatile
513 oxygenated organic aerosol (SV-OOA) concentration from the PMF analysis. The other
514 OA component also attributed to SOA, low-volatility oxygenated organic aerosol (LV-
515 OOA), is primarily from precursors emitted outside the South Coast Air Basin and is
516 used to estimate the background secondary organic aerosol (BG-SOA) as discussed
517 previously (Hayes et al., 2015).

518

519

520

521 **2.4 Correction for changes in partitioning due to emissions into a** 522 **shallower boundary layer upwind of Pasadena**

523 As described in Hayes et al. (2015), during the transport of the pollutants to
524 Pasadena, the planetary boundary layer (PBL) heights increase during the day. Using CO
525 as a conservative tracer of emissions does not account for how the shallow boundary
526 layer over Los Angeles in the morning influences gas-particle partitioning due to lower
527 vertical mixing and higher absolute POA and SOA concentrations at that time. Thus, as
528 shown in the gas-particle partitioning equation above, there will be a higher partitioning
529 of the species to the particle phase and less gas-phase oxidation of primary and secondary
530 SVOCs. Later in the morning and into the afternoon the PBL height increases (Hayes et
531 al., 2013) diluting the POA and urban SOA mass as photochemical ages increases.
532 However this is a relatively small effect as the partitioning calculation in the SOA model
533 is relatively insensitive to this effect and the absolute OA concentrations (Dzepina et al.,
534 2009; Hayes et al., 2015). Our previous work (Hayes et al., 2015) found in a sensitivity
535 study a +4/-12% variation in predicted urban SOA when various limiting cases were
536 explored for simulation of the PBL (e.g. immediate dilution to the maximum PBL height
537 measured in Pasadena versus a gradual increase during the morning).

538 To account for the effect of absolute OA mass on the partitioning calculation, the
539 absolute partitioning mass is corrected using the following method. A PBL height of
540 345 m is used for a photochemical age of 0 h and it reaches a height 855 m at a
541 photochemical age of 9.2 h, which is the maximum age for the ambient field data.
542 Between the two points, the PBL is assumed to increase linearly. The boundary layer
543 heights are determined using ceilometer measurements from Pasadena at 6:00 - 9:00 and
544 12:00 - 15:00 local time, respectively (Hayes et al., 2013). The second period is chosen
545 because it corresponds to when the maximum photochemical age is observed at the site.
546 The first period is chosen based on transport times calculated for the plume from
547 downtown Los Angeles (Washenfelder et al., 2011) that arrives in Pasadena during the
548 afternoon. There are certain limitations to this correction for the partitioning calculation.
549 First, the correction is based on a conceptual framework in which a plume is emitted and
550 then transported to Pasadena without further addition of POA or SOA precursors. A
551 second limitation is that we do not account for further dilution that may occur as the
552 plume is advected downwind of Pasadena. However, such dilution is not pertinent to the
553 OFR measurements, and so for photochemical ages beyond ambient levels observed at
554 Pasadena, we focus our analysis on the comparison with the OFR measurements.

555

556 3. RESULTS AND DISCUSSION

557 3.1 Evolution of SOA concentration over 3 days

558 We follow an approach similar to Hayes et al. (2015) in order to analyse the
559 model results. The model SOA concentration is normalized to the background subtracted
560 CO concentration to account for dilution, and the ratio is then plotted against
561 photochemical age rather than time to remove variations due to diurnal cycles of
562 precursor and oxidant concentrations. The photochemical age is calculated at a reference
563 OH radical concentration of 1.5×10^6 molec cm^{-3} (DeCarlo et al., 2010). Figure 3 shows
564 this analysis for each model case for up to 3 days of photochemical aging. Since
565 fragmentation and dry deposition are not included in the model, it has only been run to 3
566 days in order to minimize the importance of these processes with respect to SOA
567 concentrations (Ortega et al., 2016). Nevertheless, it is very likely that gas-phase
568 fragmentation of SVOCs (e.g. branching between functionalization and fragmentation)
569 occurs during oxidative aging over these photochemical ages as is discussed in further
570 detail below.

571 In each panel of Fig. 3, field measurements are included for comparison. The
572 ambient urban SOA mass at the Pasadena ground site is generally measured under
573 conditions corresponding to photochemical ages of 0.5 days or less (Hayes et al., 2013).
574 The airborne observations of SOA in the Los Angeles basin outflow are also shown as
575 the average of all data between 1 and 2 days of photochemical aging (Bahreini et al.,
576 2012). The gray region on the right serves as an estimate for very aged urban SOA based
577 on data reported by de Gouw and Jimenez (2009). The data from the OFR and a fit of the
578 ambient and reactor data (dotted black line) are also displayed in Fig. 3 (Ortega et al.,
579 2016). In addition, Figure 4 shows the ratio of modeled-to-measured SOA mass on a
580 logarithmic axis to facilitate evaluation of model performance.

581 As displayed in the graphs for Fig. 3, it should be noted the measurements from
582 the OFR (Ortega et al., 2016) and from the NOAA P3 research aircraft (Bahreini et al.,
583 2012) give quite similar results for SOA/ Δ CO. The OFR measurements are not affected
584 by particle deposition that would occur in the atmosphere at long timescales or
585 photochemical ages. Only a few percent of the particles are lost to the walls of the
586 reactor, and this process has been corrected for already in the results of Ortega et al. The
587 similarity in the two types of observations suggests that ambient particle deposition and
588 plume dispersion do not significantly change the SOA/ Δ CO ratio over the photochemical
589 ages analyzed here.

590 In ROB + TSI, as described in previous work (Hayes et al., 2015), there is a large
591 over-prediction of SOA mass at longer photochemical ages. As displayed in Fig. 3, the
592 amount of SOA produced in the model is higher than all of the field measurements taken

593 at a photochemical age longer than 0.5 days. Moreover, the ratios of model to
594 measurement are higher than the upper limit of the gray bar representing the ratios within
595 the measurement uncertainties. There is an agreement with the measurements at moderate
596 photochemical ages (between 0.25 and 0.50 days), but the SOA mass simulated by the
597 model is slightly lower than the measurements at the shortest photochemical ages (less
598 than 0.25 days) even when accounting for measurement uncertainties. In this
599 parameterization, most of the SOA produced comes from the P-S/IVOCs, and
600 uncertainties in the model with respect to these compounds likely explain the
601 overestimation observed at longer photochemical ages. As discussed in the introduction,
602 a major goal in this work is to better constrain the amount of SOA formed from the
603 oxidation of P-S/IVOCs, and the following two model cases (ROB + ZHAO + TSI and
604 WOR + ZHAO + TSI) seek to incorporate new measurements to better constrain the box
605 model with respect to the P-S/IVOCs.

606 When the yield, rate constants, and initial concentrations of P-IVOCs are
607 constrained using the field measurements reported in Zhao et al. (2014) (ROB + ZHAO +
608 TSI), the SOA mass simulated by the model shows much better agreement with the
609 measurements at longer photochemical ages (Fig. 3 and 4). There is a slight over-
610 prediction at 2 days of photochemical aging, but the model is still within the range of
611 measurements of very aged urban SOA reported by De Gouw and Jimenez (2009). The
612 parameterization reported in Robinson et al. (2007) for P-S/IVOCs is based on one study
613 of the photo-oxidation of diesel emissions from a generator (Robinson et al., 2007). The
614 results obtained here for the better constrained ROB + ZHAO + TSI case indicate that the
615 initial concentrations of P-IVOCs as well as the P-IVOC yields within ROB + TSI are too
616 high which leads to over-prediction of SOA concentration at longer photochemical ages.
617 On the other hand, the SOA mass simulated in ROB + ZHAO + TSI is biased low at
618 shorter photochemical ages (less than 1 day). Similar to other recent studies (Gentner et
619 al., 2012; Hayes et al., 2015; Ortega et al., 2016), there may be unexplained SOA
620 precursors not included in the model which rapidly form SOA or yields for fast-reacting
621 species including certain VOCs may be biased low. Both of these possibilities are
622 explored in the other model cases discussed below.

623 The WOR + ZHAO + TSI case simulates higher SOA concentrations at shorter
624 photochemical ages compared to the previous case (ROB + ZHAO + TSI), but it is still
625 biased low at shorter photochemical ages. The more rapid SOA formation is due to the
626 updated SVOC volatility distribution in this model case compared to the cases that use
627 the Robinson et al. (2007) distribution. Specifically, as shown in Fig. 2F, there is a higher
628 relative concentration of gas phase SVOCs in the $c^* = 10^2$ bin and thus a higher ratio of
629 P-SVOC to POA. Given that in the box model (and in most air quality models) the P-
630 SVOC emissions are determined by scaling the POA emissions according to their
631 volatility distribution, a higher P-SVOC to POA ratio will then result in a higher initial P-

632 SVOCs concentration. Furthermore, SOA formation from P-SVOCs is relatively fast.
633 Together these changes lead to increases in SOA formation during the first hours of
634 photochemical aging when using the Worton et al. volatility distribution. This case
635 suggests that P-SVOCs in their highest volatility bin ($c^* = 10^2 \mu\text{g m}^{-3}$ bin) that are
636 emitted by motor vehicles may be responsible for some of the observed rapid SOA
637 formation within the South Coast Air Basin. When observing the SOA mass simulated at
638 photochemical ages higher than 1 day, the simulation is similar to ROB + ZHAO + TSI.
639 There is better model/measurement agreement than for the ROB + TSI case, but a small
640 over-prediction is observed in the comparison to the reactor data at 2 days of
641 photochemical aging.

642 Also shown in the right-hand panels of Fig. 3 and 4 are the results with the
643 updated yields for the VOCs that account for gas phase chamber wall losses. For these
644 last three cases (ROB + MA, ROB + ZHAO + MA, and WOR + ZHAO + MA), the rate
645 of SOA formation at short photochemical ages is faster because the secondary SVOC
646 mass from the oxidation of the VOC precursors is distributed into lower volatility bins
647 compared to the Tsimpidi et al. (2010) parameterization. In the ROB + MA case (Fig. 3D
648 and 4D), similar to ROB + TSI, an over-prediction is obtained at longer photochemical
649 ages. There is an improvement in the model at the shortest photochemical ages, but the
650 simulated mass is still lower than the measurements even when considering the
651 measurement uncertainty. Both of these cases perform less well for SOA formation
652 within the South Coast Air Basin, and therefore the remainder of this study is focused on
653 the other four model cases. Overall, the model cases using the updated yields for V-SOA
654 show improvement for the shorter photochemical ages, and the evolution of SOA
655 concentration as a function of photochemical age better corresponds to the various
656 measurements taken at Pasadena and from the OFR.

657 Specifically, the ROB + ZHAO + MA and the WOR + ZHAO + MA cases both
658 better represent SOA formation and exhibit better model/measurement agreement among
659 the different cases used in this work. They are both consistent with the OFR reactor data
660 at longer photochemical ages as shown in Figs. 3 and 4 compared with the other cases. At
661 a qualitative level, the MA parameterization simulations are more consistent with the fit
662 of the OFR measurements in which the SOA mass remains nearly constant at longer
663 photochemical ages. In contrast, the cases with the TSI parameterization do not follow
664 this trend as the SOA mass keeps increasing between 2 and 3 days age, which is not
665 observed in the measurements. As already mentioned, the model used for this work does
666 not include fragmentation reactions, and including these reactions, in particular branching
667 between functionalization and fragmentation during gas-phase SVOC oxidation, may
668 improve the cases using a potential update of the TSI parameterization as discussed
669 below. Fig. 4F indicates that including additional P-SVOC mass in the model and
670 accounting for gas-phase wall losses in chamber studies improves SOA mass

671 concentration simulations with respect to the measurements. However, in the WOR +
672 ZHAO + MA case there is still a slight under-prediction of SOA formed at shorter
673 photochemical ages (between 0.05 and 0.5 days), and this discrepancy is observed in all
674 the other model cases. Given the uncertainties in the model set-up discussed in the
675 experimental section, it is not possible to conclude if one of the four cases (i.e. ROB +
676 ZHAO + TSI, WOR + ZHAO + TSI, ROB + ZHAO + MA, WOR + ZHAO + MA) more
677 accurately represents SOA formation in the atmosphere.

678 According to the OFR data from Ortega et al. (2016), the mass of OA starts to
679 decay due to fragmentation after heterogeneous oxidation at approximately 10 days of
680 photochemical aging. The results are consistent with other OFR field measurements
681 (George and Abbatt, 2010; Hu et al., 2016; Palm et al., 2016). In this work, the model is
682 run only up to 3 days, which is much shorter than the age when heterogeneous oxidation
683 appears to become important. In fact, when including a fragmentation pathway for each
684 of the model cases, a reduction of OA of only 6 % is observed compared to the cases
685 without fragmentation at 3 days of photochemical aging. In this sensitivity study, the
686 fragmentation is parameterized as an exponential decrease in OA concentration that has a
687 lifetime of 50 days following Ortega et al. (2016). Given the results, the inclusion of
688 fragmentation due to heterogeneous oxidation in the model does not significantly change
689 the model results or the conclusions made in this work.

690 More generally, there are at least three different fragmentation mechanisms that
691 could be responsible for the decrease of SOA formation at very high photochemical ages.
692 The first mechanism is the reaction of oxidants (e.g. OH) with the surface of an aerosol
693 particle and decomposition to form products with higher volatility, i.e. due to the
694 heterogeneous oxidation just described. The second type of fragmentation that may be
695 important for very high photochemical ages in the OFR is due to the high concentration
696 of OH (Palm et al., 2016). Most of the molecules in the gas phase will react multiple
697 times with the available oxidants before having a chance to condense, which will lead to
698 the formation of smaller products too volatile to form SOA. However, this is only
699 important at very high photochemical ages in the OFR, which are not used in this work.
700 A third type of fragmentation can occur during the aging of gas-phase SVOCs
701 (Shrivastava et al., 2013; 2015). The TSI parameterization used in the model from this
702 work and from previous modeling works (Robinson et al., 2007; Hodzic et al., 2010;
703 Shrivastava et al., 2011) only includes the functionalization of the SVOCs and neglects
704 fragmentation reactions. More recently, Shrivastava et al. (2013) have modified the VBS
705 approach in a box model by incorporating both pathways and performed several
706 sensitivity studies. The results when including fragmentation generally exhibit better
707 agreement with field observations, but as noted in that work the agreement may be
708 fortuitous given that both the emissions as well as the parameters representing oxidation
709 in the model are uncertain. This third type of fragmentation is not simulated in our

710 sensitivity study using the approach above, and it remains poorly characterized due to the
711 complexity of the chemical pathways and the number of compounds contributing to SOA
712 formation as described in Shrivastava et al. (2013).

713 Finally, Woody et al. (2016) recently proposed a meat cooking volatility
714 distribution and therefore we perform a sensitivity study by using this distribution in our
715 model for P-SVOCs coming from cooking sources. The results are displayed in the
716 supporting information (Figure S8), where this alternate approach has been implemented
717 for the WOR + ZHAO + TSI and WOR + ZHAO + MA cases. By comparing the results
718 obtained from this sensitivity study with Fig. 3, the two cases in the sensitivity study
719 display a slight decrease of SOA/ Δ CO values over 3 days of photochemical aging with a
720 difference of approximately 8% at 3 days. Thus, the model-measurement comparison
721 does not change significantly relative to the base case. Given the similarities between the
722 sensitivity study and Fig. 3, as well as the possibility of cooking SOA sources other than
723 meat-cooking (i.e. heated cooking oils, Liu et al. (2017)), the remainder of our work uses
724 the Robinson et al. volatility distribution for P-SVOCs from cooking sources.

725 **3.1.1 SOA concentration estimated at Pasadena: fossil and non-fossil** 726 **fractions**

727 In the top panel of Figure 5, the box model is compared against the urban SOA
728 determined by PMF analysis of the AMS measurements at Pasadena (Hayes et al., 2013).
729 In the bottom panel of the same figure the model is compared against the fossil and non-
730 fossil fraction of urban SOA as obtained from 14 C measurements reported in Zotter et al.
731 (2014). Both panels show measurements and predictions corresponding to 12:00 – 15:00
732 local time, when SOA concentrations peaked due to longer photochemical ages (5 hours
733 on average) as well as the arrival of emissions transported from source-rich western
734 regions of the South Coast Air Basin.

735 Similar to the results in Fig. 3 and 4 for short photochemical ages, the SOA mass
736 simulated by the ROB + ZHAO + TSI case is biased low in Fig. 5A. The ROB + ZHAO
737 + MA, WOR + ZHAO + TSI, and WOR + ZHAO + MA cases show better
738 model/measurement agreement as the simulated SOA mass is within the measurement
739 uncertainty or essentially equal to the lower limit of the concentration that is defined by
740 the measurement uncertainty. Fig. 5A also allows evaluation of the contribution of each
741 precursor type to the SOA at Pasadena. For the four cases displayed, the P-SVOCs and P-
742 IVOCs are responsible for 69 – 83 % of the urban SOA formation. Thus, more than half
743 of the urban SOA is attributed to these precursors even in the MA parameterizations
744 where the model is run with the updated yields, which doubles V-SOA compared to the
745 cases using the yields reported from Tsimpidi et al. (2010). Furthermore, 8 – 29 % of the
746 measured urban SOA is due to V-SOA where the range of values is due to the uncertainty

747 in the measurements as well as the difference in simulated V-SOA concentration for each
748 case.

749 According to the ^{14}C measurements, an average of 71 ± 3 % of urban SOA at
750 Pasadena is fossil carbon, which is thought to be due to the importance of vehicular
751 emissions, especially during the morning rush hour (Bahreini et al., 2012; Zotter et al.,
752 2014; Hayes et al., 2015). In general, the box model gives results consistent with the ^{14}C
753 measurements. To make this comparison, the simulated SOA is apportioned between
754 fossil S-SOA, fossil I-SOA, fossil V-SOA, cooking S-SOA, and biogenic V-SOA. The
755 last two apportionments correspond to non-fossil carbon. This evaluation is possible
756 following an approach similar to Hayes et al. (2015) where the identity of the precursor is
757 used to apportion SOA. Briefly, the fossil S-SOA is formed from P-SVOCs emitted with
758 hydrocarbon-like OA (HOA), which is a surrogate for vehicular POA. Second, cooking
759 S-SOA is formed from P-SVOCs emitted with cooking-influenced OA (CIOA). The
760 concentrations of HOA and CIOA were determined previously using PMF analysis.
761 Fossil V-SOA is formed from aromatics, alkanes, and olefins while isoprene and terpenes
762 are responsible for biogenic V-SOA. The treatment of IVOCs in the comparison with the
763 ^{14}C measurements has been updated from our 2015 study. Previously, it was assumed that
764 P-IVOCs were co-emitted with cooking-influenced OA, but the recent work of Zhao et
765 al. (2014) and others indicates that petroleum sources contribute substantially to IVOC
766 emissions (Dunmore et al., 2015; Ots et al., 2016). Therefore, the IVOCs are considered
767 entirely fossil carbon in order to obtain the results shown in Fig. 5B.

768 As seen in Fig. 5B, for all the model cases, cooking S-SOA dominates the non-
769 fossil fraction and biogenic VOCs have only a small contribution to non-fossil urban
770 SOA. This result is consistent with our previous work, and indicates agreement between
771 the model and ^{14}C measurements cannot be achieved without including an urban source
772 of non-fossil carbon such as P-SVOCs from cooking. With respect to fossil SOA, more
773 S-SOA is formed when using the volatility distribution of vehicular POA reported from
774 Worton et al. (2014) due to the greater proportion of gas-phase of P-SVOCs. When the
775 V-SOA yields are updated in the model (MA parameterizations), there is a corresponding
776 increase in both fossil and non-fossil V-SOA.

777 When comparing the fossil/non-fossil carbon split, all the cases are either in
778 agreement with the measurement within its uncertainty, or slightly lower. Starting with
779 the ROB + ZHAO + TSI case, the fossil fraction increases from 74 % to 79 % in each
780 case as VOCs or P-SVOCs from vehicle emissions have greater importance for SOA
781 formation. While the uncertainties reported in Zotter et al. (2014) were 71 ± 3 %, there
782 are likely additional errors due to different factors that may influence the model or
783 measurements. For example, a portion of the P-IVOCs may be from cooking sources
784 rather than entirely from fossil sources as is assumed above (Klein et al., 2016). Taking
785 the WOR + ZHAO + MA case as an example, since it is the best performing case in this

786 work according to Fig. 5A, model/measurement agreement is obtained within
787 measurement uncertainties if one assumes that 18 – 41 % of P-IVOCs come from
788 cooking emissions. Ultimately, the differences observed in the comparison with the ¹⁴C
789 data are very likely smaller than these errors discussed here, and it is concluded that all
790 the model cases perform equally well with respect to the fossil/non-fossil carbon split.

791 As reported in Gentner et al. (2012), emissions from petroleum derived fuels such
792 as diesel and gasoline have an important contribution to the formation of SOA. However,
793 there have been conflicting results regarding the relative contributions of diesel versus
794 gasoline emissions (Bahreini et al., 2012; Gentner et al., 2012). In this work, the relative
795 contribution of different SOA sources is estimated following a procedure similar to that
796 previously published in Hayes et al. (2015), and the results are shown in Figure S9 of the
797 supporting information. Briefly, the source apportionment method follows four steps.
798 First, after classifying the SOA mass from isoprene and terpenes as biogenic V-SOA, the
799 remaining V-SOA is attributed to gasoline emissions since the diesel contribution to V-
800 SOA is small (~3 %) (Hayes et al., 2015). Second, for the diesel and gasoline
801 contribution to S-SOA, 70(±10) % of HOA is emitted from diesel vehicles with the
802 remainder from gasoline vehicles (Hayes et al., 2013), and thus it is assumed for the
803 source apportionment that 70% (30%) of vehicular P-SVOCs are from diesel (gasoline)
804 vehicles. Third, the S-SOA from cooking sources is calculated separately in the model,
805 where the initial concentration of cooking P-SVOCs is estimated using the measured
806 CIOA concentration and the method described in Section 2.2.2 above. Lastly, the
807 fractional contributions to I-SOA mass is difficult to determine since there are still
808 uncertainties about the sources of IVOCs. According to Zhao et al. (2014), petroleum
809 sources other than on-road vehicles likely contribute substantially to primary IVOCs, but
810 evidence exists that cooking may be a source of IVOCs as well (Klein et al., 2016). Thus,
811 while we attribute I-SOA to these two sources, we do not distinguish the sources. The
812 estimated source apportionment in Fig. S9 attributes urban SOA as follows: 4% to
813 biogenic V-SOA, 23% to gasoline V-SOA, 9% to gasoline S-SOA, 20 % to diesel S-
814 SOA, and 17 % to cooking S-SOA. The remaining 27 % is I-SOA that is either due to
815 cooking or off-road emissions of P-IVOCs.

816 It should be noted that according to McDonald et al. (2015), the emissions from
817 vehicles have decreased over time (i.e. between 1970 and 2010) due to regulations in
818 California. Warneke et al. (2012) have observed also that the emission ratios of some
819 SOA precursors (i.e. $\Delta\text{VOC}/\Delta\text{CO}$) have remained constant between 2002 and 2010,
820 while absolute concentrations have decreased. On the other hand, cooking and off-road
821 emissions are subject to different regulations in California, and the ratios of cooking or
822 off-road emissions to vehicular emissions have likely changed with time, which means
823 that the source apportionment results for urban SOA presented here will be specific to
824 2010.

825 **3.2 SOA formation versus precursor oxidation rate constant**

826 Recent results from Ortega et al. (2016) point to the importance of fast-reacting
827 precursors for urban SOA during CalNex, and we can use their results to further evaluate
828 our box model. The fraction of SOA formed from each precursor class as a function of
829 the precursor rate constant is displayed in Figure 6. The right-axis of Fig. 6 shows the
830 correlation (R^2) of different VOCs with the maximum concentration of SOA formed
831 using the OFR as a function of their oxidation rate constants as reported in Ortega et al.
832 (2016). This analysis of the OFR data allows us to constrain the rate constants of the most
833 important SOA precursors. A detailed description of how the R^2 values were obtained can
834 be found in Ortega et al. (2016). According to the R^2 data, the VOC compounds that
835 correlate best with maximum SOA formation potential are those that have $\log k_{OH}$ rate
836 constants ranging from -10.5 to -10.0. When comparing the percentage of SOA mass
837 simulated by the model with the observed R^2 values, all of the four cases are not entirely
838 consistent with the R^2 data. According to the model, more SOA mass is formed from
839 precursors in the bin ranging from -11.0 to -10.5 (the majority of mass formed comes
840 from P-IVOCs) rather than the bin ranging from -10.5 to -10.0. In contrast, the R^2 value
841 is higher for the more reactive bin. If either fast-reacting precursors were missing in the
842 model, or if the rate constants of the currently-implemented precursors were too small,
843 then correcting either error would shift the relative distribution shown in Fig. 6 towards
844 faster-reacting SOA precursors. In turn, the trend in the percentage of modeled SOA
845 mass may more closely follow the trend in R^2 values.

846 **3.3 Volatility distribution of OA**

847 Based on the evaluations carried out up to this point on the six model cases, **the**
848 **WOR + ZHAO + MA case seems to most closely reproduce the observations.** Thus, the
849 entire volatility distribution of the OA, precursors, and secondary gas phase organics is
850 analyzed for this model case. Figure 7 shows this distribution for three selected
851 photochemical ages: 0, 5, and 36 h. The figure allows us to track the evolution of SOA
852 and secondary gas phase organics from each precursor class in terms of their
853 concentration and volatility and also to evaluate the reduction of precursor
854 concentrations. For the model results, the volatility distribution of all organics resolved
855 by precursor class, except for the VOCs and P-IVOCs, can be taken directly from the
856 model. To determine the volatility distribution of the VOCs and P-IVOCs, the SIMPOL.1
857 method (Pankow and Asher, 2008) is used to estimate the effective saturation
858 concentration of each compound or lumped species in the model. Also included in Fig. 7,
859 in the bottom-right panel, is the observed volatility distribution for the Pasadena ground
860 site, which is an average of measurements collected during 12:00 – 15:00 local time and
861 corresponds to 5 h of photochemical aging. For the measurements, the volatility
862 distribution of VOCs was determined using GC-MS data (Borbon et al., 2013) whereas

863 the IVOC distribution is taken from Zhao et al. (2014). The volatility distribution of
864 SVOCs was determined using combined thermal denuder AMS measurements (see the
865 supporting information for further details).

866 For the volatility distribution of the model at time 0, the concentrations of P-
867 SVOCs and P-IVOCs monotonically increases with the value of c^* . However, a
868 discontinuity in the mass concentration exists between the $c^* = 10^2$ and $10^3 \mu\text{g m}^{-3}$ bins.
869 This discontinuity can be explained by several factors. First, the measured IVOCs mass
870 concentration the $c^* = 10^3 \mu\text{g m}^{-3}$ bin is very low, and since the initial concentrations of
871 IVOCs in the model are constrained by the field measurements, the model will also have
872 very low concentrations. Zhao et al. (2014) have already noted that the concentration of
873 P-IVOCs in this bin is relatively low when compared to the volatility distribution from
874 Robinson et al. (2007). Another possible explanation is the presence of cooking sources,
875 which in the model are responsible for substantial P-SVOC mass (~50%) but may have a
876 smaller contribution to the P-IVOC mass.

877 During oxidation the volatility distribution evolves and the concentration of
878 secondary organics increases in the bins between $c^* = 10^{-1}$ and $10^3 \mu\text{g m}^{-3}$ (inclusive), and
879 the largest portion of SOA is found in the $c^* = 1 \mu\text{g m}^{-3}$ bin. This result is due to the
880 partitioning of the organic mass to the particle phase and the lack of particle phase
881 reactions in the model, which leads to very slow oxidation rates for species found in the
882 lower volatility bins. After 36 h, a large portion of the precursors have been reacted,
883 although some primary and secondary material remains in the gas phase giving rise to
884 more gradual SOA formation.

885 In Fig. 7, it is possible to compare the measured volatility distribution with the
886 model simulation at 5 h of photochemical aging. It should be noted that the relatively
887 high concentrations of VOCs in the model compared to the measurements are due to the
888 model containing VOCs for which measurements were not obtained in Pasadena. There
889 are 47 VOCs used in the model and only 19 VOCs were measured. However, the
890 remaining VOCs have been measured in other urban locations (Warneke et al., 2007;
891 Borbon et al., 2013) and thus it is assumed they are also present in the South Coast Air
892 Basin. For this work, we include these 28 remaining VOCs by assuming that they are also
893 emitted in the South Coast Air Basin with identical emission ratios ($\Delta\text{VOC}/\Delta\text{CO}$). When
894 comparing only VOCs measured and modeled (shown in hollow black bars), the results
895 are consistent (3.1, 3.6 and $2.2 \mu\text{g m}^{-3}$ from $c^* = 10^7$ to $10^9 \mu\text{g m}^{-3}$ bins versus 3.8, 3.7
896 and $2.2 \mu\text{g m}^{-3}$ for the measurements). On the other hand, the model appears to have a
897 low bias for the concentrations of P-IVOCs (0.16, 0.63, 0.89 and $2.3 \mu\text{g m}^{-3}$ from $c^* =$
898 10^3 to $10^6 \mu\text{g m}^{-3}$ bins versus 0.21, 1.39, 2.65 and $3.82 \mu\text{g m}^{-3}$ for the measurements).
899 This low bias is seen for each volatility bin and could possibly be explained by either
900 oxidation rate constants that are too high or $\Delta\text{IVOC}/\Delta\text{CO}$ ratios that are too low. The

901 latter explanation seems more likely given that the rate constants estimated using
902 surrogate compounds and structure-activity relationships for the unspciated P-IVOCs
903 are generally lower limits (Zhao et al., 2014), which would result in a high bias rather
904 than a low bias. The $\Delta\text{IVOC}/\Delta\text{CO}$ ratios may be low because the photochemical age
905 between 00:00 – 6:00 local time is not strictly zero, and some oxidation may have
906 occurred during the period used to determine the ratio values. Emission ratios such as
907 $\Delta\text{IVOC}/\Delta\text{CO}$ facilitate incorporating P-IVOC emissions into 3-D models that already use
908 CO emissions inventories, and the $\Delta\text{IVOC}/\Delta\text{CO}$ ratios reported here could be used for
909 this purpose. However, the resulting I-SOA concentrations should be considered lower
910 limits given that the emission ratios, and also the rate constants, are likely themselves
911 lower limits.

912 To further explore the impact of potential errors in the initial IVOC
913 concentrations, a sensitivity study has been carried out using initial concentrations
914 calculated based on the observed photochemical age and measured IVOC concentrations
915 at Pasadena as well as the estimated IVOC oxidation rate constants (Zhao et al., 2014).
916 This alternate approach is implemented for the ROB + ZHAO + MA and WOR + ZHAO
917 + MA cases and does not use nighttime IVOC-to-CO ratios. The results when using this
918 alternative approach are shown in the supporting information (Figure S10). When
919 comparing Fig. S10 with Fig. 3, differences are minor. The model/measurement
920 agreement improves slightly at shorter photochemical ages (less than 1 day). At the same
921 time a slightly larger over-prediction is observed at longer photochemical ages. However,
922 the formation of SOA modeled in this sensitivity test is similar to the original cases from
923 Fig. 3 with an average difference of only 21 %, which represent a relatively small error
924 compared to other uncertainties in SOA modeling. The IVOC initial concentrations used
925 in this sensitivity test are slightly higher than those calculated using the IVOC-to-CO
926 ratio, which explain the small increase of modeled SOA/ ΔCO . Ultimately, the different
927 approaches for determining the initial IVOC concentration in the model are reasonably
928 consistent, and both approaches perform similarly given the model and measurement
929 uncertainties.

930 For the measurements of SVOCs, all the mass in bins lower than $10^{-2} \mu\text{g m}^{-3}$ are
931 lumped into this bin for Fig. 7 since the model does not contain lower volatility bins. In
932 addition, the 10^1 and $10^2 \mu\text{g m}^{-3}$ bins are not well-resolved because the thermal denuder
933 did not consistently reach temperatures low enough (less than 37°C) to resolve SVOCs in
934 this range of volatilities. Thus, the $10^1 \mu\text{g m}^{-3}$ bin may contain some higher volatility
935 particulate mass although this contribution is expected to be small due to the low particle
936 phase fraction of compounds in the $10^2 \mu\text{g m}^{-3}$ bin. With these considerations in mind, the
937 volatility distribution of the SVOCs is somewhat different in the model compared to the
938 measurements. Most notably, the model does not form a significant amount of lower

939 volatility SOA in the $10^{-2} \mu\text{g m}^{-3}$ bin, whereas the measurements have a much higher
940 concentrations in this bin. A factor that may explain this difference between the volatility
941 distributions is the lack of particle phase reactions that continue to transform SOA into
942 lower volatility products, a process which is not considered in the model. One example of
943 a particle phase reaction is the formation of SOA within deliquesced particles, including
944 the partitioning of glyoxal to the aqueous phase to produce oligomers as discussed in
945 Ervens and Volkamer (2010), although that specific mechanism was of little significance
946 during CalNex (Washenfelder et al., 2011; Knote et al., 2014). Alternatively, the use of
947 an aging parameterization where the volatility may decrease by more than one order of
948 magnitude per oxidation reaction would also distribute some SOA mass into lower c^*
949 bins. Hayes et al. (2015) previously evaluated different parameters for aging. However,
950 the results from this previous study showed that substantial over-prediction of SOA was
951 observed when using the Grieshop et al. (2009) parameterization in which each oxidation
952 reaction reduced volatility by two orders of magnitude. New parameterizations may be
953 necessary to produce the observed SOA volatility and concentration simultaneously
954 (Cappa and Wilson, 2012). However, we note that the additional low volatility organic
955 mass will not significantly change SOA predictions in urban regions where OA
956 concentrations are relatively high. When comparing the total amount of particle phase
957 SVOCs, it seems that the model reproduces reasonably well the measurements (6.6
958 versus $9.0 \mu\text{g m}^{-3}$) as expected based on the comparisons of the total SOA concentration
959 discussed above. In addition, the total amount of SVOCs (particle and gas phase) are
960 similar (12.9 vs $11.8 \mu\text{g m}^{-3}$), although it is difficult to determine from measurements the
961 gas phase concentration of SVOCs in the $10^2 \mu\text{g m}^{-3}$ bin due to the lack of particle mass
962 in this bin under ambient concentrations as well as the limited temperature range of the
963 thermal denuder system.

964 Recently, Woody et al. (2016) published a paper that modeled SOA over
965 California using the Environmental Protection Agency's Community Multiscale Air
966 Quality Model that had been updated to include a VBS treatment of SOA (CMAQ-VBS).
967 As discussed in that paper, the modeled P-S/IVOC emission inventories remain an
968 important source of uncertainty in 3-D grid-based models. In that previous study several
969 different ratios of P-S/IVOCs-to-POA emissions were evaluated against measurements,
970 and it was found that a ratio of 7.5 gave the best agreement between the CMAQ-VBS
971 model and observations. From the results shown in Fig. 7 at a photochemical age of 0 h, a
972 P-S/IVOC-to-POA ratio of 5.2 is calculated. This ratio is different from that determined
973 by Woody et al. (2016), and may be biased low due to possibly low $\Delta\text{IVOC}/\Delta\text{CO}$
974 emission ratios as discussed earlier in this section, but it serves as both a useful lower
975 bound and has the advantage of being determined from empirical measurements of
976 aerosols rather than by tuning a model to match measured SOA concentrations. As stated
977 in Woody et al. (2016), the higher ratio may compensate for other missing (or

978 underrepresented) formation pathways in SOA models or excessive dispersion of SOA in
979 their model.

980 4. CONCLUSION

981 We have used several data sets from recently published papers to better constrain
982 and evaluate urban SOA formation pathways and precursors, especially P-SVOCs and P-
983 IVOCs, within a custom-built box model. The use of the box model facilitates the
984 incorporation of these new data sets as well as the evaluation of a number of model cases.
985 All the model cases are able to correctly simulate the fossil/non-fossil carbon split at the
986 Pasadena ground site providing support for the performance of the model. When
987 measurements of IVOCs are used to constrain the concentrations of P-IVOCs, such as in
988 the ROB + ZHAO + TSI and ROB + ZHAO + MA cases, a large improvement of the
989 model at longer photochemical age is observed. However, these model cases are still
990 biased low at shorter photochemical ages. By constraining the P-SVOCs additionally
991 with measurements of those precursors, such as in the WOR + ZHAO + TSI case, better
992 model/measurement agreement is obtained at shorter photochemical ages, yet the model
993 is still biased low. Finally, the WOR + ZHAO + MA case, which incorporates state-of-
994 the-art measurements of P-SVOCs and P-IVOCs and also accounts for the effect of
995 chamber wall-losses on VOC yields, obtains model/measurement agreement within
996 measurement uncertainties at long photochemical ages. Although, it displays also a low
997 bias at short photochemical ages, which is similar to the ROB + ZHAO + MA case. This
998 bias may be due to low $\Delta\text{IVOC}/\Delta\text{CO}$ emissions ratios or IVOC oxidation rate constants
999 for which the estimated values are too low. It is also possible that additional sources or
1000 SOA formation pathways are missing from the model. Moreover, a P-S/IVOC-to-POA
1001 ratio of 5.2 is determined, which can be combined with POA emission inventories to
1002 constrain the emissions of P-S/IVOCs in gridded chemical transport models.

1003 In addition to evaluating the model performance with respect to SOA
1004 concentration, the rates of SOA formation are compared against measurements as well.
1005 This aspect of the study was enhanced by the use of OFR data to constrain SOA
1006 formation potential for up to 3 days of photochemical aging (at 1.5×10^6 molec OH
1007 cm^{-3}). The model cases that include multi-generation oxidative aging predict substantial
1008 SOA increases after 1.5 days of aging, which is not consistent with the OFR
1009 measurements. In contrast, model cases in which aging is omitted and instead SOA yields
1010 for VOCs are corrected for gas phase wall-losses in chamber experiments predict little
1011 change in the SOA concentration after 1.5 days. These results highlight the uncertainties
1012 associated with aging schemes for SOA from VOCs, which are often implemented in
1013 SOA models. Implementing instead corrected yields for VOCs results in similar amounts
1014 of SOA but formation rates versus time that are more consistent with observations.

1015 Therefore, the model cases with updated VOC yields that account for chamber
1016 wall-losses best reproduce the ambient and OFR data. However, while the WOR +
1017 ZHAO + MA case appears to represent a slight improvement over the ROB + ZHAO +
1018 MA case, as well as over the ROB + ZHAO + TSI and WOR + ZHAO + TSI cases, it is
1019 not possible to conclude that one set of parameters is better than the other since the
1020 difference in the predictions for these 4 cases (15 % on average) is likely smaller than the
1021 uncertainties due to the model setup as well as the lack of a gas-phase fragmentation
1022 pathway during aging. Moreover, uncertainties in the vapor wall-loss corrected yields
1023 remain, and the correction of the yields has been performed here using data from a
1024 limited number of laboratory studies. In particular, the effect of temperature and humidity
1025 on gas-wall partitioning needs to be characterized. The results obtained in our work
1026 motivate future studies by showing that SOA models using wall-loss corrected yields
1027 reproduce observations for a range of photochemical ages at a level of accuracy that it is
1028 as good as or better than parameterizations with the uncorrected yields.

1029 In all six of the model cases, a large majority of the urban SOA at Pasadena is the
1030 result of P-SVOC and P-IVOC oxidation. While this result alone cannot be taken as
1031 conclusive due to the uncertainties in the model parameters, further evidence for the
1032 importance of P-SVOCs and P-IVOCs is obtained by analyzing the percentage of SOA
1033 formed at long photochemical ages (~1.5 days) as a function of the precursor rate
1034 constant. The P-SVOCs and P-IVOCs have rate constants that are similar to highly
1035 reactive VOCs that have been previously found to strongly correlate with SOA formation
1036 potential measured by the OFR.

1037 Lastly, the modeled volatility distribution of the total (gas and particle phase)
1038 organic mass between $c^* = 10^{-2}$ and 10^{10} ug m^{-3} is analyzed at three ages and compared
1039 against volatility-resolved measurements. While the total concentrations of gas and
1040 particle phase SVOCs are reasonably well simulated, at the same time there are important
1041 differences between the measured and modeled volatility distribution of SVOCs. These
1042 differences highlight the need for further studies of the chemical pathways that may give
1043 rise to SOA in low volatility bins at $c^* = 10^{-2}$ ug m^{-3} and lower.

1044

1045 **ACKNOWLEDGEMENTS**

1046 This work was partially supported by a Natural Science and Engineering Research
1047 Council of Canada (NSERC) Discovery Grant (RGPIN/05002-2014), le Fonds de
1048 recherche - Nature et technologies (FRQNT) du Québec (2016-PR-192364), and the
1049 Université de Montréal. AMO and JLJ were supported by CARB 11-305 and EPA STAR
1050 83587701-0. This manuscript has not been reviewed by EPA and thus no endorsement
1051 should be inferred. We gratefully acknowledge VOC data provided by J. de Gouw and
1052 J.B. Gilman.

1053 **REFERENCES**

- 1054 Ahmadov, R. McKeen, S. A. Robinson, A. L. Bahreini, R. Middlebrook, A. M. de Gouw,
1055 J. A. Meagher, J. Hsie, E. Y. Edgerton, E. Shaw, S. and Trainer, M.: A volatility
1056 basis set model for summertime secondary organic aerosols over the eastern
1057 United States in 2006, *J. Geophys. Res.-Atmos.*, 117, D06301, 2012
- 1058 Atkinson, R. and Arey, J.: Atmospheric degradation of volatile organic compounds,
1059 *Chem. Rev.*, 103, 4605-4638, 2003
- 1060 Bahreini, R. Middlebrook, A. M. de Gouw, J. A. Warneke, C. Trainer, M. Brock, C. A.
1061 Stark, H. Brown, S. S. Dube, W. P. Gilman, J. B. Hall, K. Holloway, J. S. Kuster,
1062 W. C. Perring, A. E. Prevot, A. S. H. Schwarz, J. P. Spackman, J. R. Szidat, S.
1063 Wagner, N. L. Weber, R. J. Zotter, P. and Parrish, D. D.: Gasoline emissions
1064 dominate over diesel in formation of secondary organic aerosol mass, *Geophys.*
1065 *Res. Lett.*, 39, L06805, 2012
- 1066 Borbon, A. Gilman, J. B. Kuster, W. C. Grand, N. Chevaillier, S. Colomb, A.
1067 Dolgorouky, C. Gros, V. Lopez, M. Sarda-Esteve, R. Holloway, J. Stutz, J.
1068 Petetin, H. McKeen, S. Beekmann, M. Warneke, C. Parrish, D. D. and de Gouw,
1069 J. A.: Emission ratios of anthropogenic volatile organic compounds in northern
1070 mid-latitude megacities: Observations versus emission inventories in Los Angeles
1071 and Paris, *J. Geophys. Res.-Atmos.*, 118, 2041-2057, 2013
- 1072 Cappa, C. D. and Wilson, K. R.: Multi-generation gas-phase oxidation, equilibrium
1073 partitioning, and the formation and evolution of secondary organic aerosol,
1074 *Atmos. Chem. Phys.*, 12, 9505-9528, 2012
- 1075 Carter, W. P. L.: Development of the SAPRC-07 chemical mechanism, *Atmos. Environ.*,
1076 44, 5324-5335, 2010
- 1077 Chan, A. W. H. Kautzman, K. E. Chhabra, P. S. Surratt, J. D. Chan, M. N. Crouse, J. D.
1078 Kuerten, A. Wennberg, P. O. Flagan, R. C. and Seinfeld, J. H.: Secondary organic
1079 aerosol formation from photooxidation of naphthalene and alkylnaphthalenes:
1080 implications for oxidation of intermediate volatility organic compounds (IVOCs),
1081 *Atmos. Chem. Phys.*, 9, 3049-3060, 2009
- 1082 Christensen, J. H. Krishna Kumar, K. Aldrian, E. An, S.-I. Cavalcanti, I. F. A. de Castro,
1083 M. Dong, W. Goswami, A. Hall, A. Kanyanga, J. K. Kitoh, A. Kossin, J. Lau, N.-
1084 C. Renwick, J. Stephenson, D. B. Xie, S.-P. and Zhou, T.: *Climate Change 2013:*
1085 *The Physical Scientific Basis. Contribution of Working Group I to the Fifth*
1086 *Assessment Report of the Intergovernmental Panel on Climate Change. 2013*

1087 De Gouw, J. and Jimenez, J. L.: Organic Aerosols in the Earth's Atmosphere, Environ.
1088 Sci. Technol., 43, 7614-7618, 2009

1089 DeCarlo, P. F. Ulbrich, I. M. Crouse, J. de Foy, B. Dunlea, E. J. Aiken, A. C. Knapp, D.
1090 Weinheimer, A. J. Campos, T. Wennberg, P. O. and Jimenez, J. L.: Investigation
1091 of the sources and processing of organic aerosol over the Central Mexican Plateau
1092 from aircraft measurements during MILAGRO, Atmos. Chem. Phys., 10, 5257-
1093 5280, 2010

1094 Dockery, D. W. and Pope, C. A.: Acute respiratory effects of particulate air-pollution,
1095 Annu. Rev. Publ. Health, 15, 107-132, 1994

1096 Donahue, N. M. Chuang, W. Epstein, S. A. Kroll, J. H. Worsnop, D. R. Robinson, A. L.
1097 Adams, P. J. and Pandis, S. N.: Why do organic aerosols exist? Understanding
1098 aerosol lifetimes using the two-dimensional volatility basis set, Envir. Chem., 10,
1099 151-157, 2013

1100 Donahue, N. M. Robinson, A. L. Stanier, C. O. and Pandis, S. N.: Coupled partitioning,
1101 dilution, and chemical aging of semivolatile organics, Environ. Sci. Technol., 40,
1102 2635-2643, 2006

1103 Dunmore, R. E. Hopkins, J. R. Lidster, R. T. Lee, J. D. Evans, M. J. Rickard, A. R.
1104 Lewis, A. C. and Hamilton, J. F.: Diesel-related hydrocarbons can dominate gas
1105 phase reactive carbon in megacities, Atmos. Chem. Phys., 15, 9983-9996, 2015

1106 Dzepina, K. Cappa, C. D. Volkamer, R. M. Madronich, S. DeCarlo, P. F. Zaveri, R. A.
1107 and Jimenez, J. L.: Modeling the Multiday Evolution and Aging of Secondary
1108 Organic Aerosol During MILAGRO 2006, Environ. Sci. Technol., 45, 3496-3503,
1109 2011

1110 Dzepina, K. Volkamer, R. M. Madronich, S. Tulet, P. Ulbrich, I. M. Zhang, Q. Cappa, C.
1111 D. Ziemann, P. J. and Jimenez, J. L.: Evaluation of recently-proposed secondary
1112 organic aerosol models for a case study in Mexico City, Atmos. Chem. Phys., 9,
1113 5681-5709, 2009

1114 Ervens, B. and Volkamer, R.: Glyoxal processing by aerosol multiphase chemistry:
1115 towards a kinetic modeling framework of secondary organic aerosol formation in
1116 aqueous particles, Atmos. Chem. Phys., 10, 8219-8244, 2010

1117 Fountoukis, C. Megaritis, A. G. Skyllakou, K. Charalampidis, P. E. Denier van der Gon,
1118 H. A. C. Crippa, M. Prévôt, A. S. H. Fachinger, F. Wiedensohler, A. Pilinis, C.
1119 and Pandis, S. N.: Simulating the formation of carbonaceous aerosol in a
1120 European Megacity (Paris) during the MEGAPOLI summer and winter
1121 campaigns, Atmos. Chem. Phys., 16, 3727-3741, 2016

1122 Gentner, D. R. Isaacman, G. Worton, D. R. Chan, A. W. H. Dallmann, T. R. Davis, L.
1123 Liu, S. Day, D. A. Russell, L. M. Wilson, K. R. Weber, R. J. Guha, A. Harley, R.
1124 A. and Goldstein, A. H.: Elucidating secondary organic aerosol from diesel and
1125 gasoline vehicles through detailed characterization of organic carbon emissions,
1126 Proc. Natl. Acad. Sci. USA, 109, 18318-18323, 2012

1127 George, I. J. and Abbatt, J. P. D.: Heterogeneous oxidation of atmospheric aerosol
1128 particles by gas-phase radicals, Nat. Chem., 2, 713-722, 2010

1129 Grieshop, A. P. Logue, J. M. Donahue, N. M. and Robinson, A. L.: Laboratory
1130 investigation of photochemical oxidation of organic aerosol from wood fires 1:
1131 measurement and simulation of organic aerosol evolution, Atmos. Chem. Phys., 9,
1132 1263-1277, 2009

1133 Hallquist, M. Wenger, J. C. Baltensperger, U. Rudich, Y. Simpson, D. Claeys, M.
 1134 Dommen, J. Donahue, N. M. George, C. Goldstein, A. H. Hamilton, J. F.
 1135 Herrmann, H. Hoffmann, T. Iinuma, Y. Jang, M. Jenkin, M. E. Jimenez, J. L.
 1136 Kiendler-Scharr, A. Maenhaut, W. McFiggans, G. Mentel, Th F. Monod, A.
 1137 Prevot, A. S. H. Seinfeld, J. H. Surratt, J. D. Szmigielski, R. and Wildt, J.: The
 1138 formation, properties and impact of secondary organic aerosol: current and
 1139 emerging issues, *Atmos. Chem. Phys.*, 9, 5155-5236, 2009
 1140 Hayes, P. L. Carlton, A. G. Baker, K. R. Ahmadov, R. Washenfelder, R. A. Alvarez, S.
 1141 Rappenglück, B. Gilman, J. B. Kuster, W. C. de Gouw, J. A. Zotter, P. Prévôt, A.
 1142 S. H. Szidat, S. Kleindienst, T. E. Offenberg, J. H. Ma, P. K. and Jimenez, J. L.:
 1143 Modeling the formation and aging of secondary organic aerosols in Los Angeles
 1144 during CalNex 2010, *Atmos. Chem. Phys.*, 15, 5773-5801, 2015
 1145 Hayes, P. L. Ortega, A. M. Cubison, M. J. Froyd, K. D. Zhao, Y. Cliff, S. S. Hu, W. W.
 1146 Toohey, D. W. Flynn, J. H. Lefer, B. L. Grossberg, N. Alvarez, S. Rappenglueck,
 1147 B. Taylor, J. W. Allan, J. D. Holloway, J. S. Gilman, J. B. Kuster, W. C. De
 1148 Gouw, J. A. Massoli, P. Zhang, X. Liu, J. Weber, R. J. Corrigan, A. L. Russell, L.
 1149 M. Isaacman, G. Worton, D. R. Kreisberg, N. M. Goldstein, A. H. Thalman, R.
 1150 Waxman, E. M. Volkamer, R. Lin, Y. H. Surratt, J. D. Kleindienst, T. E.
 1151 Offenberg, J. H. Dusanter, S. Griffith, S. Stevens, P. S. Brioude, J. Angevine, W.
 1152 M. and Jimenez, J. L.: Organic aerosol composition and sources in Pasadena,
 1153 California, during the 2010 CalNex campaign, *J. Geophys. Res.-Atmos.*, 118,
 1154 9233-9257, 2013
 1155 Heald, C. L. Coe, H. Jimenez, J. L. Weber, R. J. Bahreini, R. Middlebrook, A. M.
 1156 Russell, L. M. Jolleys, M. Fu, T. M. Allan, J. D. Bower, K. N. Capes, G. Crosier,
 1157 J. Morgan, W. T. Robinson, N. H. Williams, P. I. Cubison, M. J. DeCarlo, P. F.
 1158 and Dunlea, E. J.: Exploring the vertical profile of atmospheric organic aerosol:
 1159 comparing 17 aircraft field campaigns with a global model, *Atmos. Chem. Phys.*,
 1160 11, 12673-12696, 2011
 1161 Hodzic, A. and Jimenez, J. L.: Modeling anthropogenically controlled secondary organic
 1162 aerosols in a megacity: a simplified framework for global and climate models,
 1163 *Geosci. Model Dev.*, 4, 901-917, 2011
 1164 Hodzic, A. Jimenez, J. L. Madronich, S. Canagaratna, M. R. DeCarlo, P. F. Kleinman, L.
 1165 and Fast, J.: Modeling organic aerosols in a megacity: potential contribution of
 1166 semi-volatile and intermediate volatility primary organic compounds to secondary
 1167 organic aerosol formation, *Atmos. Chem. Phys.*, 10, 5491-5514, 2010
 1168 Hodzic, A. Kasibhatla, P. S. Jo, D. S. Cappa, C. D. Jimenez, J. L. Madronich, S. and
 1169 Park, R. J.: Rethinking the global secondary organic aerosol (SOA) budget:
 1170 stronger production, faster removal, shorter lifetime, *Atmos. Chem. Phys.*, 16,
 1171 7917-7941, 2016
 1172 Hu, W. Palm, B. B. Day, D. A. Campuzano-Jost, P. Krechmer, J. E. Peng, Z. de Sá, S. S.
 1173 Martin, S. T. Alexander, M. L. Baumann, K. Hacker, L. Kiendler-Scharr, A.
 1174 Koss, A. R. de Gouw, J. A. Goldstein, A. H. Seco, R. Sjostedt, S. J. Park, J. H.
 1175 Guenther, A. B. Kim, S. Canonaco, F. Prévôt, A. S. H. Brune, W. H. and Jimenez,
 1176 J. L.: Volatility and lifetime against OH heterogeneous reaction of ambient
 1177 isoprene-epoxydiols-derived secondary organic aerosol (IEPOX-SOA), *Atmos.*
 1178 *Chem. Phys.*, 16, 11563-11580, 2016

1179 Jimenez, J. L. Canagaratna, M. R. Donahue, N. M. Prevot, A. S. H. Zhang, Q. Kroll, J. H.
 1180 DeCarlo, P. F. Allan, J. D. Coe, H. Ng, N. L. Aiken, A. C. Docherty, K. S.
 1181 Ulbrich, I. M. Grieshop, A. P. Robinson, A. L. Duplissy, J. Smith, J. D. Wilson,
 1182 K. R. Lanz, V. A. Hueglin, C. Sun, Y. L. Tian, J. Laaksonen, A. Raatikainen, T.
 1183 Rautiainen, J. Vaattovaara, P. Ehn, M. Kulmala, M. Tomlinson, J. M. Collins, D.
 1184 R. Cubison, M. J. Dunlea, E. J. Huffman, J. A. Onasch, T. B. Alfarra, M. R.
 1185 Williams, P. I. Bower, K. Kondo, Y. Schneider, J. Drewnick, F. Borrmann, S.
 1186 Weimer, S. Demerjian, K. Salcedo, D. Cottrell, L. Griffin, R. Takami, A.
 1187 Miyoshi, T. Hatakeyama, S. Shimono, A. Sun, J. Y. Zhang, Y. M. Dzepina, K.
 1188 Kimmel, J. R. Sueper, D. Jayne, J. T. Herndon, S. C. Trimborn, A. M. Williams,
 1189 L. R. Wood, E. C. Middlebrook, A. M. Kolb, C. E. Baltensperger, U. and
 1190 Worsnop, D. R.: Evolution of Organic Aerosols in the Atmosphere, *Science*, 326,
 1191 1525-1529, 2009
 1192 Klein, F. Platt, S. M. Farren, N. J. Detournay, A. Bruns, E. A. Bozzetti, C. Daellenbach,
 1193 K. R. Kilic, D. Kumar, N. K. Pieber, S. M. Slowik, J. G. Temime-Roussel, B.
 1194 Marchand, N. Hamilton, J. F. Baltensperger, U. Prevot, A. S. H. and El Haddad,
 1195 I.: Characterization of Gas-Phase Organics Using Proton Transfer Reaction Time-
 1196 of-Flight Mass Spectrometry: Cooking Emissions, *Environ. Sci. Technol.*, 50,
 1197 1243-1250, 2016
 1198 Knote, C. Hodzic, A. Jimenez, J. L. Volkamer, R. Orlando, J. J. Baidar, S. Brioude, J.
 1199 Fast, J. Gentner, D. R. Goldstein, A. H. Hayes, P. L. Knighton, W. B. Oetjen, H.
 1200 Setyan, A. Stark, H. Thalman, R. Tyndall, G. Washenfelder, R. Waxman, E. and
 1201 Zhang, Q.: Simulation of semi-explicit mechanisms of SOA formation from
 1202 glyoxal in aerosol in a 3-D model, *Atmos. Chem. Phys.*, 14, 6213-6239, 2014
 1203 Krechmer, J. E. Pagonis, D. Ziemann, P. J. and Jimenez, J. L.: Quantification of Gas-
 1204 Wall Partitioning in Teflon Environmental Chambers Using Rapid Bursts of Low-
 1205 Volatility Oxidized Species Generated in Situ, *Environ. Sci. Technol.*, 50, 5757-
 1206 5765, 2016
 1207 Kroll, J. H. Ng, N. L. Murphy, S. M. Flagan, R. C. and Seinfeld, J. H.: Secondary organic
 1208 aerosol formation from isoprene photooxidation, *Environ. Sci. Technol.*, 40,
 1209 1869-1877, 2006
 1210 Liu, T. Li, Z. Chan, M. and Chan, C. K.: Formation of secondary organic aerosols from
 1211 gas-phase emissions of heated cooking oils, *Atmos. Chem. Phys. Discuss.*, 2017,
 1212 1-30, 2017
 1213 Matsunaga, A. and Ziemann, P. J.: Gas-Wall Partitioning of Organic Compounds in a
 1214 Teflon Film Chamber and Potential Effects on Reaction Product and Aerosol
 1215 Yield Measurements, *Aerosol Sci. Technol.*, 44, 881-892, 2010
 1216 McDonald, B. C. Goldstein, A. H. and Harley, R. A.: Long-Term Trends in California
 1217 Mobile Source Emissions and Ambient Concentrations of Black Carbon and
 1218 Organic Aerosol, *Environ. Sci. Technol.*, 49, 5178-5188, 2015
 1219 Ng, N. L. Kroll, J. H. Chan, A. W. H. Chhabra, P. S. Flagan, R. C. and Seinfeld, J. H.:
 1220 Secondary organic aerosol formation from m-xylene, toluene, and benzene,
 1221 *Atmos. Chem. Phys.*, 7, 3909-3922, 2007
 1222 Odum, J. R. Hoffmann, T. Bowman, F. Collins, D. Flagan, R. C. and Seinfeld, J. H.:
 1223 Gas/particle partitioning and secondary organic aerosol yields, *Environ. Sci.*
 1224 *Technol.*, 30, 2580-2585, 1996

1225 Ortega, A. M. Hayes, P. L. Peng, Z. Palm, B. B. Hu, W. Day, D. A. Li, R. Cubison, M. J.
 1226 Brune, W. H. Graus, M. Warneke, C. Gilman, J. B. Kuster, W. C. de Gouw, J.
 1227 Gutiérrez-Montes, C. and Jimenez, J. L.: Real-time measurements of secondary
 1228 organic aerosol formation and aging from ambient air in an oxidation flow reactor
 1229 in the Los Angeles area, *Atmos. Chem. Phys.*, 16, 7411-7433, 2016
 1230 Ots, R. Young, D. E. Vieno, M. Xu, L. Dunmore, R. E. Allan, J. D. Coe, H. Williams, L.
 1231 R. Herndon, S. C. Ng, N. L. Hamilton, J. F. Bergström, R. Di Marco, C. Nemitz,
 1232 E. Mackenzie, I. A. Kuenen, J. J. P. Green, D. C. Reis, S. and Heal, M. R.:
 1233 Simulating secondary organic aerosol from missing diesel-related intermediate-
 1234 volatility organic compound emissions during the Clean Air for
 1235 London (ClearfLo) campaign, *Atmos. Chem. Phys.*, 16, 6453-6473, 2016
 1236 Palm, B. B. Campuzano-Jost, P. Ortega, A. M. Day, D. A. Kaser, L. Jud, W. Karl, T.
 1237 Hansel, A. Hunter, J. F. Cross, E. S. Kroll, J. H. Peng, Z. Brune, W. H. and
 1238 Jimenez, J. L.: In situ secondary organic aerosol formation from ambient pine
 1239 forest air using an oxidation flow reactor, *Atmos. Chem. Phys.*, 16, 2943-2970,
 1240 2016
 1241 Pankow, J. F.: An absorption model of the gas aerosol partitioning involved in the
 1242 formation of secondary organic aerosol, *Atmos. Environ.*, 28, 189-193, 1994
 1243 Pankow, J. F. and Asher, W. E.: SIMPOL.1: a simple group contribution method for
 1244 predicting vapor pressures and enthalpies of vaporization of multifunctional
 1245 organic compounds, *Atmos. Chem. Phys.*, 8, 2773-2796, 2008
 1246 Parrish, D. D. Stohl, A. Forster, C. Atlas, E. L. Blake, D. R. Goldan, P. D. Kuster, W. C.
 1247 and de Gouw, J. A.: Effects of mixing on evolution of hydrocarbon ratios in the
 1248 troposphere, *J. Geophys. Res.-Atmos.*, 112, 2007
 1249 Presto, A. A. Miracolo, M. A. Donahue, N. M. and Robinson, A. L.: Secondary Organic
 1250 Aerosol Formation from High-NO_x Photo-Oxidation of Low Volatility
 1251 Precursors: n-Alkanes, *Environ. Sci. Technol.*, 44, 2029-2034, 2010
 1252 Robinson, A. L. Donahue, N. M. Shrivastava, M. K. Weitkamp, E. A. Sage, A. M.
 1253 Grieshop, A. P. Lane, T. E. Pierce, J. R. and Pandis, S. N.: Rethinking organic
 1254 aerosols: Semivolatile emissions and photochemical aging, *Science*, 315, 1259-
 1255 1262, 2007
 1256 Ryerson, T. B. Andrews, A. E. Angevine, W. M. Bates, T. S. Brock, C. A. Cairns, B.
 1257 Cohen, R. C. Cooper, O. R. de Gouw, J. A. Fehsenfeld, F. C. Ferrare, R. A.
 1258 Fischer, M. L. Flagan, R. C. Goldstein, A. H. Hair, J. W. Hardesty, R. M.
 1259 Hostetler, C. A. Jimenez, J. L. Langford, A. O. McCauley, E. McKeen, S. A.
 1260 Molina, L. T. Nenes, A. Oltmans, S. J. Parrish, D. D. Pederson, J. R. Pierce, R. B.
 1261 Prather, K. Quinn, P. K. Seinfeld, J. H. Senff, C. J. Sorooshian, A. Stutz, J.
 1262 Surratt, J. D. Trainer, M. Volkamer, R. Williams, E. J. and Wofsy, S. C.: The
 1263 2010 California Research at the Nexus of Air Quality and Climate Change
 1264 (CalNex) field study, *J. Geophys. Res.-Atmos.*, 118, 5830-5866, 2013
 1265 Shrivastava, M. Easter, R. C. Liu, X. H. Zelenyuk, A. Singh, B. Zhang, K. Ma, P. L.
 1266 Chand, D. Ghan, S. Jimenez, J. L. Zhang, Q. Fast, J. Rasch, P. J. and Tiitta, P.:
 1267 Global transformation and fate of SOA: Implications of low-volatility SOA and
 1268 gas-phase fragmentation reactions, *J. Geophys. Res.-Atmos.*, 120, 4169-4195,
 1269 2015

1270 Shrivastava, M. Fast, J. Easter, R. Gustafson Jr, W. I. Zaveri, R. A. Jimenez, J. L. Saide,
1271 P. and Hodzic, A.: Modeling organic aerosols in a megacity: comparison of
1272 simple and complex representations of the volatility basis set approach, *Atmos.*
1273 *Chem. Phys.*, 11, 6639-6662, 2011

1274 Shrivastava, M. Zelenyuk, A. Imre, D. Easter, R. Beranek, J. Zaveri, R. A. and Fast, J.:
1275 Implications of low volatility SOA and gas-phase fragmentation reactions on
1276 SOA loadings and their spatial and temporal evolution in the atmosphere, *J.*
1277 *Geophys. Res.-Atmos.*, 118, 3328-3342, 2013

1278 Spracklen, D. V. Jimenez, J. L. Carslaw, K. S. Worsnop, D. R. Evans, M. J. Mann, G. W.
1279 Zhang, Q. Canagaratna, M. R. Allan, J. Coe, H. McFiggans, G. Rap, A. and
1280 Forster, P.: Aerosol mass spectrometer constraint on the global secondary organic
1281 aerosol budget, *Atmos. Chem. Phys.*, 11, 12109-12136, 2011

1282 Tsimpidi, A. P. Karydis, V. A. Zavala, M. Lei, W. Molina, L. Ulbrich, I. M. Jimenez, J.
1283 L. and Pandis, S. N.: Evaluation of the volatility basis-set approach for the
1284 simulation of organic aerosol formation in the Mexico City metropolitan area,
1285 *Atmos. Chem. Phys.*, 10, 525-546, 2010

1286 Volkamer, R. Jimenez, J. L. San Martini, F. Dzepina, K. Zhang, Q. Salcedo, D. Molina,
1287 L. T. Worsnop, D. R. and Molina, M. J.: Secondary organic aerosol formation
1288 from anthropogenic air pollution: Rapid and higher than expected, *Geophys. Res.*
1289 *Lett.*, 33, 2006

1290 Warneke, C. de Gouw, J. A. Holloway, J. S. Peischl, J. Ryerson, T. B. Atlas, E. Blake, D.
1291 Trainer, M. and Parrish, D. D.: Multiyear trends in volatile organic compounds in
1292 Los Angeles, California: Five decades of decreasing emissions, *J. Geophys. Res.-*
1293 *Atmos.*, 117, 2012

1294 Warneke, C. McKeen, S. A. de Gouw, J. A. Goldan, P. D. Kuster, W. C. Holloway, J. S.
1295 Williams, E. J. Lerner, B. M. Parrish, D. D. Trainer, M. Fehsenfeld, F. C. Kato, S.
1296 Atlas, E. L. Baker, A. and Blake, D. R.: Determination of urban volatile organic
1297 compound emission ratios and comparison with an emissions database, *J.*
1298 *Geophys. Res.-Atmos.*, 112, D10s47, 2007

1299 Washenfelder, R. A. Young, C. J. Brown, S. S. Angevine, W. M. Atlas, E. L. Blake, D.
1300 R. Bon, D. M. Cubison, M. J. de Gouw, J. A. Dusanter, S. Flynn, J. Gilman, J. B.
1301 Graus, M. Griffith, S. Grossberg, N. Hayes, P. L. Jimenez, J. L. Kuster, W. C.
1302 Lefer, B. L. Pollack, I. B. Ryerson, T. B. Stark, H. Stevens, P. S. and Trainer, M.
1303 K.: The glyoxal budget and its contribution to organic aerosol for Los Angeles,
1304 California, during CalNex 2010, *J. Geophys. Res.-Atmos.*, 116, 2011

1305 Watson, J. G.: Visibility: Science and regulation, *J. Air Waste Manag. Assoc.*, 52, 628-
1306 713, 2002

1307 Woody, M. C. Baker, K. R. Hayes, P. L. Jimenez, J. L. Koo, B. and Pye, H. O. T.:
1308 Understanding sources of organic aerosol during CalNex-2010 using the CMAQ-
1309 VBS, *Atmos. Chem. Phys.*, 16, 4081-4100, 2016

1310 Worton, D. R. Isaacman, G. Gentner, D. R. Dallmann, T. R. Chan, A. W. H. Ruehl, C.
1311 Kirchstetter, T. W. Wilson, K. R. Harley, R. A. and Goldstein, A. H.: Lubricating
1312 Oil Dominates Primary Organic Aerosol Emissions from Motor Vehicles,
1313 *Environ. Sci. Technol.*, 48, 3698-3706, 2014

1314 Ye, P. Ding, X. Hakala, J. Hofbauer, V. Robinson, E. S. and Donahue, N. M.: Vapor wall
1315 loss of semi-volatile organic compounds in a Teflon chamber, *Aerosol Sci.*
1316 *Technol.*, 50, 822-834, 2016

1317 Yuan, B. Veres, P. R. Warneke, C. Roberts, J. M. Gilman, J. B. Koss, A. Edwards, P. M.
1318 Graus, M. Kuster, W. C. Li, S. M. Wild, R. J. Brown, S. S. Dubé, W. P. Lerner,
1319 B. M. Williams, E. J. Johnson, J. E. Quinn, P. K. Bates, T. S. Lefer, B. Hayes, P.
1320 L. Jimenez, J. L. Weber, R. J. Zamora, R. Ervens, B. Millet, D. B. Rappenglück,
1321 B. and de Gouw, J. A.: Investigation of secondary formation of formic acid: urban
1322 environment vs. oil and gas producing region, *Atmos. Chem. Phys.*, 15, 1975-
1323 1993, 2015

1324 Zhang, Q. Jimenez, J. L. Canagaratna, M. R. Allan, J. D. Coe, H. Ulbrich, I. Alfarra, M.
1325 R. Takami, A. Middlebrook, A. M. Sun, Y. L. Dzepina, K. Dunlea, E. Docherty,
1326 K. DeCarlo, P. F. Salcedo, D. Onasch, T. Jayne, J. T. Miyoshi, T. Shimono, A.
1327 Hatakeyama, S. Takegawa, N. Kondo, Y. Schneider, J. Drewnick, F. Borrmann,
1328 S. Weimer, S. Demerjian, K. Williams, P. Bower, K. Bahreini, R. Cottrell, L.
1329 Griffin, R. J. Rautiainen, J. Sun, J. Y. Zhang, Y. M. and Worsnop, D. R.: Ubiquity
1330 and dominance of oxygenated species in organic aerosols in anthropogenically-
1331 influenced Northern Hemisphere midlatitudes, *Geophys. Res. Lett.*, 34, 2007

1332 Zhang, X. Cappa, C. D. Jathar, S. H. McVay, R. C. Ensberg, J. J. Kleeman, M. I. J. and
1333 Seinfeld, J. H.: Influence of vapor wall loss in laboratory chambers on yields of
1334 secondary organic aerosol, *Proc. Natl. Acad. Sci. USA*, 111, 5802-5807, 2014

1335 Zhao, Y. Hennigan, C. J. May, A. A. Tkacik, D. S. de Gouw, J. A. Gilman, J. B. Kuster,
1336 W. C. Borbon, A. and Robinson, A. L.: Intermediate-Volatility Organic
1337 Compounds: A Large Source of Secondary Organic Aerosol, *Environ. Sci.*
1338 *Technol.*, 48, 13743-13750, 2014

1339 Zotter, P. El-Haddad, I. Zhang, Y. M. Hayes, P. L. Zhang, X. Lin, Y.-H. Wacker, L.
1340 Schnelle-Kreis, J. Abbaszade, G. Zimmermann, R. Surratt, J. D. Weber, R. J.
1341 Jimenez, J. L. Szidat, S. Baltensperger, U. and Prevot, A. S. H.: Diurnal cycle of
1342 fossil and nonfossil carbon using radiocarbon analyses during CalNex, *J.*
1343 *Geophys. Res.-Atmos.*, 119, 6818-6835, 2014

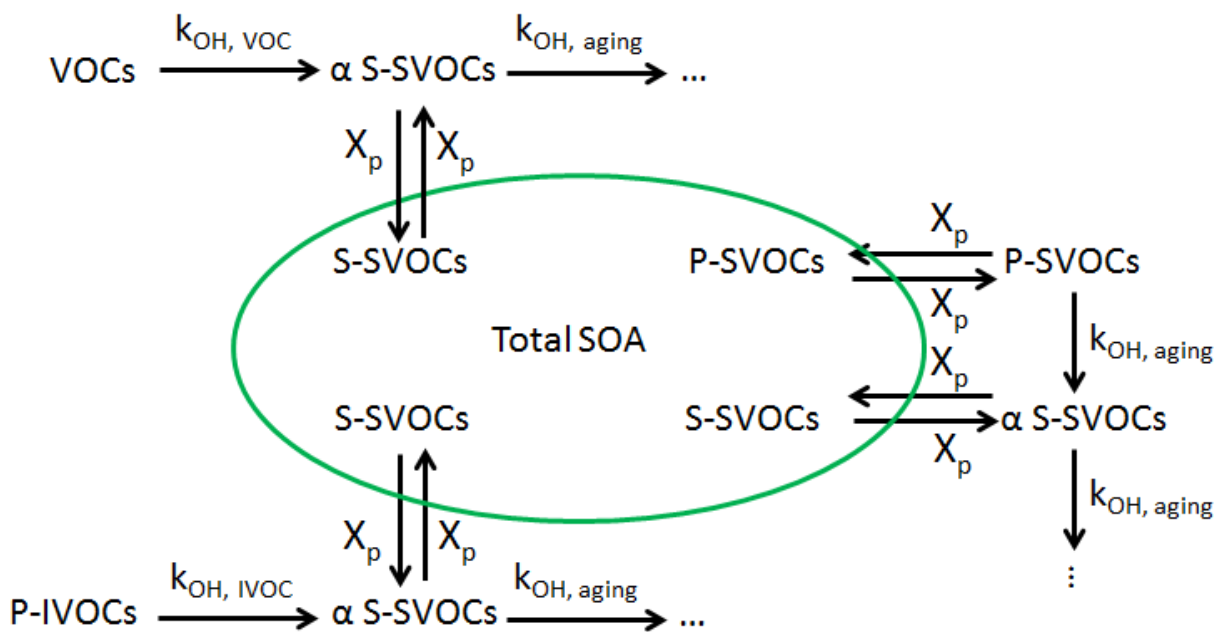
1344

1345 **Table 1.** Summary of the model cases used in this paper.

Case	Notes	References
1) ROB + TSI	<u>P-S/IVOCs</u> : Robinson et al. parameterization, and all SOA treated within VBS framework	Hayes et al. (2015) Robinson et al. (2007) Tsimpidi et al. (2010)
	<u>VOCs</u> : Tsimpidi et al. parameterization with aging	
2) ROB + ZHAO + TSI	<u>P-SVOCs</u> : Robinson et al. parameterization, and all SOA treated within VBS framework	Robinson et al. (2007) Zhao et al. (2014) Tsimpidi et al. (2010)
	<u>P-IVOCs</u> : Zhao et al. parameterization with aging <u>VOCs</u> : Tsimpidi et al. parameterization with aging	
3) WOR + ZHAO + TSI	<u>P-SVOCs</u> : Worton et al. volatility distribution for vehicular P-SVOCs, Robinson et al. volatility distribution for cooking P-SVOCs	Robinson et al. (2007) Worton et al. (2014) Zhao et al. (2014) Tsimpidi et al. (2010)
	<u>P-IVOCs</u> : Zhao et al. parameterization with aging <u>VOCs</u> : Tsimpidi et al. parameterization with aging	
4) ROB + MA	<u>P-S/IVOCs</u> : Robinson et al. parameterization, and all SOA treated within VBS framework	Robinson et al. (2007) This work
	<u>VOCs</u> : VOCs yields corrected for wall-losses, no aging of VOC oxidation products	
5) ROB + ZHAO + MA	<u>P-SVOCs</u> : Robinson et al. parameterization, and all SOA treated within VBS framework	Robinson et al. (2007) Zhao et al. (2014) This work
	<u>P-IVOCs</u> : Zhao et al. IVOC parameterization with aging <u>VOCs</u> : VOCs yields corrected for wall-losses, no aging of VOC oxidation products	
6) WOR + ZHAO + MA	<u>P-SVOCs</u> : Worton et al. volatility distribution for vehicular P-SVOCs, Robinson et al. volatility distribution for cooking P-SVOCs	Robinson et al. (2007) Worton et al. (2014) Zhao et al. (2014) This work
	<u>P-IVOCs</u> : Zhao et al. IVOC parameterization with aging <u>VOCs</u> : VOCs yields corrected for wall-losses, no aging of VOC oxidation products	

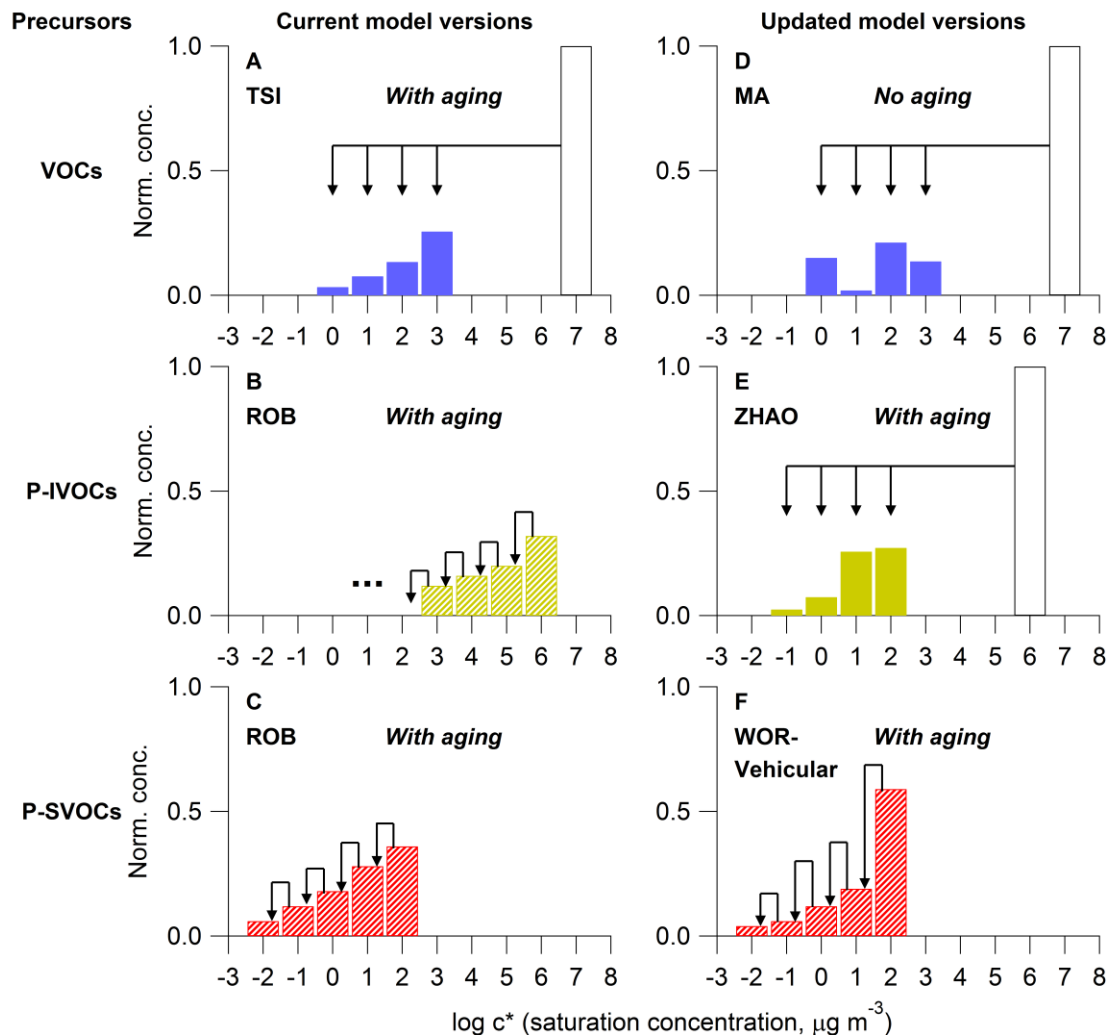
1346

1347



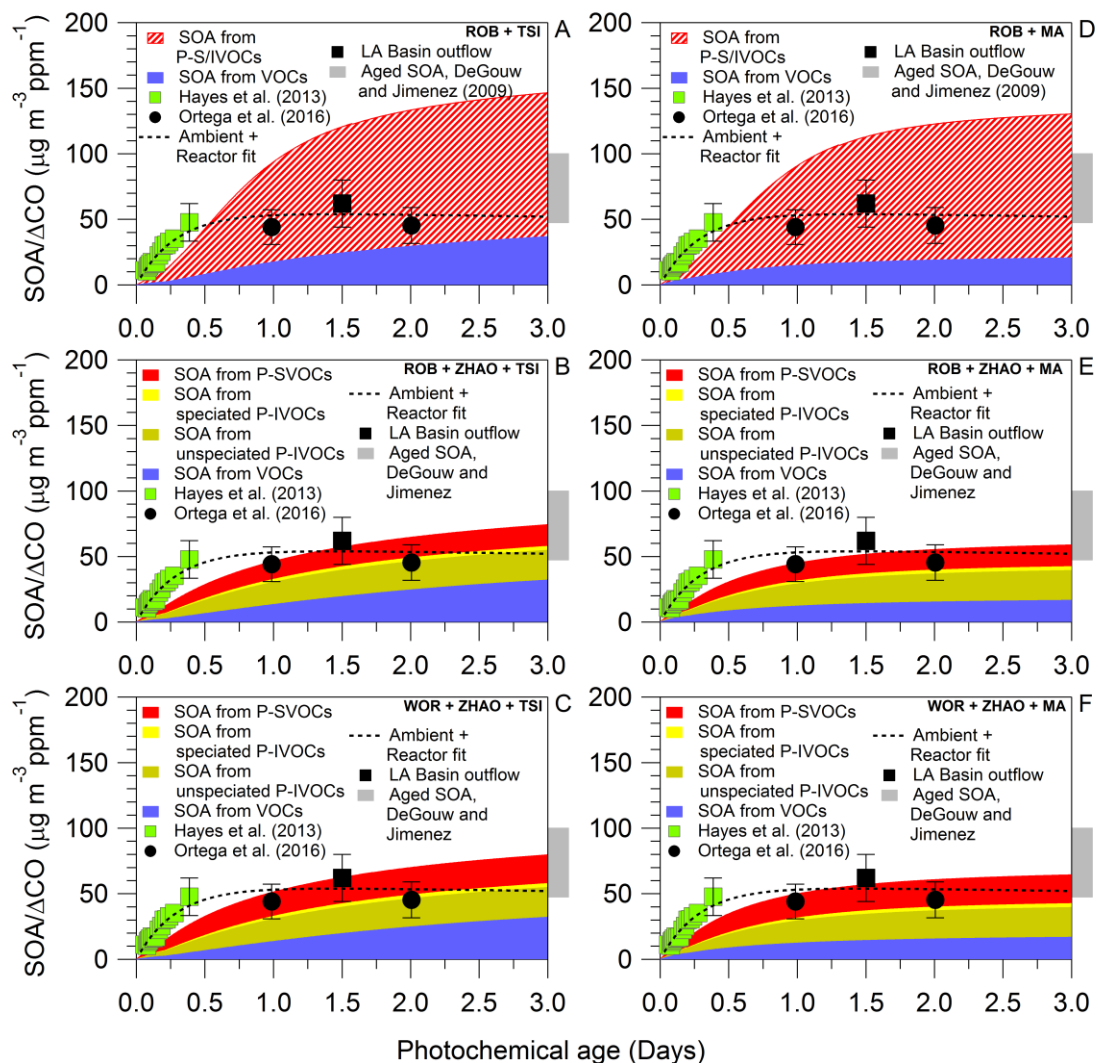
1348

1349 **Figure 1.** Schematic of the chemical pathways leading to the formation of SOA in the box model
 1350 where α is the SOA yield, $k_{OH, VOC}$ and $k_{OH, IVOC}$ are the rate constants of a VOC or an IVOC
 1351 species respectively for oxidation by OH radicals, and X_p is the particle-phase fraction of a
 1352 species.



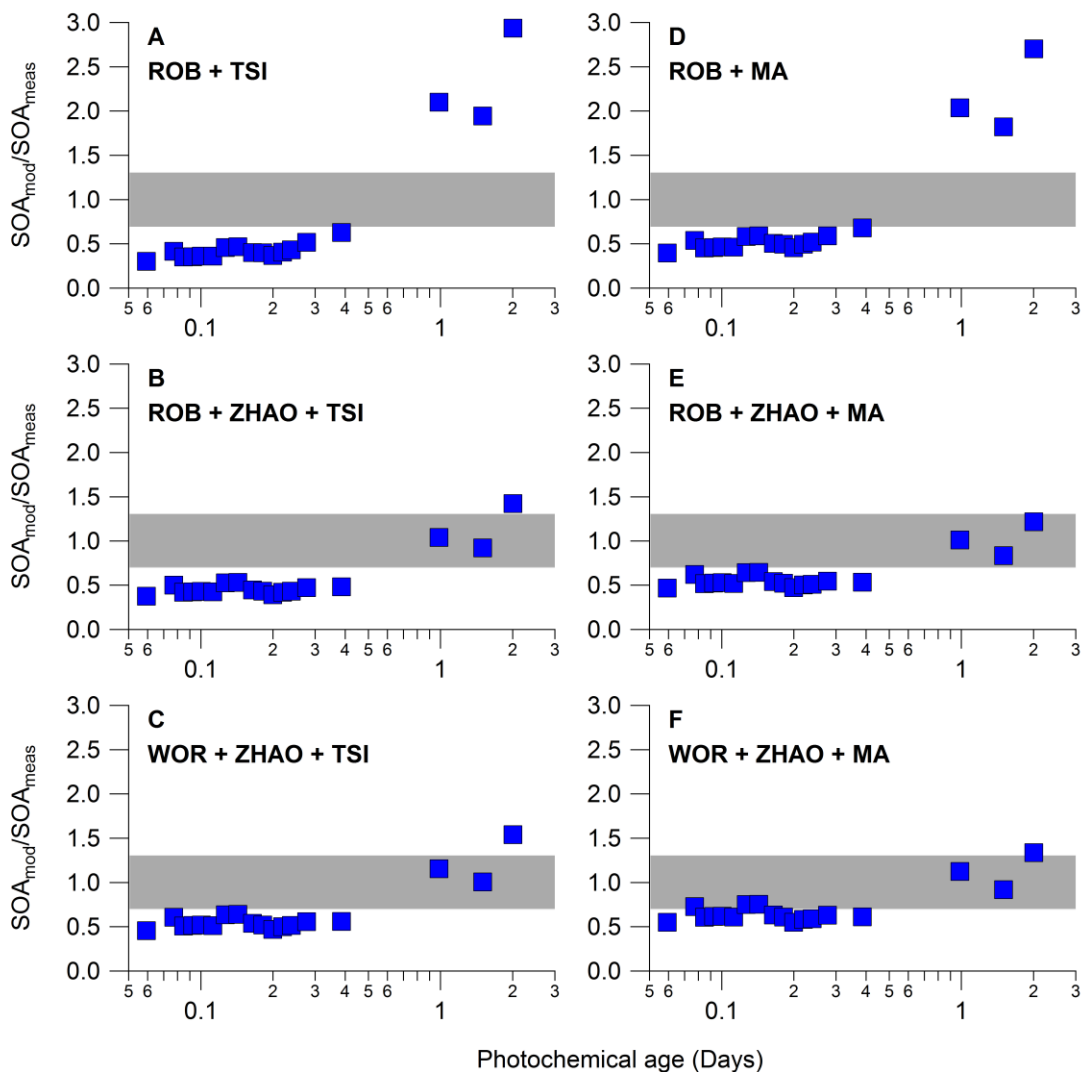
1353

1354 **Figure 2.** Schematic of the SOA formation parameterizations used in the model. The products
 1355 formed are shown in different colors for each precursor. Note that the striped color bars indicate
 1356 that the bins contain both primary and secondary organics. In panel (A) the parameterization of
 1357 Tsimpidi et al. (2010) distributes the products of VOCs oxidation into four volatility bins. Panels
 1358 (B) and (C), show the parameterization of Robinson et al. (2007) in which the volatility of the
 1359 SOA precursors, specifically IVOCs and SVOCs, decrease by one order of magnitude per
 1360 oxidation reaction. For P-IVOCs, aging continues to transfer mass to lower volatility bins ($\log c^*$
 1361 < 2). Panel (D) shows the updated parameterization for VOC oxidation that accounts for gas
 1362 phase wall losses, and Panel (E) shows the updated parameterization for P-IVOC oxidation that
 1363 uses the speciated measurements of IVOCs from Zhao et al. (2014). In Panel (F), for the
 1364 parameterization based on the measurements of Wornton et al. (2014), the Robinson et al. (2007)
 1365 volatility distribution is still used for the P-SVOCs emitted from cooking sources. Arrows
 1366 representing the aging of SOA are omitted for clarity.



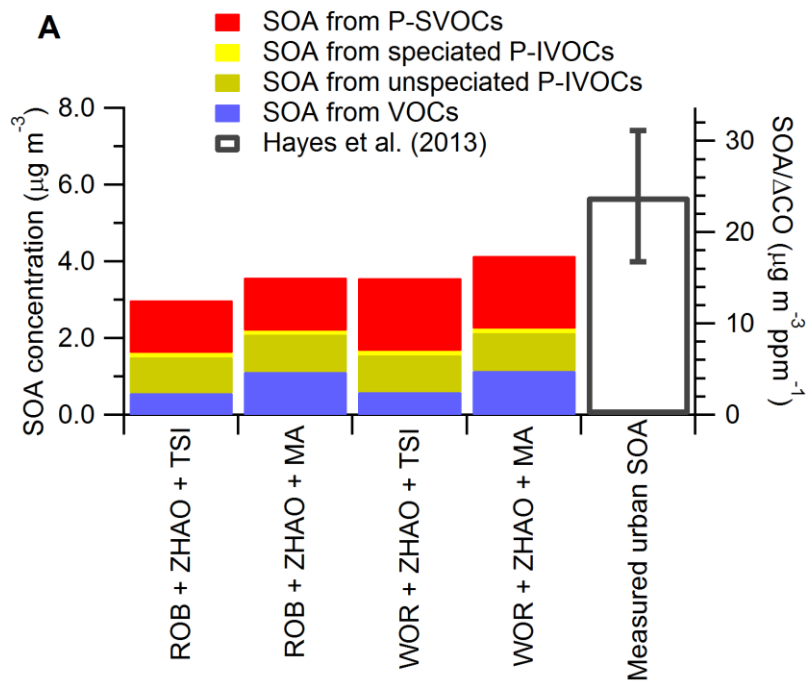
1367

1368 **Figure 3.** Predicted urban SOA mass by all six cases for up to 3 days of photochemical aging
 1369 using a reference OH radical concentration of 1.5×10^6 molec cm^{-3} . Background SOA is not
 1370 included in the figure. The SOA concentrations have been normalized to the background
 1371 subtracted CO (ΔCO) concentration to account for changes in emission strengths and dilution.
 1372 The SOA/ ΔCO data determined from the ambient and OFR measurements at Pasadena as
 1373 reported by Hayes et al. (2013) (green squares) and Ortega et al. (2016) (black circles) are
 1374 shown. Also shown is SOA/ ΔCO determined from measurements performed aboard the NOAA
 1375 P3 research aircraft (black square) reported by Bahreini et al. (2012) and highly aged urban air
 1376 masses (gray bar) reported by de Gouw and Jimenez (2009). The fit for ambient and reactor data
 1377 reported by Ortega et al. (2016) is also shown (dotted black line).

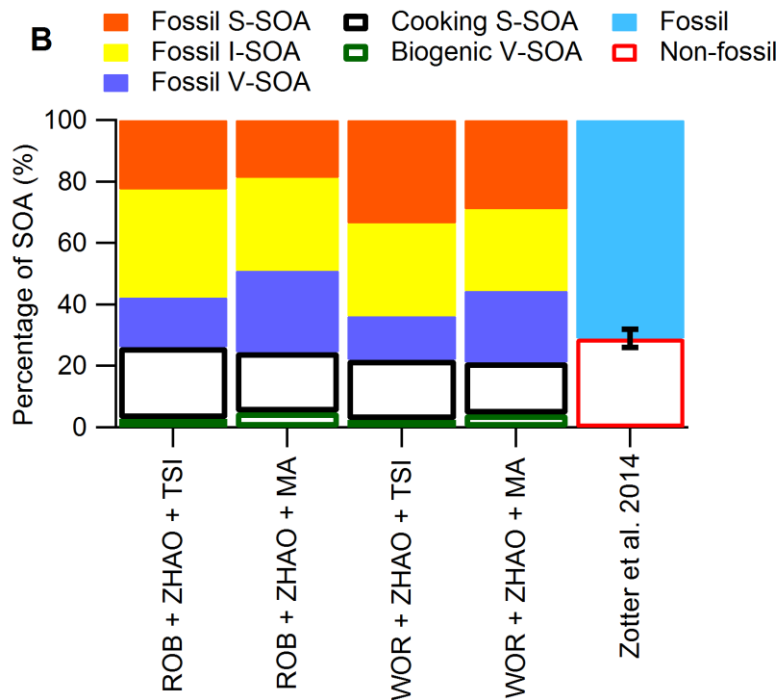


1378

1379 **Figure 4.** The ratio of the modeled-to-measured SOA concentrations (blue squares) for all model
 1380 cases. The measurements are the same as used in Figure 3. The gray bar indicates ratios that
 1381 would correspond to model results that are within the estimated $\pm 30\%$ uncertainty of the
 1382 measurements.

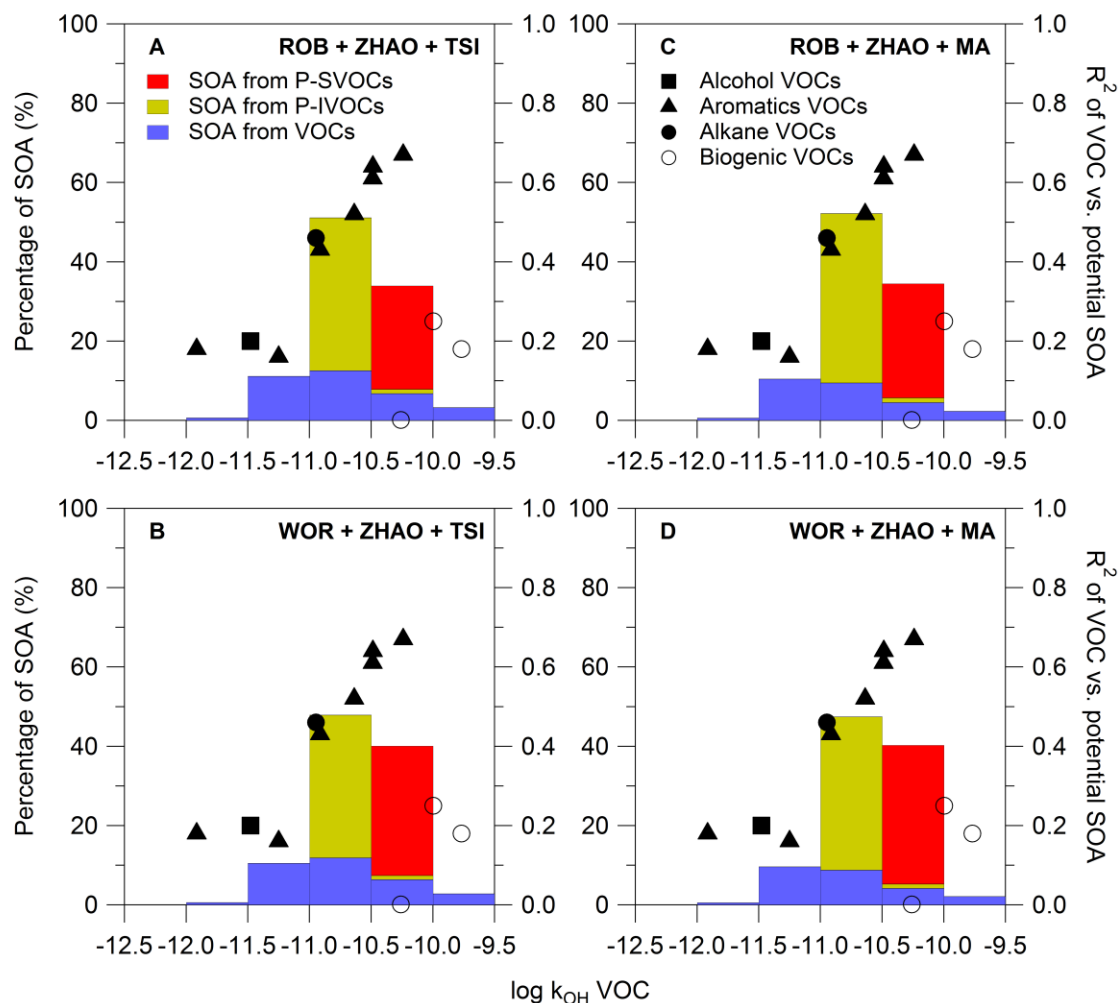


1383



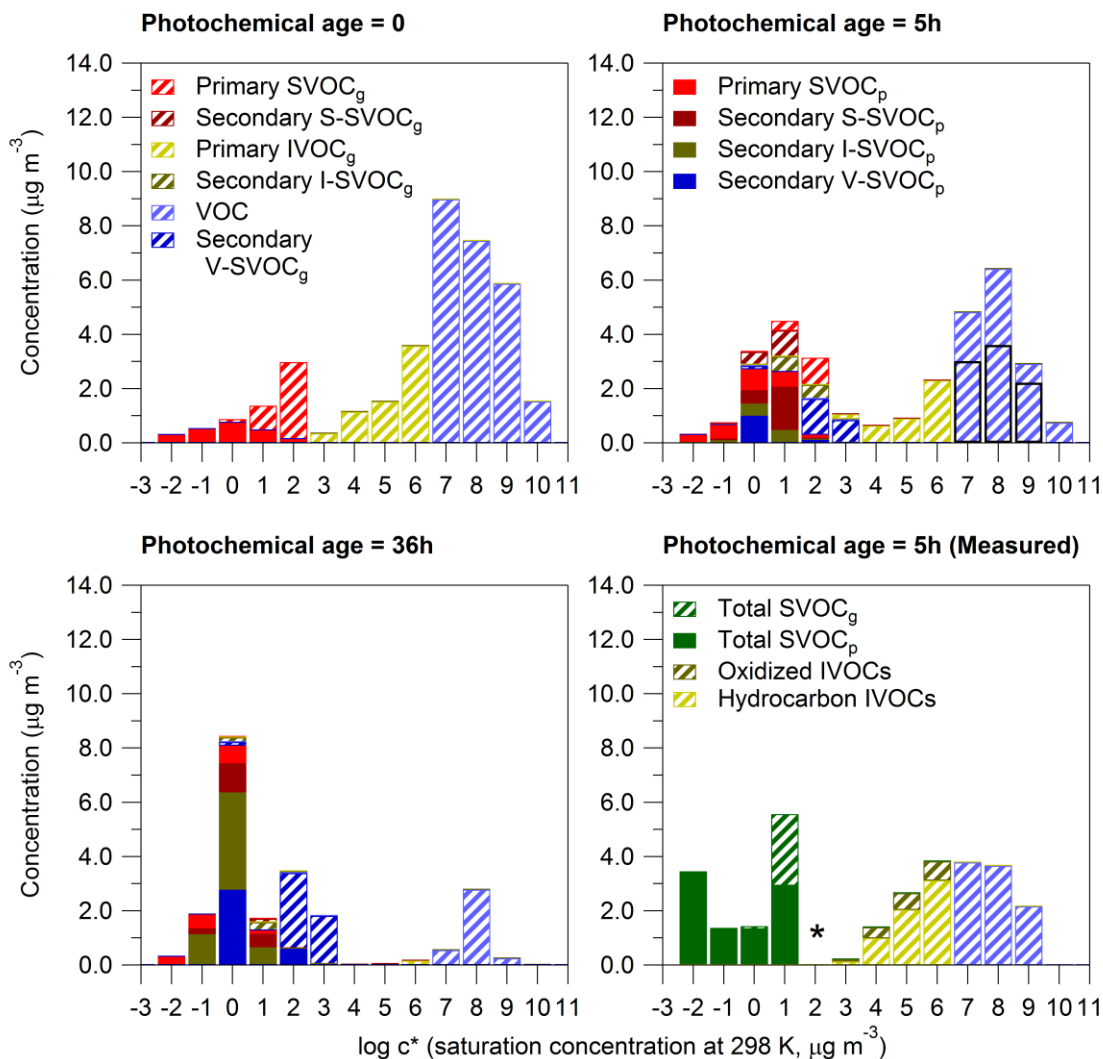
1384

1385 **Figure 5.** (A) Predicted and measured urban SOA mass for 12:00 – 15:00 local time at the
 1386 Pasadena ground site. (B) The fractional mass of fossil S-SOA, fossil I-SOA, and fossil V-SOA,
 1387 as well as cooking S-SOA and biogenic V-SOA for the same time and location. The percentage
 1388 of urban SOA from fossil and non-fossil sources as reported in Zotter et al. (2014) is also
 1389 displayed. The fossil sources are shown as solid bars and the non-fossil sources as hollow bars.



1390

1391 **Figure 6.** Percentage of SOA mass formed from different precursors at 1.5 days of
 1392 photochemical aging (at $1.5 \times 10^6 \text{ molec OH cm}^{-3}$) binned according to precursor rate constant.
 1393 The correlations (R^2) between the concentrations of different VOCs and the maximum SOA
 1394 concentration formed in the OFR as reported by Ortega et al. (2016) are represented by the
 1395 markers. The shape of the marker indicates the chemical family to which each compound
 1396 belongs. For the VOCs and the P-IVOCs the rate constant is the constant for the initial oxidation
 1397 reaction. The measurements of IVOCs used here allow the rate constants of these precursors to
 1398 be taken from published work or estimated using structure-activity relationships as described
 1399 previously (Zhao et al., 2014). For S-SOA, the rate constant is the aging rate constant reported
 1400 originally by Robinson et al. (2007).



1401

1402 **Figure 7.** OA volatility distribution as simulated by the WOR + ZHAO + MA case displayed at
 1403 different photochemical ages (0, 5, and 36 h). The partitioning of the species is indicated using
 1404 patterned bars for gas phase and solid bars for particle phase mass. The bottom-right graph also
 1405 shows the measured volatility distribution of OA. The SVOC volatility distribution is determined
 1406 using a combined thermal denuder AMS system as described in the supporting information. The
 1407 IVOC volatility distribution was previously published in Zhao et al. (2014), and the VOC
 1408 distribution was determined from GC-MS measurements using the SIMPOL.1 model to estimate
 1409 the volatility of each VOC. The asterisk in the bin $\log c^* = 2$ indicates that measurements are not
 1410 available for this bin. It should be noted that not all the VOCs in the model were measured at
 1411 Pasadena (see text for details). For direct visual comparison with the measurements, the
 1412 simulated concentrations of only the VOCs measured at Pasadena are indicated by the black
 1413 hollow bars in the bins $\log c^* = 7, 8,$ and $9 \mu\text{g m}^{-3}$.

1 *Supporting Information for*

2 **Evaluating the impact of new observational constraints on P-S/IVOC emissions, multi-**
3 **generation oxidation, and chamber wall losses on SOA modeling for Los Angeles, CA**

4 Prettina K. Ma et al.

5 *Correspondence to: patrick.hayes@umontreal.ca

6 Estimation of SOA yields for the MA model cases by accounting for chamber vapor losses

7 The approach used here to estimate SOA yields for VOC oxidation that account for losses of gas phase organic compounds to the
8 walls of Teflon environmental chambers uses a set of recently published parameters for modeling gas-wall partitioning in chamber
9 experiments (Krechmer et al., 2016). This previous work found that the fraction of each compound that partitioned to the walls at
10 equilibrium followed absorptive partitioning theory with an equivalent wall mass concentration that could be calculated from the
11 following equation.

$$12 \quad c_w = 16(c^*)^{0.6} \mu g m^{-3} \quad \text{for } c^* = 1, 10, 100, \text{ or } 1000 \mu g m^{-3} \quad (1)$$

13 Our approach assumes equilibrium between the organic material found in the gas phase, particle phase, and the chamber walls. The
14 limitations of this assumption and its potential impact on the model results are discussed below. The partitioning of the SVOCs
15 between the particle and gas phases and the chamber walls can be calculated using the particle concentration, C_{OA} as well as the
16 equivalent wall mass concentration calculated from Equation 1 above.

$$\frac{[SVOC]_w}{[SVOC]_g} = \frac{c_w}{c^*} \quad (2)$$

$$\frac{[SVOC]_p}{[SVOC]_g} = \frac{C_{OA}}{c^*} \quad (3)$$

17 Furthermore, the yield, α_i , is the total amount of SVOC at a given volatility, i , formed from a given VOC.

$$[SVOC]_{g,i} + [SVOC]_{p,i} + [SVOC]_{w,i} = \alpha_i [\Delta VOC] \quad (4)$$

18 Combining Equations 2, 3, and 4, one can obtain the following equation.

$$[SVOC]_{p,i} = \alpha_i \left(1 + \frac{C_i^*}{C_{OA}} + \frac{C_{w,i}}{C_{OA}} \right)^{-1} [\Delta VOC] \quad (5)$$

19 If a four bin basis set is used where $i = 1, 10, 100, \text{ or } 1000 \mu g m^{-3}$, then the total SOA yield, Y , measured during an environmental
20 chamber experiment can be fit with Equation 6, which is simply Equation 5 summed over the four volatilities and then rearranged.

$$Y = \alpha_1 \left(1 + \frac{1}{C_{OA}} + \frac{C_{w,1}}{C_{OA}}\right)^{-1} + \alpha_{10} \left(1 + \frac{10}{C_{OA}} + \frac{C_{w,10}}{C_{OA}}\right)^{-1} + \alpha_{100} \left(1 + \frac{100}{C_{OA}} + \frac{C_{w,100}}{C_{OA}}\right)^{-1} + \alpha_{1000} \left(1 + \frac{1000}{C_{OA}} + \frac{C_{w,1000}}{C_{OA}}\right)^{-1} \quad (6)$$

21 The corrected yields in this work were determined by simulating yield curves using the parameters published in Tsimpidi et al. (2010)
 22 and then refitting the curves using Equation 6.

23 For clarity, c_w is the equivalent organic mass concentration of the walls, and it is an empirically determined value. Equations 2
 24 and 3 are the partitioning equations that describe either the partitioning between the gas phase and walls or the gas phase and the
 25 particles, which both depend on the volatility of the organic vapors, c^* . The significance of c_w can be understood by comparing
 26 equations 2 and 3. In equation 3, the partitioning is dependent on the total particle phase, c_{OA} . Similarly, the parameter c_w is the
 27 amount of mass in the chamber walls available for partitioning expressed as an effective mass concentration based on the work of
 28 Krechmer et al. (2016). However, the value of c_w is a function of c^* as shown in equation 1.

29 As mentioned above, the approach described here assumes equilibrium between the particle and gas phases as well as the
 30 chamber walls. For higher volatility compounds ($c^* \geq 10 \mu\text{g m}^{-3}$), this assumption is reasonable given recently published results that
 31 show transfer of mass between particles and walls on the timescale of an hour (Ye et al., 2016). The same paper has shown however
 32 that for compounds with a volatility of $c^* = 1 \mu\text{g m}^{-3}$, the organic material condensed on particles evaporates and partitions to the
 33 chamber walls on timescales that are longer than typical chamber experiments. The α value for the $c^* = 1 \mu\text{g m}^{-3}$ bin would then be
 34 biased high since the model described above would attribute mass to the chamber walls that is not actually present. Therefore, the
 35 amount of V-SOA in model cases that use the corrected yields determined here should be considered an upper limit. Furthermore, the
 36 original yields (without aging) should be considered lower limits.

37 **Estimation of the SVOC volatility distribution at Pasadena from Thermonuder Aerosol Mass Spectrometry** 38 **Measurements (TD-AMS)**

39 The TD-AMS measurements at Pasadena were carried out using the system previously described by Huffman et al. (2008).
 40 Briefly, switching valves were used to sample both ambient air as well as ambient air passed through a thermodenuder (TD) that was
 41 scanned between 37 and 260°C. The mass fraction remaining (MFR) as a function of temperature, also known as a thermogram, is

42 then calculated from the ratio of the TD measurements and the linearly-interpolated ambient measurements. In order to compare
43 against the model, the thermogram was only determined for the period between 12:00 – 15:00 local time, which corresponded to 5 h of
44 photochemical aging at a reference OH concentration of 1.5×10^6 molec OH cm⁻³. This thermogram is shown below in **Figure S11**.
45 The thermogram is then converted to a volatility distribution using the method described by Faulhaber et al. (2009).

46 The lowest volatility bin modeled is $c^* = 0.01 \mu\text{g m}^{-3}$, but similar to previous measurements (Dzepina et al., 2011), the TD
47 volatility distribution extends to lower volatility bins. The mass in these lower bins is lumped into the $c^* = 0.01$ bins to allow
48 comparison with the model. In addition, since the background SOA is treated as non-volatile in the box model, we subtract the amount
49 of background SOA from the lowest bin ($c^* = 0.01 \mu\text{g m}^{-3}$) after lumping to determine the volatility distribution of urban OA at
50 Pasadena. Both of these approximations will bias the measured urban OA towards higher volatilities. When subtracting the
51 background SOA, this bias would be due to the possibility that some of the background SOA is found in c^* bins greater than $0.01 \mu\text{g}$
52 m^{-3} . Thus, some of the mass subtracted from the $c^* = 0.01 \mu\text{g m}^{-3}$ bin should instead be subtracted from more volatile bins. Given the
53 measured urban OA is already lower volatility than that predicted in the model, correcting these potential sources of error would not
54 change the conclusion in the main text that the measured SOA is less volatile than the modeled SOA.

55

56 **REFERENCES**

- 57 Dzepina, K. Cappa, C. D. Volkamer, R. M. Madronich, S. DeCarlo, P. F. Zaveri, R. A. and Jimenez, J. L.: Modeling the Multiday
58 Evolution and Aging of Secondary Organic Aerosol During MILAGRO 2006, *Environ. Sci. Technol.*, 45, 3496-3503, 2011
- 59 Faulhaber, A. E. Thomas, B. M. Jimenez, J. L. Jayne, J. T. Worsnop, D. R. and Ziemann, P. J.: Characterization of a thermodenuder-
60 particle beam mass spectrometer system for the study of organic aerosol volatility and composition, *Atmos. Meas. Tech.*, 2,
61 15-31, 2009
- 62 Huffman, J. A. Ziemann, P. J. Jayne, J. T. Worsnop, D. R. and Jimenez, J. L.: Development and characterization of a fast-
63 stepping/scanning thermodenuder for chemically-resolved aerosol volatility measurements, *Aerosol Sci. Technol.*, 42, 395-
64 407, 2008
- 65 Krechmer, J. E. Pagonis, D. Ziemann, P. J. and Jimenez, J. L.: Quantification of Gas-Wall Partitioning in Teflon Environmental
66 Chambers Using Rapid Bursts of Low-Volatility Oxidized Species Generated in Situ, *Environ. Sci. Technol.*, 50, 5757-5765,
67 2016
- 68 Tsimpidi, A. P. Karydis, V. A. Zavala, M. Lei, W. Molina, L. Ulbrich, I. M. Jimenez, J. L. and Pandis, S. N.: Evaluation of the
69 volatility basis-set approach for the simulation of organic aerosol formation in the Mexico City metropolitan area, *Atmos.*
70 *Chem. Phys.*, 10, 525-546, 2010
- 71 Ye, P. Ding, X. Hakala, J. Hofbauer, V. Robinson, E. S. and Donahue, N. M.: Vapor wall loss of semi-volatile organic compounds in
72 a Teflon chamber, *Aerosol Sci. Technol.*, 50, 822-834, 2016

73

74 **Table S1.** Parameters for VOC oxidation used in the model. The aging rate constant for the multi-generation oxidation of VOCs is
 75 $1 \times 10^{-11} \text{ cm}^3 \text{ molec}^{-1} \text{ s}^{-1}$.

Classification	Compounds	Molecular weight (g mol ⁻¹)	k_{OH} (cm ³ molec ⁻¹ s ⁻¹)	$\Delta\text{VOC}/\Delta\text{CO}$ (ppt ppb ⁻¹)	Stoichiometric SOA yield High-NO _x , 298 K (μg m ⁻³)				
					0.1	1	10	100	1000
Alk5	Methylcyclopentane	84.2	5.68×10^{-12}	0.566	0.000	0.150	0.000	0.000	0.000
	Cyclohexane		6.97×10^{-12}	0.285					
	Methylcyclohexane	98.2	9.64×10^{-12}	0.202					
	n-Heptane	100.2	6.76×10^{-12}	0.398					
	2-Methylhexane		6.89×10^{-12}	0.385					
	3-Methylhexane		7.17×10^{-12}	0.460					
	2,3-Dimethylpentane		7.15×10^{-12}	0.252					
	2,4-Dimethylpentane		4.77×10^{-12}	0.171					
	2,2,3-Trimethylbutane	114.2	3.81×10^{-12}	0.031					
	n-Octane		8.11×10^{-12}	0.197					
	3-Methylheptane		8.59×10^{-12}	0.131					
	2-Methylheptane		8.31×10^{-12}	0.171					
	2,2,4-Trimethylpentane		3.34×10^{-12}	0.476					
	2,3,4-Trimethylpentane		6.60×10^{-12}	0.171					
	2,3,3-Trimethylpentane	4.40×10^{-12}	0.194						
	n-Nonane	128.3	9.70×10^{-12}	0.220					
n-Decane	142.3	1.10×10^{-11}	0.180						
Undecane	156.3	1.23×10^{-11}	0.290						
Ole1	Propene	42.1	2.63×10^{-11}	3.740	0.000	0.001	0.005	0.038	0.150
	1-Butene	56.1	3.14×10^{-11}	0.340					
	1-Pentene	70.1	3.14×10^{-11}	0.112					
	2-Methyl-1-Butene		6.10×10^{-11}	0.250					
	3-Methyl-1-Butene		3.18×10^{-11}	0.058					
Ole2	1,3-butadiene	54.1	6.66×10^{-11}	0.350	0.000	0.003	0.026	0.083	0.270
	<i>trans</i> -2-pentene	70.1	6.70×10^{-11}	0.097					
	<i>cis</i> -2-pentene		6.50×10^{-11}	0.050					

76 **Table S1 (continued).**

Classification	Compounds	Molecular weight (g mol ⁻¹)	k_{OH} (cm ³ molec ⁻¹ s ⁻¹)	$\Delta VOC/\Delta CO$ (ppt ppb ⁻¹)	Stoichiometric SOA yield High-NO _x , 298 K (μg m ⁻³)				
					0.1	1	10	100	1000
Ole2	Styrene	104.2	5.80×10^{-11}	0.220	0.000	0.003	0.026	0.083	0.270
Ald	Benzaldehyde	106.1	1.15×10^{-11}	1.15×10^{-9}	0.000	0.000	0.000	0.000	0.000
	<i>o</i> -Tolualdehyde	120.1							
	<i>m</i> -Tolualdehyde								
	<i>p</i> -Tolualdehyde								
2,5-Dimethylbenzaldehyde	134.2								
Aro1	Toluene	92.1	5.63×10^{-12}	3.180	0.000	0.003	0.165	0.300	0.435
	Ethylbenzene	106.2	7.00×10^{-12}	0.570					
	<i>i</i> -Propylbenzene	120.2	6.30×10^{-12}	0.030					
	<i>n</i> -Propylbenzene		5.80×10^{-12}	0.110					
	Benzene	78.1	1.22×10^{-12}	1.300					
Aro2	<i>o</i> -Ethyltoluene	120.2	1.19×10^{-11}	0.120	0.000	0.002	0.195	0.300	0.435
	<i>m/p</i> -Ethyltoluene		1.52×10^{-11}	0.349					
	1,2,3-Trimethylbenzene		3.27×10^{-11}	0.240					
	1,2,4-Trimethylbenzene		3.25×10^{-11}	0.620					
	1,3,5-Trimethylbenzene		5.67×10^{-11}	0.310					
	<i>m/p</i> -Xylene	106.2	1.87×10^{-11}	1.790 ^a					
	<i>o</i> -Xylene		1.36×10^{-11}	0.459 ^b					
Isop	Anthropogenic isoprene	68.1	1.00×10^{-10}	0.300	0.000	0.001	0.023	0.015	0.000
	Biogenic isoprene			N/A					
Terp	α -pinene + β -pinene + limonene	136.2	9.82×10^{-11}	N/A	0.000	0.012	0.122	0.201	0.500

77 ^aAverage of both emission ratios; ^bZhao et al. 2014

78

79 **Table S2.** Parameters for P-IVOC oxidation used in the model. Measurements of the IVOCs were reported in Zhao et al. 2014. The
 80 aging rate constant for the multi-generation oxidation of P-IVOCs is $4 \times 10^{-11} \text{ cm}^3 \text{ molec}^{-1} \text{ s}^{-1}$.

Classification	Compounds	k_{OH} ($\text{cm}^3 \text{ molec}^{-1} \text{ s}^{-1}$)	$\Delta\text{IVOC}/\Delta\text{CO}$ ($\text{ng m}^{-3} \text{ ppb}^{-1}$)	Stoichiometric SOA yield High-NOx, 298 K ($\mu\text{g m}^{-3}$)				
				0.1	1	10	100	1000
Naph	Naphtalene	2.44×10^{-11}	0.341	0.000	0.165	0.005	0.516	0.881
	1-Methylnaphtalene	4.09×10^{-11}	0.058					
	2-Methylnaphtalene	4.86×10^{-11}	0.110					
	Phenanthrene	3.20×10^{-11}	0.187					
Alk10	B12 alkane	1.32×10^{-11}	1.718	0.000	0.150	0.000	0.000	0.000
Alk11	B13 alkane	1.51×10^{-11}	1.513					
Alk12	Dodecane	1.32×10^{-11}	0.446	0.000	0.014	0.110	0.160	0.000
	B14 alkane	1.68×10^{-11}	0.951					
	B12 cyclic	1.32×10^{-11}	8.950					
Alk13	Tridecane	1.51×10^{-11}	0.310	0.014	0.059	0.220	0.400	0.000
	Heptylcyclohexane	1.91×10^{-11}	0.049					
	B15 alkane	1.82×10^{-11}	0.574					
	B13 cyclic	1.51×10^{-11}	5.868					
Alk14	Tetradecane	1.68×10^{-11}	0.479	0.022	0.094	0.300	0.350	0.000
	Octylcyclohexane	2.05×10^{-11}	0.049					
	B16 alkane	1.96×10^{-11}	0.486					
	B14 cyclic	1.68×10^{-11}	5.009					
Alk15	Pentadecane	1.82×10^{-11}	0.277	0.044	0.071	0.410	0.300	0.000
	Nonylcyclohexane	2.19×10^{-11}	0.036					
	Pristane	2.44×10^{-11}	0.062					
	B17 alkane	2.10×10^{-11}	0.795					
	B15 cyclic	1.82×10^{-11}	2.758					
Alk16	Hexadecane	1.96×10^{-11}	0.204	0.053	0.083	0.460	0.250	0.000
	Decylcyclohexane	2.33×10^{-11}	0.029					
	Phytane	2.61×10^{-11}	0.031					
	B18 alkane	2.24×10^{-11}	0.278					

81 Table S2 (Continued).

Classification	Compounds	k_{OH} ($\text{cm}^3 \text{ molec}^{-1} \text{ s}^{-1}$)	$\Delta\text{IVOC}/\Delta\text{CO}$ ($\text{ng m}^{-3} \text{ ppb}^{-1}$)	Stoichiometric SOA yield High-NO _x , 298 K ($\mu\text{g m}^{-3}$)				
				0.1	1	10	100	1000
Alk16	B16 cyclic	1.96×10^{-11}	1.855	0.053	0.083	0.460	0.250	0.000
Alk17	Heptadecane	2.10×10^{-11}	0.141	0.063	0.089	0.550	0.200	0.000
	Octadecane	2.24×10^{-11}	0.070					
	Nonadecane	2.38×10^{-11}	0.030					
	Eicosane	2.52×10^{-11}	0.015					
	Heneicosane	2.67×10^{-11}	0.010					
	B19 alkane	2.38×10^{-11}	0.123					
	B20 alkane	2.52×10^{-11}	0.072					
	B21 alkane	2.67×10^{-11}	0.028					
	B17 cyclic	2.10×10^{-11}	2.473					
	B18 cyclic	2.24×10^{-11}	0.939					
	B19 cyclic	2.38×10^{-11}	0.526					
	B20 cyclic	2.52×10^{-11}	0.311					
	B21 cyclic	2.67×10^{-11}	0.142					

82

83 **Table S3.** Parameters for P-SVOC oxidation and the P-SVOC volatility distribution used in the model. The volatility distribution of P-
 84 SVOCs reported by Worton et al. (2014) is used for vehicular emissions whereas the volatility distribution of P-SVOCs reported by
 85 Robinson et al. (2007) is used for cooking emissions.

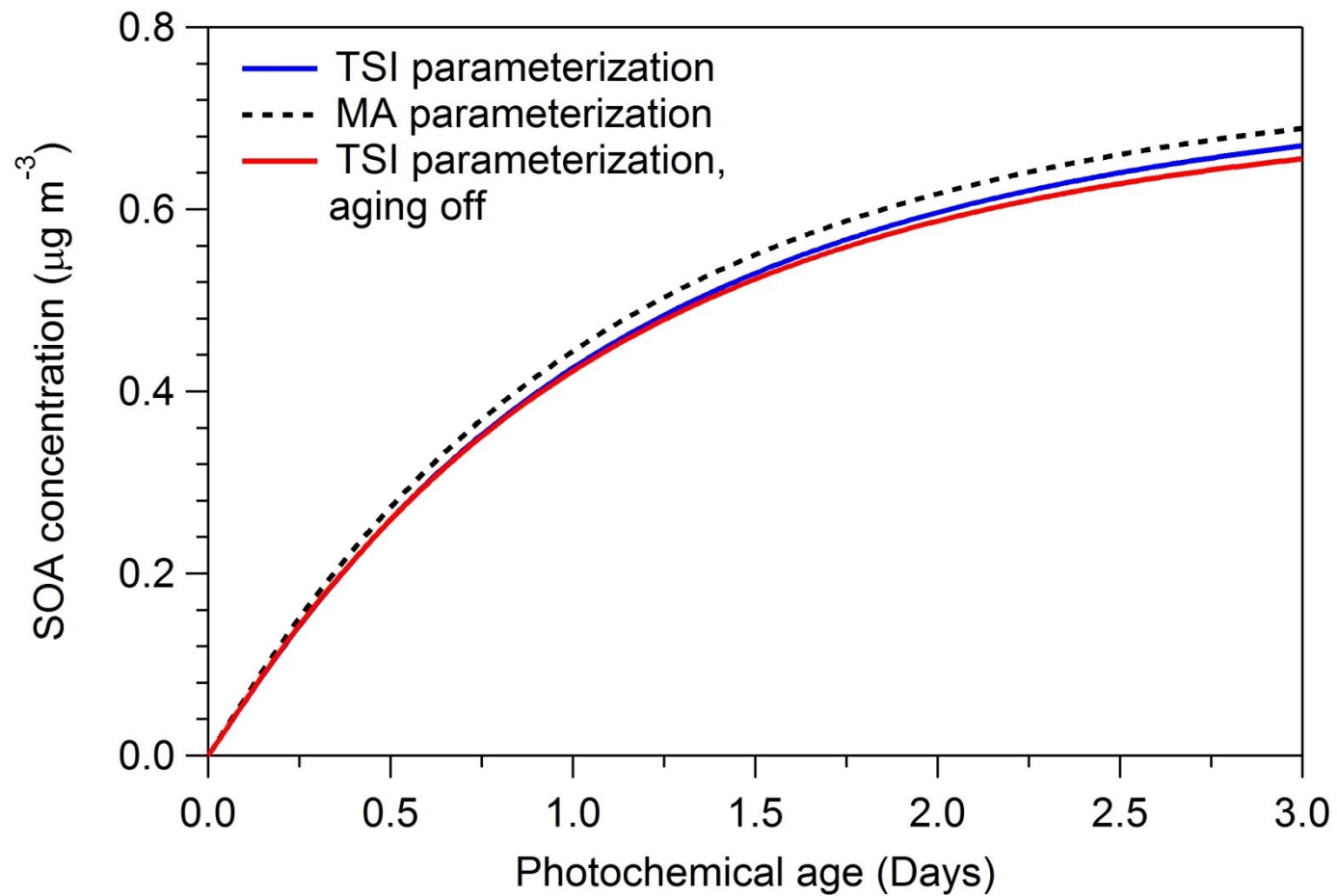
c* ($\mu\text{g m}^{-3}$)	$\Delta\text{H}_{\text{vap}}$ (kJ mol^{-1})	Molecular Weight (g mol^{-1})	Fraction of total P-SVOC (%)	
			ROB	WOR
ROB & WOR	ROB & WOR	ROB & WOR		
10^{-2}	112	250	6	4
10^{-1}	106		12	6
10^0	100		18	12
10^1	94		28	19
10^2	88		36	59
K_{OH} ($\text{cm}^3 \text{molec}^{-1} \text{s}^{-1}$)	4×10^{-11}			
Oxygen mass gain per oxidation generation (%)	7.5			
Volatility decrease per oxidation generation	1 order of magnitude			

86

87 **Table S4.** Updated version of the SOA yields for VOCs accounting for losses of semi-volatile gases to chamber walls.

Classification	Stoichiometric SOA yield, High-NO _x , at 298 K (μg m ⁻³)			
	1	10	100	1000
Alk5	0.157	0.000	0.000	0.000
Ole1	0.014	0.000	0.098	0.088
Ole2	0.052	0.000	0.183	0.157
Ald	0.000	0.000	0.000	0.000
Aro1	0.276	0.002	0.431	0.202
Aro2	0.310	0.000	0.420	0.209
Isop	0.034	0.000	0.005	0.000
Terp	0.210	0.000	0.348	0.297

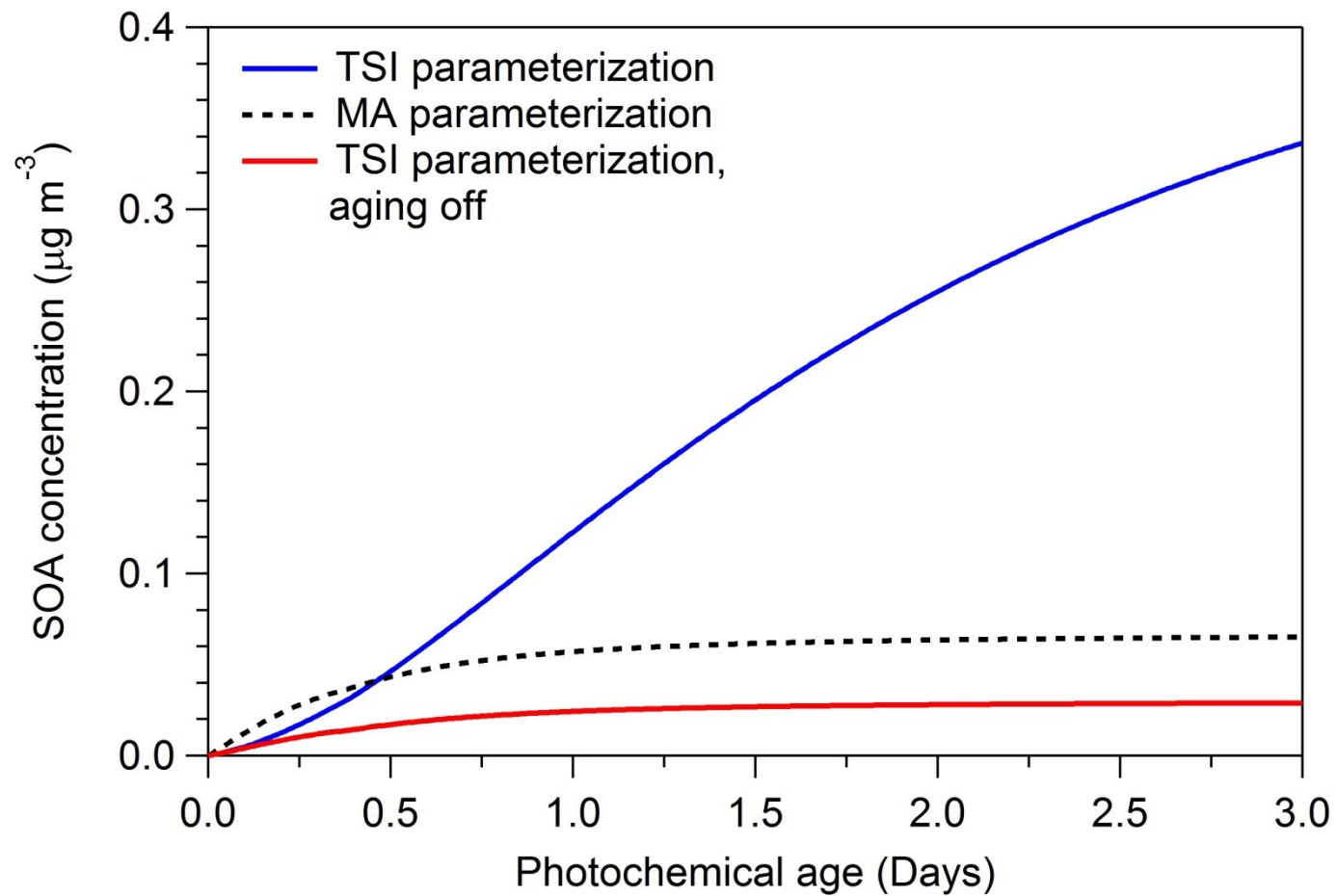
88



89

90 **Figure S1.** Predicted urban SOA mass from the alkane VOCs (Alk5) for different SOA formation parameterizations.

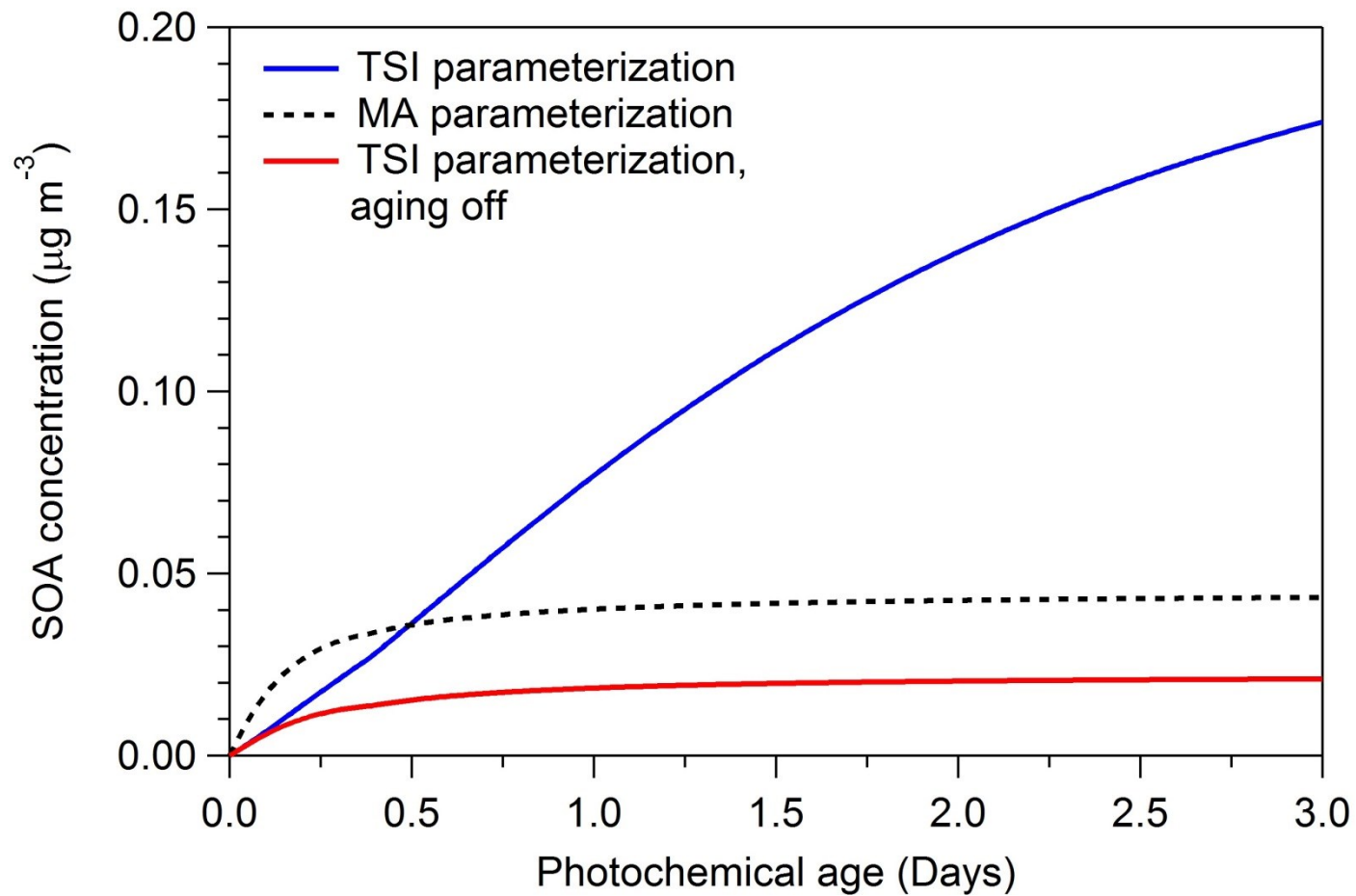
91



92

93 **Figure S2.** Predicted urban SOA mass from the olefin VOCs (Ole1) for different SOA formation parameterizations.

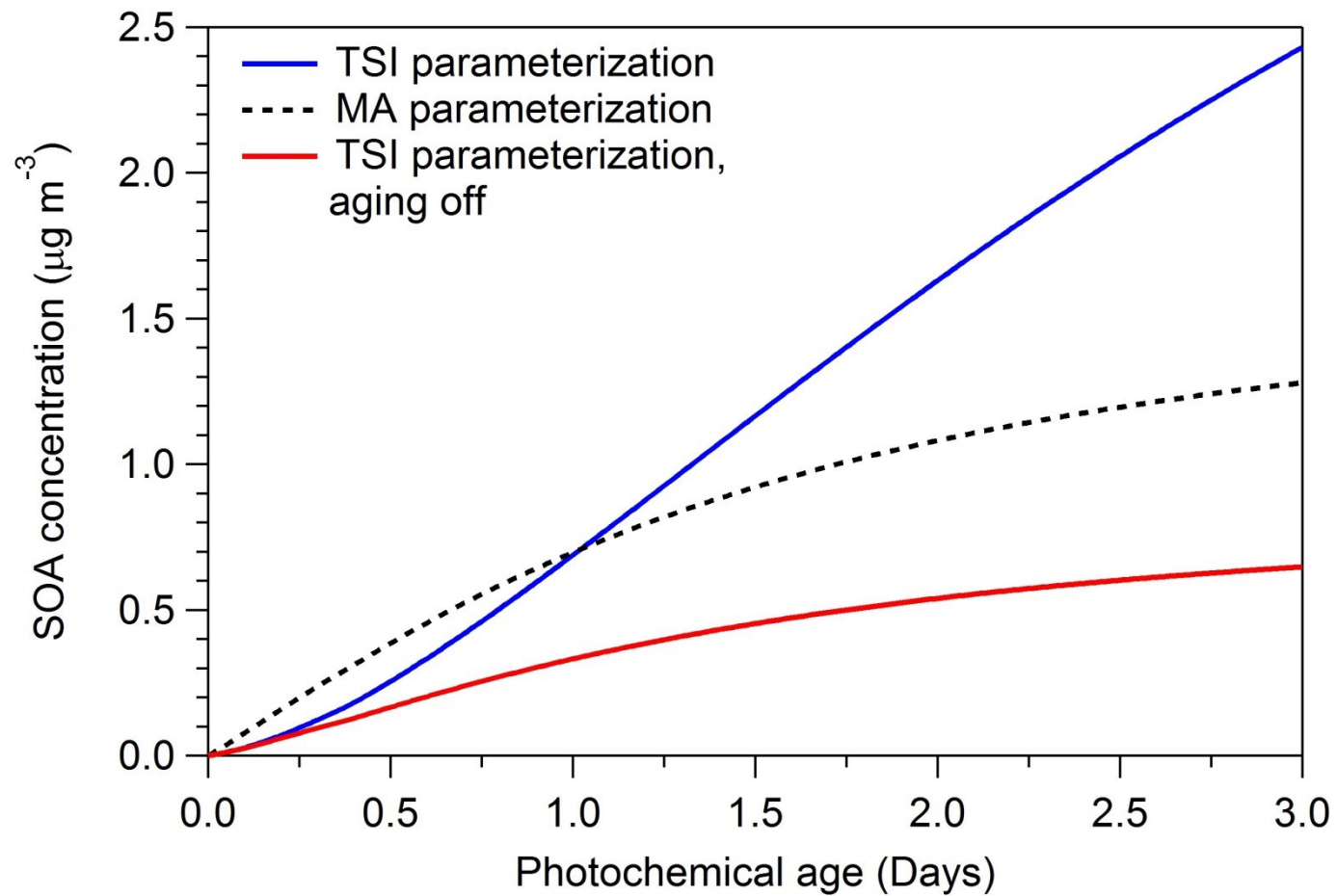
94



95

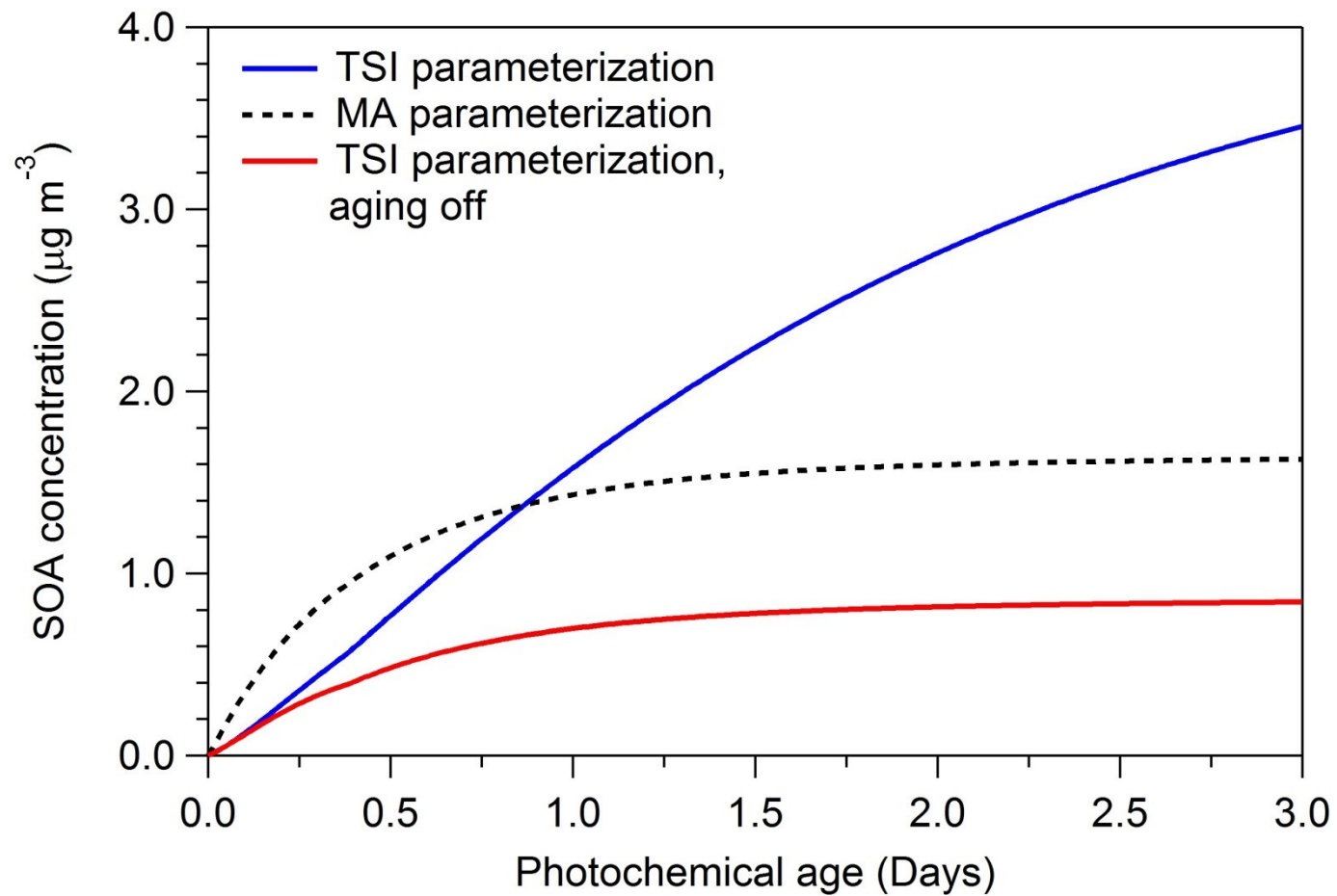
96 **Figure S3** Predicted urban SOA mass from the olefin VOCs (Ole2) for different SOA formation parameterizations.

97



98

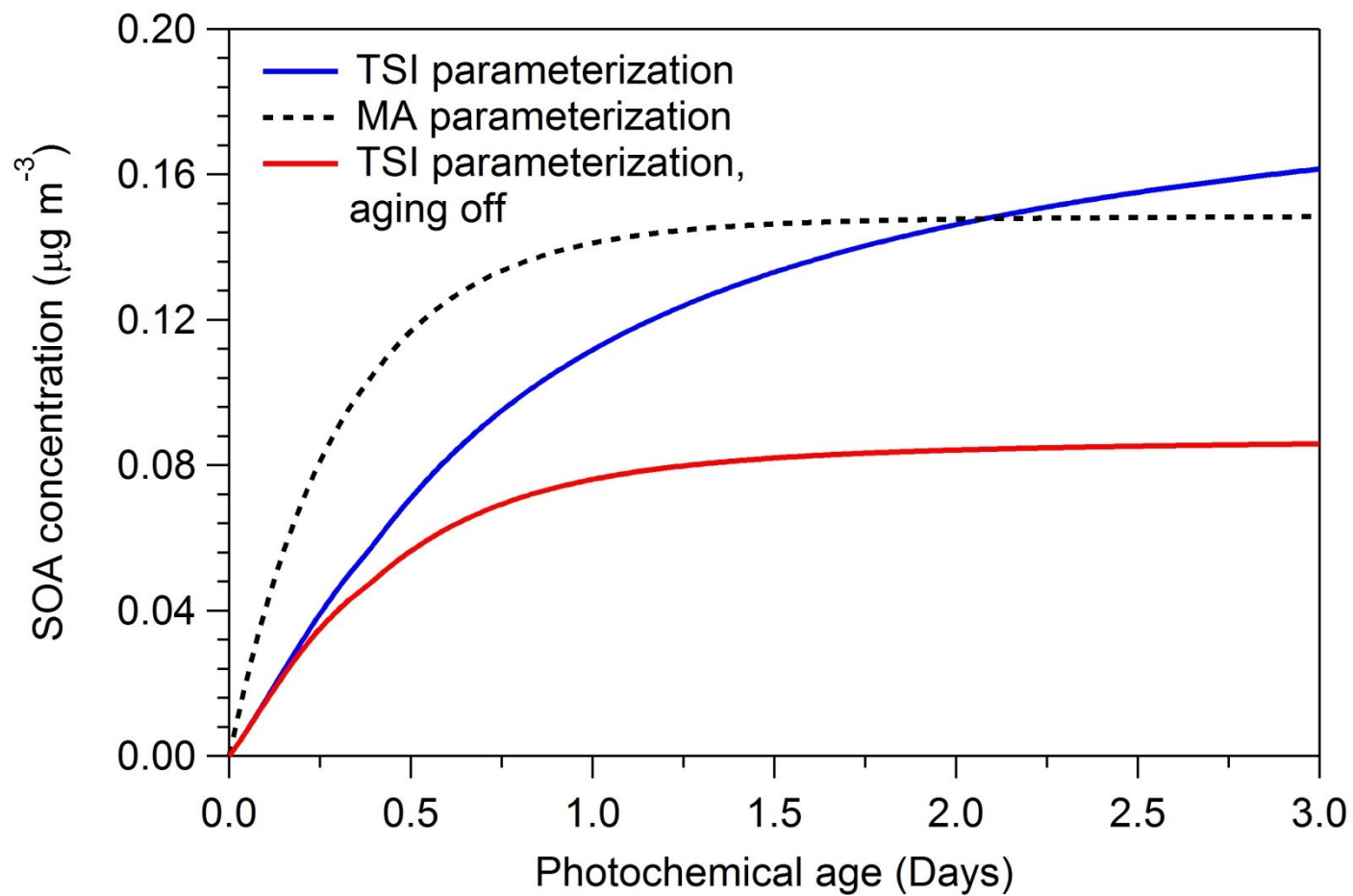
99 **Figure S4.** Predicted urban SOA mass from the aromatic VOCs (Aro1) for different SOA formation parameterizations.



100

101 **Figure S5.** Predicted urban SOA mass from the aromatic VOCs (Aro2) for different SOA formation parameterizations.

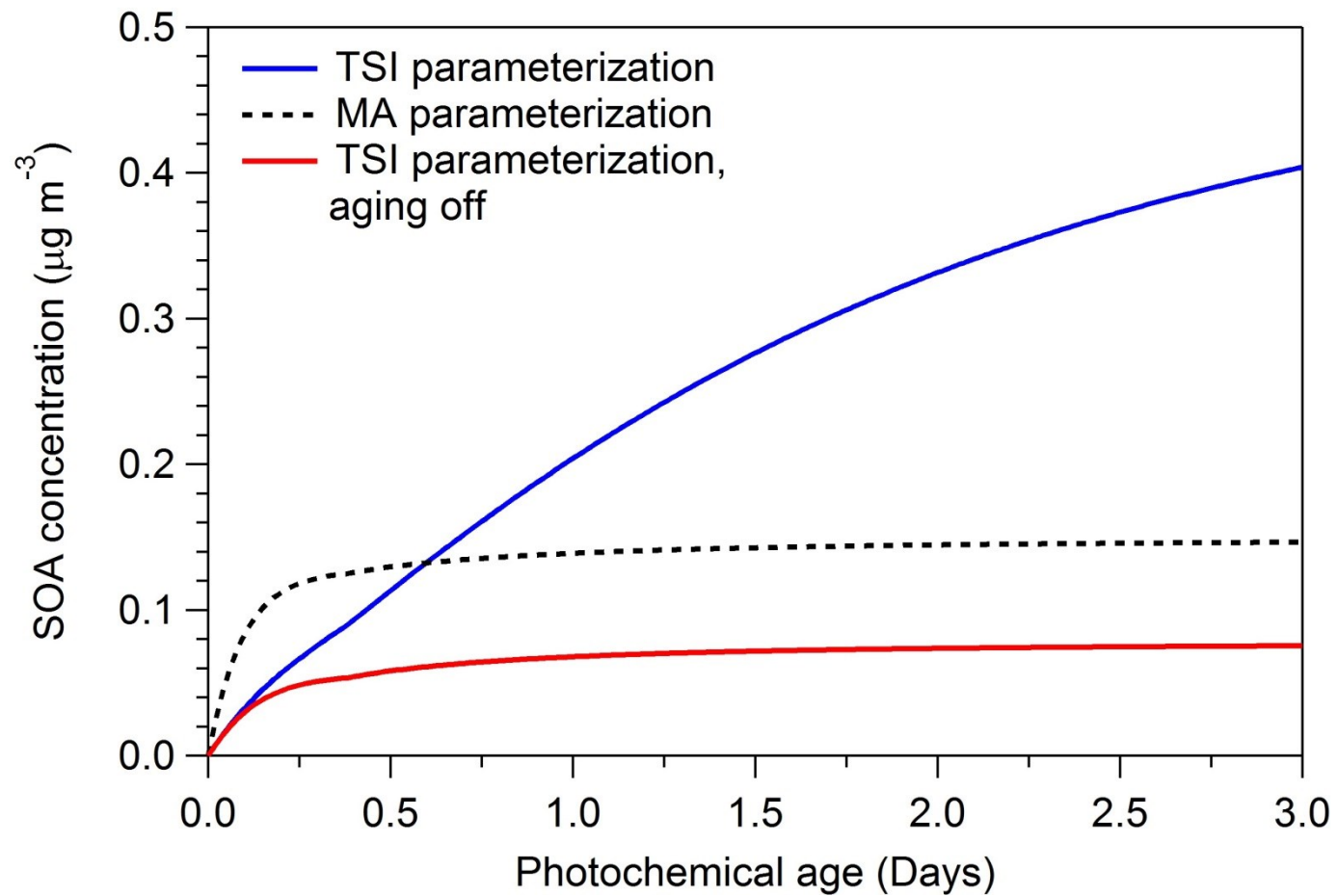
102



103

104 **Figure S6.** Predicted urban SOA mass from isoprene (Isop) for different SOA formation parameterizations.

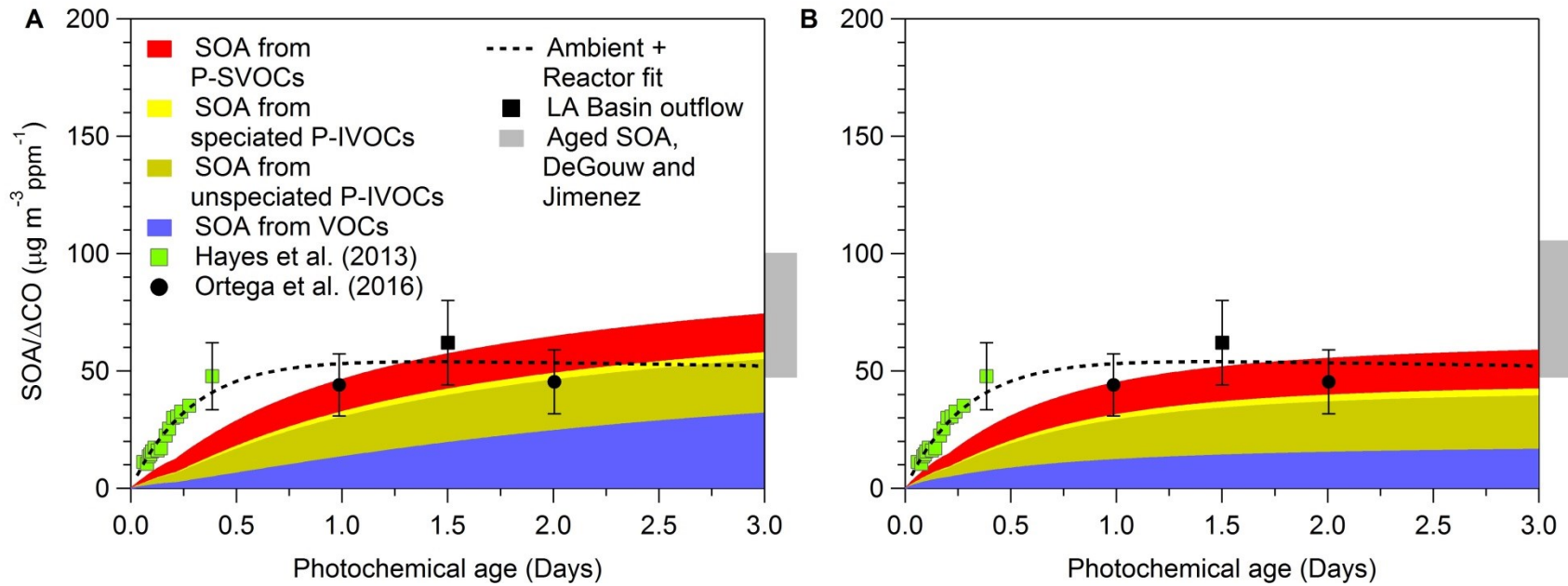
105



106

107 **Figure S7.** Predicted urban SOA mass from terpenes (Terp) for different SOA formation parameterizations.

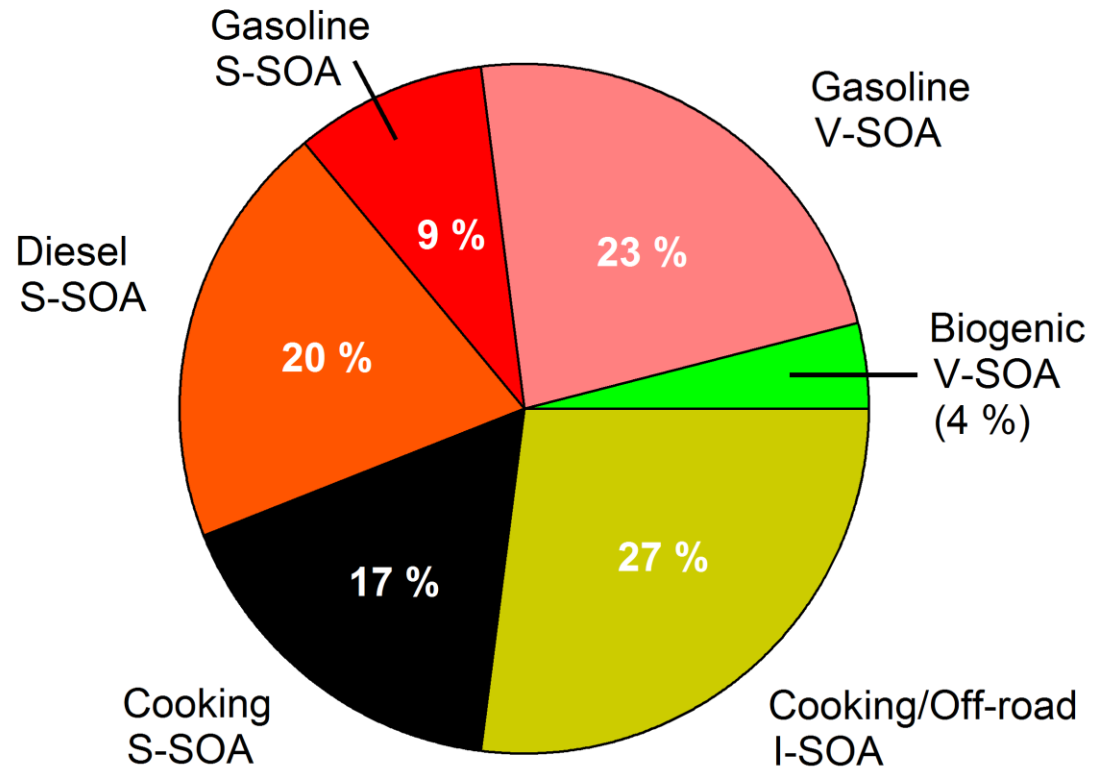
108



109

110 **Figure S8.** Predicted urban SOA mass by the A) WOR + ZHAO + TSI and B) WOR + ZHAO + MA cases when using the meat
 111 cooking volatility distribution reported by Woody et al. (2016).

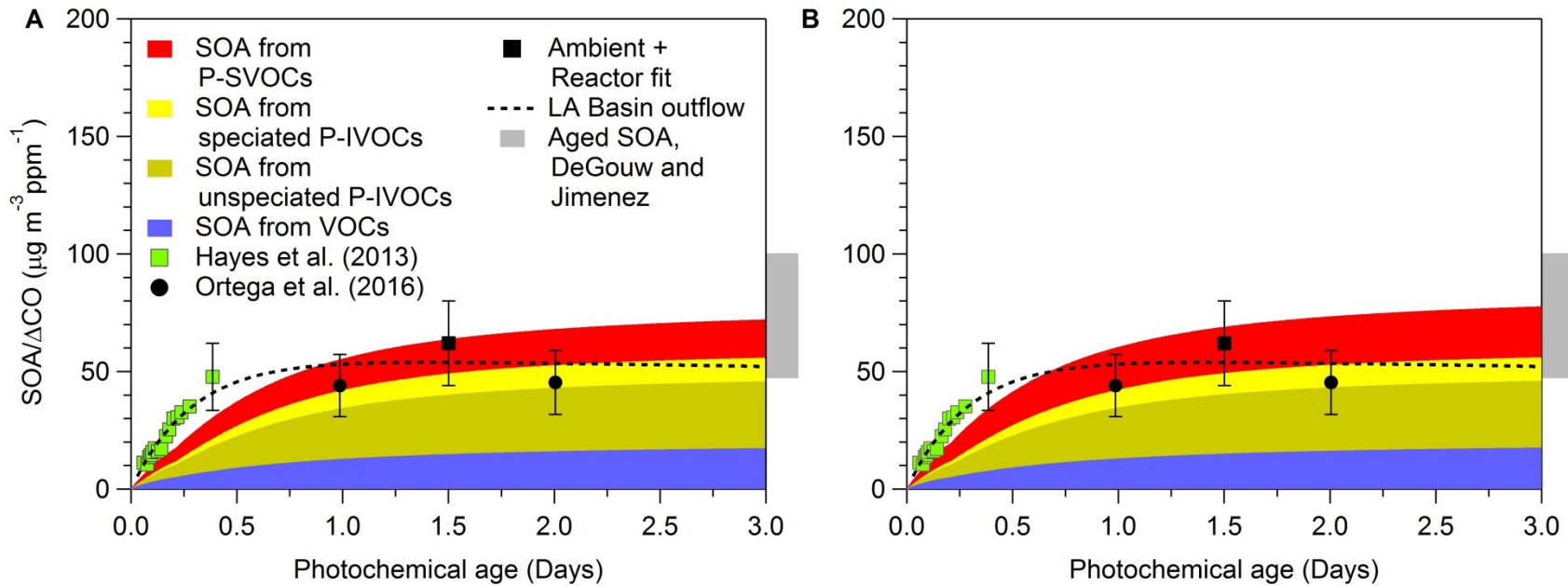
112



113

114 **Figure S9.** Estimated fractional contributions to urban SOA mass concentration using the WOR + ZHAO + MA case.

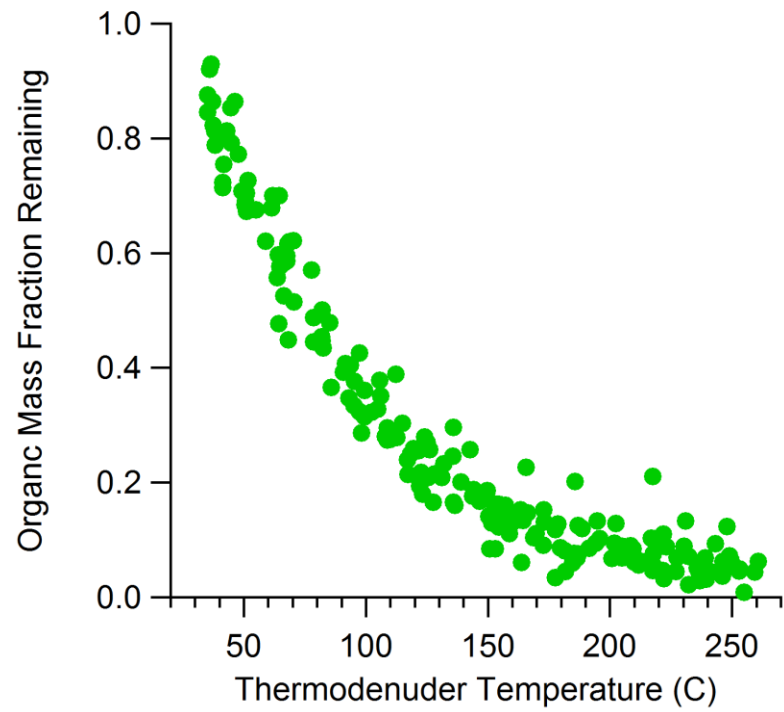
115



116

117 **Figure S10.** Predicted urban SOA mass for the A) ROB + ZHAO + MA and B) WOR + ZHAO + MA cases when using IVOC initial
 118 concentrations determined using photochemical age, the Pasadena IVOC concentrations and the estimated IVOC oxidation rate
 119 constants.

120



121

122 **Figure S11.** Organic mass fraction remaining as a function of temperature for Pasadena, California during CalNex 2010. Data
123 correspond to 12:00 – 15:00 local time.

124